UNIVERSITÀ
DEGLI STUDI
DI PADOVA

Università degli Studi di Padova

Dipartimento di Scienze Biomediche

SCUOLA DI DOTTORATO DI RICERCA IN: Scienze Biomediche

CICLO 31°

Exploring the role of astrocytic Ca^{2+} signaling in Alzheimer's Disease.

Tesi redatta con il contributo finanziario della Fondazione Cariparo.

Direttore della Scuola: Ch.mo Prof. Paolo Bernardi

Supervisore: Dott. Giorgio Carmignoto

Co-supervisore: Dott.ssa Cristina Fasolato

Dottoranda: Annamaria Lia

To Matteo,

who is the wind beneath my wings.

Contents

Abbreviations

2P: two-photon

ACSF: artificial cerebrospinal fluid

Aβ: β-Amyloid

Aβo: Aβ Oligomers

AD: Alzheimer's Disease

ApoE4: Apolipoprotein E Epsilon Allele 4

APP: Amyloid Precursor Protein

ATP: Adenosine triphosphate

BDNF: Brain Derived Neurotrophic Factor

BS: blocking serum

CCE: Capacitative Ca^{2+} Entry

CSF: Cerebrospinal fluid

CPA: Cyclopiazonic acid

DG: Dentate gyrus

ER: Endoplasmic Reticulum

FAD: Familial Alzheimer's Disease

fMRI: functional magnetic resonance imaging

GABA: γ-Aminobutyric Acid

GECIs: Genetically Encoded Calcium Indicators

GFAP: Glial Fibrillary Acidic Protein

GPCRs: G-Protein Coupled Receptors

INS: intrinsic optic signal

IP_3: inositol (1,4,5)-triphosphate

IP_3R: IP_3 Receptor

LTP: Long- Term Potentiation

LTD: Long- Term Depression

mGluRs: metabotropic glutamate receptors

MCI: Mild Cognitive Impairments

NA: noradrenaline

NMDARs: N-methyl-D-aspartate receptors

NVU: neurovascular unit

OGB: Oregon-Green BAPTA1

PBS: phosphate saline buffer

PiB-PET: Pittsburgh compound B positron emission tomography

PMCA: plasma membrane Ca^{2+}-ATPase

PLC: phospholipase C

PS1: Presenilin 1

PS2: Presenilin 2

ROIs: Region Of Interests

RyR: Ryanodine Receptor

SERCA: sarco/endoplasmic reticulum Ca^{2+}-ATPase

SSCx: Somato-Sensory Cortex

STAT3: signal transducer and activator of transcription 3

TREM2: triggering receptor expressed on myeloid cells 2

TRPA1: transient receptor potential ankyrin 1

TTX: Tetrodotoxin

WT: wild-type

1. Summary

Alzheimer's disease (AD) is a chronic incurable neurodegenerative disease, characterized by severe and progressive memory loss and cognitive dysfunctions. The molecular and cellular mechanisms of AD pathogenesis and the early events that anticipate the cognitive decline remain poorly understood. Over the last decades research on neurodegenerative diseases has always been conducted by starting from the aetiology of the disease and proceeding then by looking at the effect of the different hallmarks mainly on neuronal physiology.

Noteworthy, a fundamental albeit neglected aspect is the accumulating evidence of the existence in the brain of dynamic interactions between neurons and astrocytes. Astrocytes are the most abundant type of glial cells in the central nervous system, they are electrically unexcitable but express a form of excitability based on variations of the intracellular concentration of Ca^{2+} ions. It is now largely recognized that astrocytes play crucial roles in brain function, from the control of tissue homeostasis to the modulation of both neurovascular coupling and synaptic transmission. Considering the variety of functions exerted by astrocytes in the brain, it is reasonable to hypothesize an involvement of this cell type in the pathogenesis of brain disorders, including AD.

The main goal of my PhD project is to shed light onto the relationship between astrocytic Ca^{2+} signaling and AD. We focused on astrocytic Ca^{2+} dysfunctions in mouse models of AD along the progression of the disease, by clarifying whether astrocytic Ca^{2+} signal dysfunctions precede or follow Aβ plaque deposition. We evaluated the nature of these alterations in terms of signaling pathways, astrocytic compartments, *i.e.* soma, proximal processes and microdomains, and brain areas involved. To this aim, we employed three FAD mouse models, PS2.30H and APPSwe, which express the human PS2-N141I

mutation and the human APP Swedish mutation alone respectively, and the PS2APP (B6.152H) model that expresses both mutants.

All the experiments were carried out in mice at 3 and 6 months of age, before and after, respectively, the onset of plaque deposition in the PS2APP model. To investigate astrocytic activity, I carried out Ca^{2+} imaging experiments in brain slice and *in vivo* preparations from somato-sensory cortex (SSCx) and hippocampal brain slices by using the genetically encoded Ca^{2+} indicator (GECI) GCaMP6f which allows to study Ca^{2+} signals with high spatial resolution at different astrocytic compartments, including Ca^{2+} microdomains at the thin processes in close contact with the synapses. We found that along with the progression of AD, astrocyte Ca^{2+} activity in the SSCx exhibits a sequence of changes: in 3-month-old PS2APP mice, spontaneous activity is significantly increased, while in 6-month-old PS2APP mice, *i.e.* after the appearance of amyloid plaques, both spontaneous activity and the responsiveness to different metabotropic agonists are drastically reduced in all astrocytic territories. The decrease in evoked responses is likely due to a general IP_3-dependent mechanism. Moreover, we verified that these alterations are not present in APPSwe and PS2.30H mice, demonstrating that the expression of APP or PS2 mutant alone is not sufficient to fully recapitulate the astrocytic Ca^{2+} defects observed in PS2APP mice. Although these defects start in concomitance with Aβ plaque deposition, astrocytic hypoactivity is unrelated to plaque proximity. We are currently investigating whether these alterations are maintained in the real *in vivo* context. Preliminary experiments reveal that, as in brain slices, spontaneous activity is drastically reduced in the SSCx of anesthetized mice. In conclusion, astrocytic Ca^{2+} activity is strongly affected in AD. Additional experiments are currently under development, to assess the

relevance of these astrocytic Ca^{2+} defects in the disturbances of synaptic plasticity and learning/memory functions characterizing AD.

2. Riassunto

Il morbo di Alzheimer è una malattia neurodegenerativa, ancora oggi incurabile, che rappresenta circa il 60% dei casi di demenza. I pazienti AD mostrano un lento e progressivo declino delle funzioni cognitive. I meccanismi molecolari e cellulari alla base del morbo di Alzheimer sono ancora largamente ignoti. Negli ultimi anni la ricerca scientifica si è focalizzata sullo studio degli effetti dei principali marcatori della malattia, *i.e.* placche amiloidi e grovigli neurofibrillari, sulla fisiologia neuronale. Un aspetto cruciale, sebbene a lungo trascurato, è l'esistenza di complesse interazioni fra i neuroni e gli astrociti, le cellule gliali più abbondanti del nostro cervello. Al contrario dei neuroni, gli astrociti sono cellule elettricamente non eccitabili, che tuttavia posseggono una forma diversa di eccitabilità basata su variazioni della concentrazione intracellulare dello ione Ca^{2+}. Gli astrociti svolgono una grande varietà di funzioni che vanno dal controllo dell'omeostasi cerebrale alla modulazione del *coupling* neurovascolare e della trasmissione sinaptica. L'obiettivo della mia tesi di dottorato è quello di esplorare il possibile ruolo di queste cellule nel morbo di Alzheimer. In particolare, la nostra attenzione si è focalizzata sullo studio di possibili disfunzioni del segnale Ca^{2+} astrocitario in modelli murini del morbo di Alzheimer, studiando i cambiamenti dell'attività Ca^{2+} negli astrociti durante la progressione della malattia, verificando quindi se le disfunzioni astrocitarie siano precedenti o successive alla deposizione delle placche amiloidi. Abbiamo caratterizzato queste disfunzioni in termini di vie di segnale, compartimenti astrocitari, *i.e.* soma, processi prossimali e microdomini, e aree cerebrali coinvolte. Nello specifico, abbiamo usato tre modelli murini che presentano mutazioni correlate con le forme familiari di morbo di Alzheimer. I modelli PS2.30H e APPSwe esprimono rispettivamente una forma umana mutata di

PS2 (PS2-N141I) e di APP (APPSwe). Il terzo modello, PS2APP (B6.152H), esprime entrambe le proteine mutate. Gli esperimenti sono stati condotti a 3 e 6 mesi, rispettivamente prima e dopo la comparsa delle placche amiloidi nel modello PS2APP. Per studiare l'attività astrocitaria abbiamo condotto esperimenti di Ca^{2+} imaging in preparazioni *ex vivo* ed *in vivo* di corteccia somato-sensoriale e in fettine ippocampali. Per studiare il segnale Ca^{2+} astrocitario a livello del soma e dei processi, inclusi quelli più a contatto con le sinapsi, abbiamo usato un indicatore genetico per il Ca^{2+}, il GCaMP6f. Dai nostri risultati si evince che durante la progressione della patologia nei topi PS2APP l'attività degli astrociti subisce diversi cambiamenti: a 3 mesi l'attività spontanea è significativamente aumentata, mentre a 6 mesi, dopo la comparsa delle placche amiloidi, sia l'attività spontanea che quella evocata dall'attivazione di diversi recettori metabotropici sono drasticamente ridotte in tutti i compartimenti astrocitari. La riduzione della risposta evocata sembra essere dovuta ad un meccanismo generale dipendente dal segnale IP_3. Queste alterazioni non sono presenti negli altri due modelli murini di Alzheimer usati, dimostrando che l'espressione dell'APP o della PS2 mutata da sola non è sufficiente a ricapitolare i difetti astrocitari del segnale Ca^{2+} presenti nel modello PS2APP. Sebbene nel modello PS2APP le alterazioni si presentino in concomitanza con le placche amiloidi, l'ipoattività astrocitaria non è influenzata dalla vicinanza delle placche. Inoltre, esperimenti preliminari *in vivo* confermano che nei topi PS2APP l'attività astrocitaria a 6 mesi è drasticamente ridotta. In conclusione, nel modello PS2APP l'attività Ca^{2+} degli astrociti è severamente alterata. Ulteriori esperimenti, anche di tipo comportamentale, atti ad investigare le conseguenze di queste alterazioni del segnale Ca^{2+} astrocitario sono attualmente in sviluppo.

3. Introduction

AD, Parkinson disease, amyotrophic lateral sclerosis and Huntington's disease are among the most severe brain disorders and represent a major threat for human health. They differ in their pathophysiology; indeed, some cause memory impairments and other affect the ability to speak or move. Several attempts have been made to find therapeutic targets to stop or delay the progression of these pathologies. Over the last decades, this research has always been conducted by starting from the aetiology of the disease and proceeding then by looking at the effect of the different hallmarks on neuronal physiology. AD makes no exception to this rule. Basic and clinical research have been, indeed, focused mainly on main hallmarks of AD, *i.e.* amyloid-β (Aβ) plaques and neurofibrillary tangles, and their detrimental effects on neuronal physiology. In this "searching for a cure", a fundamental albeit neglected aspect is that brain function depends on dynamic interactions between neurons and different cell types among which a prominent role is played by astrocytes, a rather heterogenous type of glial cells [3].

Astrocytes are the most abundant class of glial cells in the brain. Their importance has been restricted for long time to a merely passive role as mechanical and metabolic supporters of neurons. Nowadays, astrocytes are considered active cellular elements in brain circuits that through dynamic bidirectional signaling with neurons contribute to the regulation of fundamental phenomena in brain function. Astrocytes detect synaptic activity through activation of neurotransmitter receptors which induce distinct intracellular Ca^{2+} elevations. In turn, these astrocytic Ca^{2+} changes trigger the release of gliotransmitters that modulate neuronal transmission and synaptic

plasticity. Despite the growing interest on astrocytic role in brain physiology, much less information is available on a possible contribution of astrocytes to AD. Deeply understanding the link between AD and astrocytes could help to find new therapeutic strategies to contrast this lethal brain disease.

The aim of this thesis is to shed light onto the relationship between astrocytic Ca^{2+} signaling and AD. We aim to clarify whether astrocytic Ca^{2+} dysfunctions are present in a mouse model of AD and, if so, to dissect out the nature of these alterations in terms of signaling pathway, astrocytic structures involved, and brain areas implicated. Our main purpose is to clarify whether astrocytic Ca^{2+} activity changes along AD progression, and possibly precedes or follows Aβ plaque deposition.

This study will also open the possibility to dissect the role of astrocytic Ca^{2+} signaling in connection with neuronal activity and, more important, in behavioural functions and dysfunctions.

3.1 Alzheimer's Disease

AD is a common and incurable neurodegenerative disease. It has been identified in 1979 from Robert Katzman as the most common form of dementia and possibly contributing to 60-80% of cases.

World Health Organization considers dementia as a public health priority and in May 2017, the World Health Assembly endorsed the *Global action plan on the public health response to dementia 2017-2025*. The goal of this plan is to improve how we face this extremely diffuse disease, both in terms of increasing awareness about dementia, support to patients and of funding research projects that could help to identify new therapeutic targets. Current treatments are unable to halt AD progression, they can only slow down the worsening of

dementia symptoms. The greatest known risk factor is increasing age, the majority of people with AD being over 65 years. However, AD is not just a disease of the old age. According to Alzheimer's Association, indeed, approximately 200,000 Americans under 65 are affected by early-onset AD.

As to the clinical manifestations of the disease, the most common early sign is the difficulty remembering of newly learned information. Later on with the pathology, the symptoms become more severe, including disorientation, mood and behavioural changes and more serious memory loss.

From the anatomical and structural point of view, the two main hallmarks of AD are Aβ plaques and neurofibrillary tangles, although their role in AD is still hotly debated.

3.1.1 Historical Background

"I have lost myself"

With these few words, pronounced at the beginning of the last century by Auguste Deter, Alzheimer's history begins.

In 1906, based on the observation of Auguste's symptoms, Alois Alzheimer described for the first time a form of dementia, which subsequently became known as AD, at suggestion of Emily Kraepelin. [4]

Among the symptoms, Auguste D. showed profound and increasingly memory impairments, unfounded suspicions about her family, hallucinations and other worsening psychological changes. Alzheimer characterized the histopathological features of this disease, performing *post-mortem* analysis on the brain of Auguste D. through the reduced silver staining methods described by Max Bielschowsky [5].

About neurofibrillary tangles (Fig.1) he said:

"*In the centre of an otherwise almost normal cell there stands out one or several fibrils due to their characteristic thickness and peculiar impregnability". [6]*

Figure 1. Neurofibrillary Tangles from Auguste D., drawn by Alzheimer. [7]

At the same time, he described also senile plaques as:

"Numerous small military foci are found in the superior layers. They are determined by the storage of a peculiar material in the cortex".[6]

It was not until the late 1980s that it was discovered that neurofibrillary tangles are due to intracellular aggregation of tau proteins [8] and that senile plaques were derived from the extracellular deposition and aggregation of Aβ peptides [9].

3.1.2 Genetics

AD can be divided in two main groups: sporadic AD and familial AD (FAD). FAD results from a mutation in one of the following genes: *APP*, *PSEN1* and *PSEN2*.

The *APP* gene, identified in 1987 [10], is located on chromosome 21 and encodes for amyloid precursor protein (APP), the protein from which Aβ is

formed. Families presenting *APP* mutations undergo an early onset disorder, often in their 50s. Beside *APP* mutations, also the overexpression of normal APP, as in the case of elevated gene dosage in trisomy 21 (Down's syndrome), can lead to an early development of AD [11].

PSEN1 gene, located on chromosome 14, was discovered in 1995 [12]. It encodes for presenilin-1 (PS1), one of the catalytic components of γ-secretase, an enzyme involved in the cleavage of APP. *PSEN1* mutations lead to the earliest and most aggressive form of AD, with onset around 40s. In the same year, the third gene involved in FAD was discovered, *PSEN2* [13]. This gene is an homologous of *PSEN1*, it is located on chromosome 1 and encodes for presenilin-2 (PS2), that, as PS1, is involved in the amyloidogenic cleavage of APP. Beside these three genes, other genes can influence the probability to develop AD. Various studies have assessed the role of the Apolipoprotein E epsilon allele 4 (*ApoE4*) [14], that can be considered the strongest genetic risk factor associated with late-onset AD.

APOE has three common isoforms in humans: APOE2, APOE3, and APOE4. They are products of alleles at a single gene locus. APOE3 is the most common isoform and mediates intermediate risk for AD. Conversely, the *ApoE4* allele is significantly overrepresented in late-onset AD patients and has a dose-dependent effect on the risk and age of onset of AD, whereas *ApoE2* is protective [15]. Another gene that has been recently linked to AD is triggering receptor expressed on myeloid cells 2 (TREM2), which is almost exclusively expressed by microglia in the brain. It is involved in all phases of Aβ phagocytosis [16] and increasing TREM2 gene dosage reduces plaque area and associated toxicity [17].

Apparently, there is a sharp distinction between FAD and sporadic AD, but it is important to notice that subjects presenting FAD-related mutations sometimes develop the disease after 65 years, and that early onset AD can affect also patients without FAD-related mutations. Hence, while these categories are useful for research and clinical purposes, it is important to clarify that AD is a complex disease: real life of patients often represents an exception to our attempts to make clear distinctions in the manifestations of an unclear pathology.

3.1.3 Pathogenesis

The pathogenesis of AD is still object of debate in the scientific community. In 1992 John Hardy and Gerald Higgins proposed the amyloid cascade hypothesis [18], which remains nowadays the most widely accepted. According to this hypothesis, an imbalance in Aβ production and/or clearance leads to its accumulation in the brain and this should represent the starting point of a process that ultimately causes AD. Aβ production involves all the three genes implicated in FAD. Indeed, while a non-amyloidogenic product is released if APP is cleaved by α-secretase, Aβ peptides are released from APP after the sequential cleavage of two different secretases, β-secretase and γ-secretase (Fig.2).

Most of the Aβ produced by γ-secretase in physiological conditions is the 40-residue form ($A\beta_{40}$), while the 42-residue variant ($A\beta_{42}$) is less common. However, the major Aβ species deposited in the plaques is the $A\beta_{42}$, the most prone to aggregate. Noteworthy, in the presence of FAD mutations the ratio $A\beta_{42}/A\beta_{40}$ is significantly increased [19].

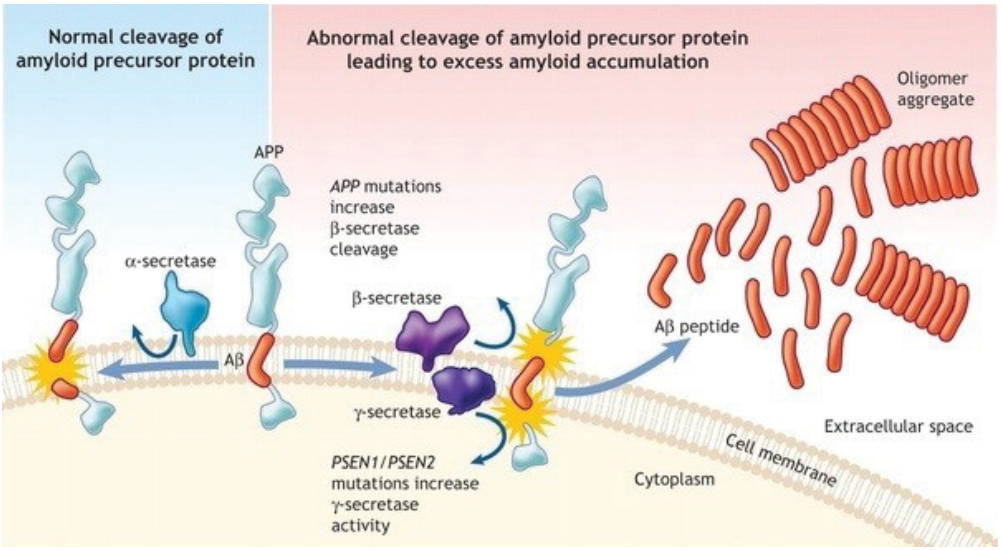

Figure 2. APP processing. The scheme shows the two different pathways that are involved in the APP cleavage. The α-secretase activity (left) leads to the production of a non-amyloidogenic product. Instead, the sequential cleavage mediated by β- and γ-secretase leads to the production of Aβ-peptides that possibly culminate in the production of aggregates and senile plaques. Image adapted from [2].

Several lines of evidence have recently challenged this relatively simple and clear picture that poses Aβ plaques at the centre of the story. As a matter of fact, other players are likely involved in determining the conversion of the disease from preclinical AD to overt AD.

Noteworthy, the attention now focused from large insoluble aggregates, i.e. plaques, to small soluble oligomeric intermediates, Aβ oligomers (Aβo). They are increased in AD patients and represent the earliest component of amyloid plaques [20]. Moreover, it has been demonstrated that Aβo affect synaptic plasticity, dendritic spine density and memory [21, 22].

In light of these changes, amyloid cascade hypothesis has been readapted, introducing the role of Aβo. Indeed, it has been stated that soluble Aβo cause a variety of alterations such as gliosis, oxidative stress and Ca^{2+} dysregulations ultimately leading to synaptic loss and neuronal death. It is noteworthy that the

link between AD and Ca^{2+} homeostasis is older with respect to amyloid cascade hypothesis, as it was suggested by Khachaturian in 1987 [23]. The role of Ca^{2+} alterations in AD is supported also from the importance of presenilins in regulating Ca^{2+} homeostasis at the level of plasma membrane, endoplasmic reticulum (ER) and mitochondria [24].

The amyloid cascade hypothesis is not, however, completely accepted. In 2015, Karl Herrup examined the case of rejecting amyloid cascade hypothesis [25]. For instance, he highlighted that I) overexpression of human APP in mouse produces plaques, but it is not sufficient to have AD, II) tangles correlate better with neurodegeneration with respect to plaques, III) immunoclearing of plaques does not improve cognition, IV) no phase 3 clinical trials based on amyloid cascade hypothesis have been successful. Remarkably, at the time of Herrupp's analysis the study related to the human monoclonal antibody aducanumab was not published yet. This antibody reduces soluble and insoluble Aβ, and phase 3 clinical trial reports showed that it also slows cognitive decline [26]. Recent findings pointed out also a new role for Aβ peptide as antimicrobial peptide, suggesting that Aβ deposition is a protective immune response to infection. This is named the antimicrobial hypothesis of AD, and this aspect may have some importance in the aetiology of AD [27]. Altogether, many aspects are still unclear about the pathogenesis of AD and probably Aβ is not the only basis of AD. Beside Aβ deposition there are other alterations concerning different aspects of brain function and beside neurons, different cell types, such as microglia and astrocytes, are involved in the disease.

3.1.4 Biomarkers

A biomarker generally refers to a measurable indicator of some biological state or condition. Biomarkers are often measured and evaluated to examine both physiological and pathological processes. Classical AD biomarkers are Aβ plaques and neurofibrillary tangles.

In the past, AD was defined with certainty only at autopsy. In the last year, a paradigm shift has characterized the approach related to AD diagnosis. Nowadays, diagnosis of either prodromal or overt AD is exclusively based on progressive biomarkers that are independent of the clinical state of the subject [28, 29]. This is possible thanks to *in vivo* identification of Aβ plaques and neurofibrillary tangles by positron emission tomography (PET), hippocampal atrophy and cortex thinning as well as hypometabolism by anatomic and functional magnetic resonance imaging (fMRI) (see below).

Yet, there is an ever-growing need to find biomarkers for the early diagnosis of AD at the occurrence of mild cognitive impairment (MCI) or even before and to follow the progression of the disease. Clinically accepted and validated biomarkers are the assessment of $A\beta_{42}$ decrease combined with phosphor-tau increase at the level of cerebrospinal fluid (CSF) and plasma, but also brain Aβ deposition measurements by Pittsburgh compound B positron emission tomography (PiB-PET). CSF measurements are based on the concept that Aβ accumulation in the brain, due to overproduction or lower extrusion through the blood-brain barrier (BBB), leads to a reduction of $A\beta_{42}$ in CSF [30]. Interestingly, it has been evaluated the diagnostic potential of $A\beta_{42}/A\beta_{40}$ ratio in CSF [31]. Its accuracy is similar with respect to the measurements of $A\beta_{42}$ allowing to discriminate between AD and non-AD subjects.

Surprisingly, the use of $A\beta_{40}/A\beta_{42}$ ratio reduces the number of indeterminate CSF profiles, thus it is reasonable to hypothesize that it will be preferred to $A\beta_{42}$ measurement alone.

Sampling CSF requires a lumbar puncture and it is considered to be invasive also because it may cause post-lumbar puncture headache (PLPH) [32]. PiB-PET (Fig.3) is a less invasive procedure; it is performed by using PiB, a radioactive analogue of thioflavin-T, to bind $A\beta_{40}$ and $A\beta_{42}$ fibrils and insoluble plaques [33]. Neuroimaging techniques, because of their minimally invasive nature and sensitivity to the earliest changes within the brain substrate, are hopefully the more adequate techniques to disclose subjects with a higher risk to develop AD. Among the negative aspects of neuroimaging, it must be considered that these techniques are very expensive in terms of cost of the radioligands, structural facilities and analytical tools. Noteworthy, both in the case of CSF measurements and PiB-PET, information related to *in vivo* amyloid plaque presence in elderly subjects remains to be adequately correlated with preclinical (asymptomatic) stages of AD.

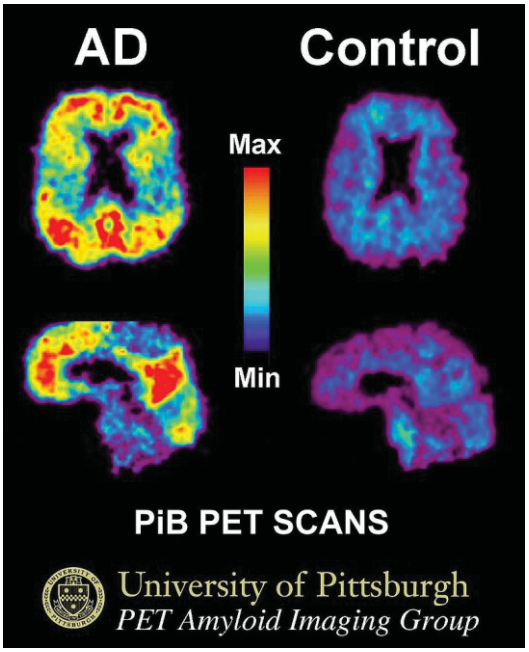

Figure 3. PiB-PET scan of a patient with AD compared with an elderly person with normal memory. Areas of red and yellow show high concentrations of PiB in the brain and suggest high amounts of amyloid deposits in these areas.

One important aspect that must be considered in preclinical diagnosis of AD is the importance to discriminate between AD and MCI. This latter is a condition characterized by measurable cognitive decline that doesn't satisfy the criteria for AD. It does not always precede - or progress to - AD, but when it involves

memory dysfunctions there is more risk of developing AD. Therefore, to accurately predict conversion from MCI to AD it is fundamental to integrate the analysis of different biomarkers [34]. Finally, the detection of brain atrophy and hypo-metabolism, especially at the hippocampal level, further confirms the progression of the disease, becoming a valuable tool in different clinical trials. Large scale studies with both FAD and SAD patients, support the idea that the two forms of the disease share very similar stages, only with decades of anticipation for FAD patients. Moreover, given the debated role of Aβ plaques and the general complexity of AD pathogenesis, a crucial aspect is to move our attention from the classical biomarkers of AD to new ones that are as much as possible specific features of AD, allowing to perform an early diagnosis. Indeed, an explanation for the failure of clinical trials based on amyloid cascade hypothesis is that the drugs are given at the wrong point in the progression of AD [35].

"The general view is these are the right drugs, but they're too late,

it's like taking statins when you're having a heart attack."

John Hardy

3.2 Astrocytes

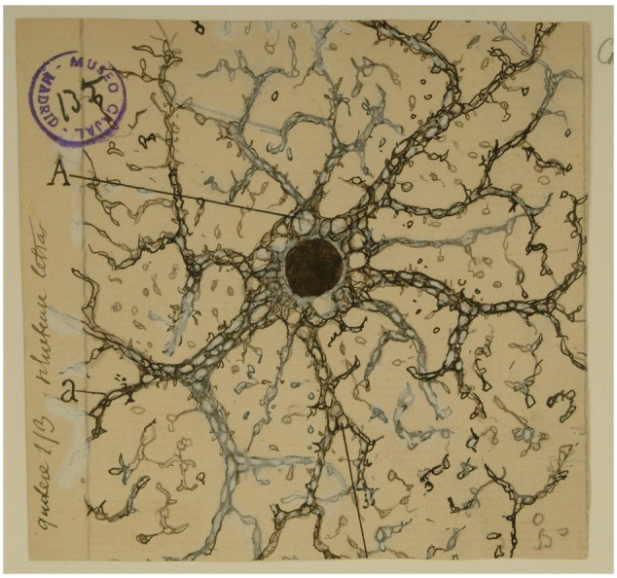

Figure 4. Cajal's drawing showing a "neuroglia" of the pyramidal layer and stratum radiatum of the Ammon horn from an adult man autopsied 3 h after death. [1]

The concept of *Nervenkitt*, later defined as neuroglia, was introduced in 1856 by Rudolph Virchow. He conceived neuroglia as a kind of connective tissue that contained also cellular elements. Camillo Golgi disclosed glia as a cellular population, he identified glial cells as round cells with different fine processes extended in all directions and recognized glial endfeet contacting blood vessels (Fig. 4) [36]. The term a*strocyte* was introduced in 1893 by Michael von Lenhossék [37] and popularized by Ramón y Cajal, awarded the Nobel Prize in 1906 for his work on neuronal structures and connections. As a result of his work on astrocytes, Cajal confirmed some of the astrocytic features by using an astroglia-specific staining technique and proposed also pioneering concepts regarding their functions (Fig. 5). Unfortunately, at the end of the nineteenth century it was impossible to confirm those concepts. Indeed, Cajal in 1899 wrote:

"What functional significance can be attributed to the neuroglia? Unfortunately, the present state of science does not allow to answer this important question but through more or less rational conjectures. When facing this problem, the physiologist is totally disarmed for lack of methods."

One century after, the technological advancements allowed to confirm different Cajal's theories.

Indeed, from a variety of studies, it is now well established that astrocytes are star-shaped glial cells involved in brain information processing, which actively communicate with neurons, regulate neurovascular coupling and are implicated in brain superior functions [38].

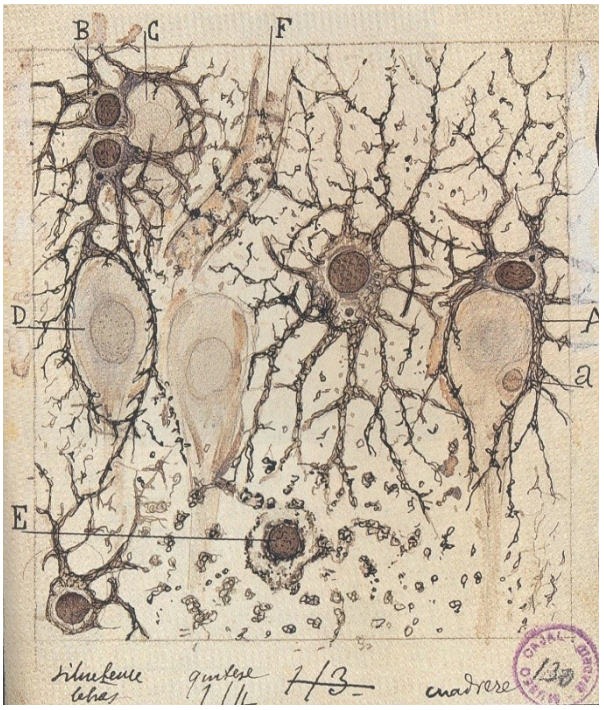

Figure 5. Cajal's drawing. Original labels: A, large astrocyte embracing a Pyramidal neuron; B, twin astrocytes forming a nest around a cell, C, while one of them sends two branches forming another nest, D; E, cell with signs of "autolysis"; F, capillary vessel. Sublimated gold chloride method.

3.2.1 Star-shaped, omnipresent, always different: astrocytes

Astrocytes are highly heterogenous and, at present, a marker capable to label all astroglial cell types does not exist. As an example, recently Lin and colleagues identified a subset of astrocytes that exhibits an enhanced capacity to support synapse formation and demonstrated differential migratory and proliferative properties among different astrocytes [39]. Beyond (and perhaps as a result of) this heterogeneity, astrocytes have fundamental roles in all aspects of physiology, ranging from neurotransmission and synaptogenesis to metabolic support and blood-brain barrier formation [40, 41].

To better understand how astrocytes can exert such a plethora of functions in the brain, it is worth looking at their morphology and distribution. Astrocytes

are star-shaped cells that are present in all brain regions. Their morphology hides a huge complexity both in terms of anatomical appearance and functionality. They are characterized by a central soma, a variable number of principal processes that depart from the soma and a huge number of thin processes, *i.e.* microdomains. Microinjection of hippocampal astrocytes with fluorescent dyes demonstrated that each astrocyte covers a discrete area that is free of processes from adjacent astrocytes. A contact between different astrocytes might occur only at the level of microdomains (Fig. 6A) [42].

Microdomains are also in close contact with the synapses. They enwrap the pre- and postsynaptic neuronal elements, creating a structural and functional entity that represents the information transfer unit of the brain (Fig. 6B) [43]. This special organization leads to the concept of tripartite synapse, in which astrocytes eavesdrop neuronal chatting and actively modulate it. The effects of astrocyte neuromodulation depend firstly on which and where the gliotransmitter targets are located. In the CA1-CA3 hippocampal region, astrocytic glutamate has been reported to potentiate excitatory transmission by

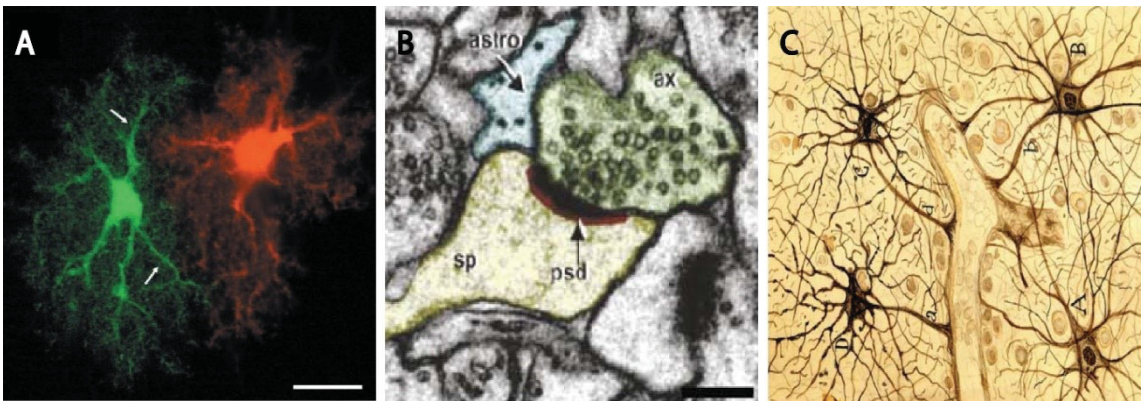

Figure 6. Astrocytic morphology. (A) Astrocytes in the stratum radiatum of CA1 filled with a green fluorescent dye (Alexa 488) and a red fluorescent dye (Alexa 568). Astrocyte territories are non-overlapping, except for peripheral microdomains [42]. **(B)** Electron microscopy image of astrocyte process at the axon-spine interface revealing the presence of tripartite synapse [43]. **(C)** Cajal's drawing showing the contact between astrocytes and blood vessels.

acting on postsynaptic N-methyl-D-aspartate receptors (NMDARs) favouring neuronal synchrony [44, 45]. On the other hand, in the hippocampal dentate gyrus (DG) the same gliotransmitter glutamate can activate presynaptic NMDARs to transiently potentiate excitatory transmission [46]. The astrocytic release of gliotransmitters is also associated to the modulation of long-term potentiation (LTP) and long-term depression (LTD) of synaptic transmission. For instance, astrocytic glutamate mediates a form of spike-timing dependent depression of excitatory transmission in the neocortex [47], as well as a form of mGluR-dependent and NMDA-independent form of LTP in hippocampal CA1 region. This form of plasticity was demonstrated to require the coincidence between postsynaptic activity and astrocyte Ca^{2+} signaling [46]. Noteworthy, the concept of tripartite synapse in the last few years has been updated, also microglial cells seem to be involved in neuron-glia conversation. Beth Stevens proposed the hypothesis of quad-partite synapse, which is based on several findings suggesting that microglia play dynamic roles at developing and mature synapses [48].

Last but not least, it is worth underlining that astrocytes are implicated in neurovascular coupling. As already highlighted in Cajal's drawing, the intraparenchymal vasculature is extensively covered by astrocytic endfeet (Fig. 6C). Astrocytes are part of the neurovascular unit (NVU) and can act as a bridge between neuronal elements and blood vessels. The close contacts of astrocytes with both synapses and blood vessels make astrocytes the ideal cells for preserving the balance between the high energy demand of active neurons and the supply of oxygen and nutrients from the blood by maintaining both resting blood flow and activity-evoked changes in vascular tone [49]. These findings

confirm an active role of astrocytes both in synaptic transmission and neurovascular coupling.

3.2.2 Mechanisms of Ca^{2+} excitability

Astrocytes unlike neurons, are not electrically excitable cells. Their excitability is based on variations of the intracellular Ca^{2+} concentration, therefore astrocytes encode information as Ca^{2+} signals at the cytoplasmic and organelle level. The development of ion-sensitive fluorescent indicators together with the advancement of imaging techniques provided the necessary tools to study astrocytes excitability. In the early 90s, for the first time, Cornell Bell showed that transmitters released from neurons induce transient elevations of astrocytic Ca^{2+} levels [50]. Two main forms of astrocyte excitation are well documented: one is neuron-dependent, thus generated by chemical signals released from neuronal circuits, and the other occurs spontaneously, thus independently of neuronal input [51]. Astrocytes can finely tune the intracellular Ca^{2+} concentrations because they express a huge variety of molecules involved in Ca^{2+} flows, such as metabotropic receptors coupled to intracellular Ca^{2+} stores via G proteins and Ca^{2+} permeable ligand-gated channels. Stimulation of these signalling pathways leads to phospholipase C (PLC) activation and formation of inositol (1,4,5)-triphosphate (IP_3), which increases the intracellular Ca^{2+} concentration through Ca^{2+} release from IP_3-sensitive Ca^{2+} stores and through store-operated Ca^{2+} influx [52, 53]. Ca^{2+} release is a fundamental event in astrocytic physiology, indeed both G_q and G_s G-Protein Coupled Receptors (GPCRs) signaling pathways have been shown to regulate gliotransmitter release [54]. The intracellular Ca^{2+} concentration is re-established to its basal values by the sarco/endoplasmic reticulum Ca^{2+}-ATPase (SERCA) that transports Ca^{2+}

ions from the cytosol into the ER and the plasma membrane Ca^{2+}-ATPase (PMCA) that pumps Ca^{2+} out into the extracellular space. In addition, also the Na^{+}/Ca^{2+} exchanger cooperates to extrude Ca^{2+} outside the cell [55]. Historically, Ca^{2+} signal dynamics and significance have been studied in astrocytic somata. Somatic Ca^{2+} elevations are characterized by slow dynamics (1-10 second timescale) and occur mainly in response to an intense neuronal firing [56]. In 2011, Rusakov concluded that:

> *"In striking contrast to the rapid and highly space- and time-constrained machinery of neuronal spike propagation and synaptic release, astroglia appear slow and imprecise."* [57]

Over the last few years, researchers have focused their attention on Ca^{2+} signaling at the level of astrocytic processes. Indeed, astrocytes enwrap synapses with their tiny processes, thus it is reasonable to hypothesize that synaptic activity is detected by astrocytes at the level of microdomains and that microdomains are crucial for the astrocytic modulatory function. In 2011, two different laboratories demonstrated that physiological synaptic activity is sufficient to activate Ca^{2+} signals in astrocytic processes and that this activation is sufficient for astrocytes to modulate synaptic transmission [58, 59]. The advent of GCaMP-based GECIs allowed to overcome limitations of existing methods, and their use revealed unexpectedly high numbers of localized Ca^{2+} microdomains in entire astrocyte territories, allowing to study the relevance of these Ca^{2+} signals in brain pathophysiology [60]. The possibility to study Ca^{2+} signals at astrocytic microdomains sheds light on the spontaneous activity of astrocytes. At the level of thin astrocytic processes, the spatio-temporal dynamics are completely different with respect to the somatic ones. Indeed, Ca^{2+} events are more frequent and transient compared with somatic activity. The

mechanisms that govern spontaneous astrocytic activity are still under debate (Fig. 7).

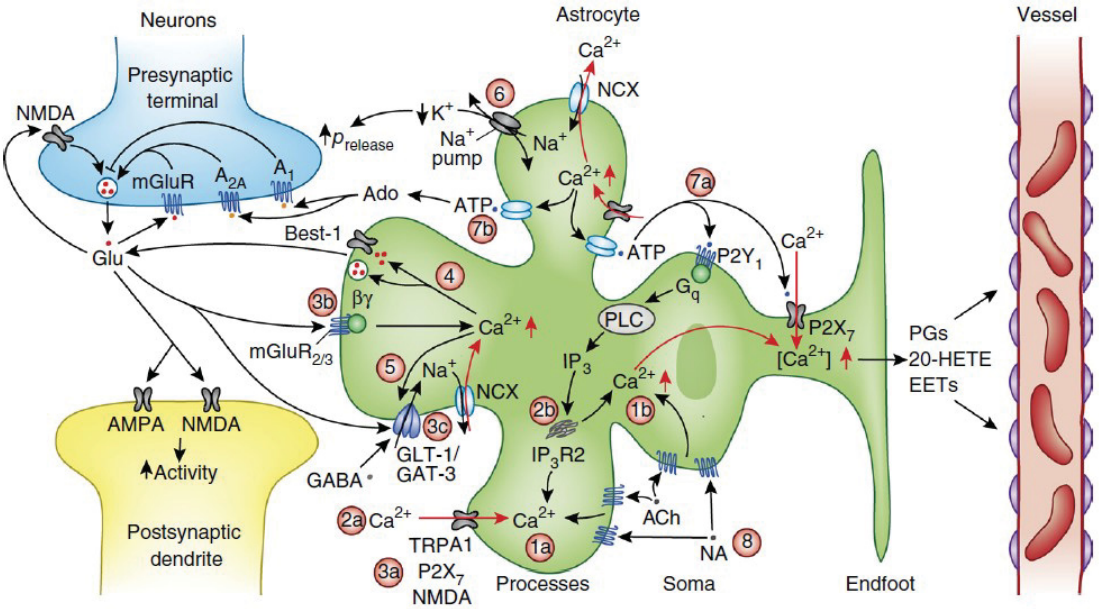

Figure 7. Mechanisms of Ca^{2+} activity at astrocytic thin processes. 1. $[Ca^{2+}]_i$ transients in the processes of astrocytes (1a) differ from those in the soma (1b) in terms of frequency, kinetics and spatial spread. 2. $[Ca^{2+}]_i$ transients in the processes of astrocytes depend roughly equally on Ca^{2+} entry (2a) from the extracellular space through ion channels (40%) and on Ca^{2+} release from intracellular stores (60%), while those in the soma (2b) depend largely (90%) on Ca^{2+} release from the intracellular stores. 3. $[Ca^{2+}]_i$ transients can be generated by Ca^{2+} entry through spontaneously opening TRPA1 channels or neurotransmitter-gated channels (3a), by mGluR2 or mGluR3 (3b), and by neurotransmitter uptake raising $[Na^+]_i$ and reversing Na^+/Ca^{2+} exchange (3c). 4. $[Ca^{2+}]_i$ rises may release transmitters via ion channels as well as via exocytosis. 5. $[Ca^{2+}]_i$ rises alter the surface expression of neurotransmitter transporters. 6. Activation of Na^+/Ca^{2+} exchange by a $[Ca^{2+}]_i$ rise can raise $[Na^+]_i$ and activate the sodium pump, lowering $[K^+]_o$ and hyperpolarizing nearby neurons. This increases the release probability for action potential–driven vesicle release and thus decreases synaptic failure rate. 7. ATP released by a $[Ca^{2+}]_i$ rise may act on P2X or P2Y receptors to raise $[Ca^{2+}]_i$ farther along the cell, propagating a Ca^{2+} wave along the cell (7a), or be converted to adenosine, which acts on presynaptic receptors to increase (A_{2A}) or decrease (A_1) transmitter release (7b). 8. Noradrenaline (NA) released from locus coeruleus neurons and acetylcholine released from nucleus basalis neurons produce large $[Ca^{2+}]_i$ rises in astrocytes. Adapted from [65].

Different works corroborated the idea that spontaneous activity depends mainly on Ca^{2+} influx from the extracellular matrix and it seems to be independent from IP_3 related pathway [61]. In particular, it has been recognized a role in

regulating spontaneous Ca^{2+} activity for transient receptor potential ankyrin 1 (TRPA1) channels, that seem also to regulate D-serine constitutive release and GABA uptake [62, 63]. In 2017, Agarwal and colleagues instead suggested that during periods of high oxidative phosphorylation the "cell-intrinsic" spontaneous Ca^{2+} transients that persist in astrocytic processes reflect stochastic opening of the mitochondrial Permeability Transition Pore (mPTP) [64]. All in all, much work is needed to arrive to a full comprehension of the mechanisms that govern Ca^{2+} signaling in astrocytes. Over the last decades a lot of studies focused their attention on somatic Ca^{2+} signaling unveiling fundamental astrocytic properties in brain function, but now the astrocyte field is focused on the significance of Ca^{2+} signaling at thin processes, thus composing the *third wave*, as it has been defined by Bazargani in 2016 [65]. Indeed, the *first wave* disclosed the role of astrocytes as active players in synaptic transmission, with somatic Ca^{2+} elevations as crucial mediators, while the *second wave* arose doubts about the possibility that the slow Ca^{2+} signals at astrocytic somata could effectively be responsible of astrocytic modulation of synaptic transmission. Nowadays, the *third wave* pointed out the role of Ca^{2+} activity at astrocytic thin processes as possible fast mediator of astrocytic response to synaptic transmission. Astrocytic Ca^{2+} signaling has thus acquired a multi-faceted identity, with a complex spatial-temporal profile ranging from small, local fast responses that can modulate synaptic transmission, to larger, global, albeit slower responses of all astrocytic territories that result from the integration of multiple signals at fine astrocytic processes.

3.2.3 Reactive astrocytes

Pathological conditions such as brain injury, ischemia or exposure to toxic materials (in AD identified as Aβ oligomers, fibrils and plaques) induce the formation of reactive astrocytes. The process, known as astrogliosis, involves a wide range of both molecular and functional changes. Astrogliosis varies from subtle changes to gross morphological alterations, and differs between brain diseases [66]. Non-reactive astrocytes are highly ramified cells with spongiform processes that extend from main processes arising from the soma. In reactive astrocytes the main processes are characterized by hypertrophy and upregulation of different proteins such as Glial Fibrillary Acidic Protein (GFAP) (Fig. 8) and vimentin [67]. Reactive astrocytes release a huge variety of molecules, including neurotrophic factors, inflammatory modulators, chemokines and cytokines. These factors can be either neuroprotective or neurotoxic [66]. Among the neuroprotective signaling pathways, one is related to the signal transducer and activator of transcription 3 (STAT3), indeed astrocyte-specific deletion of STAT3 increases inflammation and tissue damage [68]. In AD, astrocytes undergo differential pathological alterations along the progression of the disease. Reactive astrocytes are found at the site of Aβ deposits in post-mortem human AD brains and in animal models of AD [69-71]. In the early stages of the disease, activated astrocytes have neuroprotective action by internalizing and degrading Aβ, whereas in the later stages amyloid plaque deposits cause astrocytic death [72]. The atrophic changes of astrocytes appear with a different timing in different brain areas. For instance, in the 3xTG-AD mouse model, the entorhinal cortex presents atrophic astrocytes by 1 month of age, but in hippocampus atrophic astrocytes appear only by 6 months [73].

Astroglial atrophy and degeneration most likely lead to a decrease in the astroglial envelope of cerebral vessels and synapses, thus contributing to dysfunctions in the NVU and tripartite synapses. Given the evidences of a fundamental role of astrocytes in brain physiology, in the latest years researchers tried to better classify astrocytic changes when they become reactive.

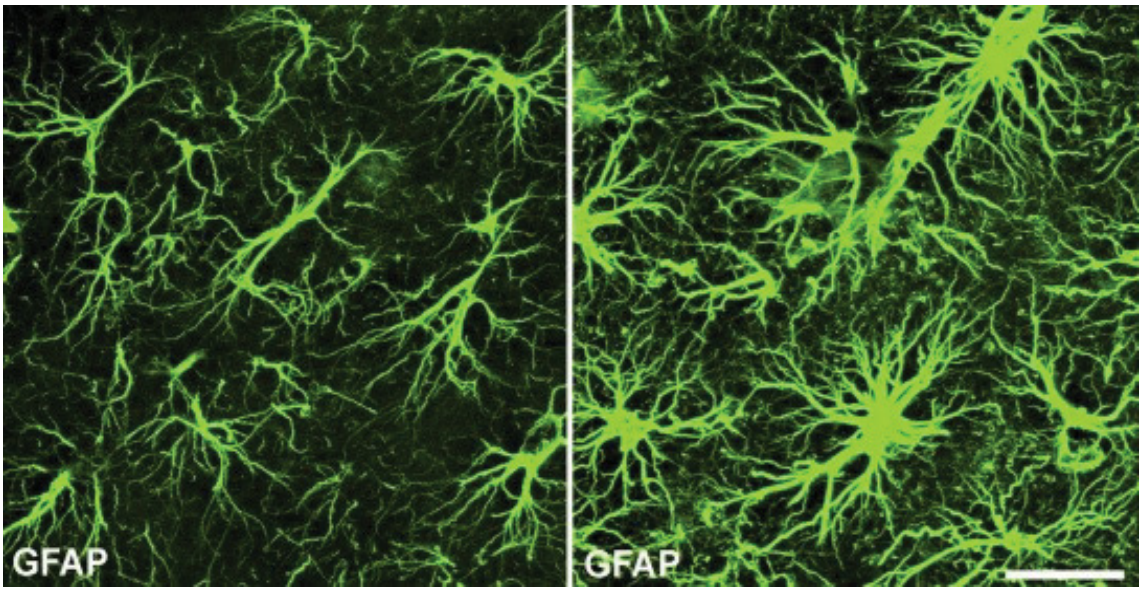

Figure 8. Reactive astrocytes. On the left, non-reactive astrocytes expressing GFAP, which forms bundles of intermediate filaments. On the right, astrocytes expressing GFAP with main processes that show reactive hypertrophy, 4 days after entorhinal cortex lesion. From Wilhelmsson et al. [74]

In 2017 Barres's laboratory classified reactive astrocytes in two main subgroups, A1 and A2. A1 astrocytes are induced by microglia and gain neurotoxic functions, thereby releasing an unidentified neurotoxin that induces neuronal death. A1 astrocytes are also present in human brain tissues of patients affected by AD. On the opposite, A2 astrocytes up-regulate neurotrophic factors, thus they are protective [75]. On the same line, Chun and co-workers investigated the different role of hypertrophic astrocytes in different contexts. Hypertrophy has always been considered a feature of reactive astrocytes, a condition that implies either positive or detrimental effects on neurons and brain functions in

general. Chun and colleagues [76] in their work made a distinction between hypertrophic reactive astrocytes and hypertrophic active astrocytes. More in detail, brain injury that induces hypertrophy in astrocytes is accompanied by increased γ-aminobutyric acid (GABA) expression and GABA tonic release causing an abnormal inhibition of neuronal activity. Astrocytes that show these GABA-related alterations are defined hypertrophic reactive astrocytes. Noteworthy, increase in GABA expression and GABA tonic release are present also in different mouse models of AD [77], and PET studies reported that reactive astrocytes are present in patients at early stages of AD [78]. On the contrary, hypertrophic active astrocytes are characterized by activation in the presence of physiological and environmental beneficial stimulation and show enhanced expression of pro-brain derived neurotrophic factor (BDNF) which, once released, may result in brain plasticity and enhanced cognition [17, 79]. All together these findings claim out the importance of considering astrocytes not as a unique type of cell but as a big category that contains functionally and morphologically different subtypes. Pursuing in studying astrocytes in pathogenic conditions both in terms of protective and neurotoxic roles, thus investigating possible astrocytic multi-faceted roles in brain pathology, could open new possibilities to understand the complex pathogenesis of brain diseases and to reveal new therapeutic targets.

3.3 Calcium and AD

3.3.1 Presenilins and Ca^{2+} homeostasis

PS1 and PS2 were initially recognized for their role in APP processing, as catalytic component of γ-secretase. Their mutations are related to FAD and lead

to an increase in the $A\beta_{42}/A\beta_{40}$ ratio [80]. In addition to APP processing, the PS1 γ-secretase activity is also involved in Notch signaling pathway, however Notch processing is not affected by FAD-linked PS1 mutations. PS1 and PS2 have also independent roles in different processes, not requiring the catalytic activity, such as signal transduction and Ca^{2+} homeostasis [81, 82], and recently it has been recognized a role for PS2 in mediating ER-mitochondria coupling [24, 83]. Presenilins have been reported to function as ER Ca^{2+}-leak channels [84]. These findings were however questioned by different groups [24, 85, 86]. PS1 and PS2 when overexpressed in cell lines are able to alter ER Ca^{2+} handling [87]. To date there has been little agreement on the exact role of presenilins in the context of AD and Ca^{2+} alterations. Indeed, on one side the extensive work of Bezprozvanny led to the "Ca^{2+} overload" hypothesis of AD, sustaining that in the presence of FAD mutations, presenilins lose their Ca^{2+}-leak function leading to abnormal increase of Ca^{2+} in the ER and to increased Ca^{2+} release under IP_3Rs or ryanodine receptors (RyR) stimulation [84]. On the other side, this hypothesis it is not completely accepted. In fact, by using organelle-targeted Ca^{2+} probes, it has been shown that PS2 mutants reduce the ER Ca^{2+} content not only in cell lines but also in neurons from hippocampal brain slices. PS1 mutants have no effect or partially mimic the effects of PS2 mutants [82, 88, 89]. Both PS2 an PS1 mutations, instead, seem to have the same effect on activating RyRs [90, 91].

3.3.2 Astrocytic Ca^{2+} signaling and AD

For a long time, researchers have focused their attention on studying the effect of the different hallmarks of AD on neuronal cells. Aß may damage synapses and kill neurons by a mechanism involving oxidative stress and disruption of

cellular-Ca^{2+} homeostasis [92]. The multi-faceted role of astrocytic Ca^{2+} signaling in brain physiology led to a growing interest of the scientific community on its role in brain diseases. Nowadays, a growing body of literature recognizes the role of astrocytic Ca^{2+} signaling in AD.

The first pioneering work that explored the influence of $A\beta_{42}$ in astrocytic cell cultures has been published in 2003 by Haughey and Mattson [93]. They reported that rat cortical astrocytes exposed to $A\beta_{42}$ showed altered Ca^{2+} wave signaling. Indeed, by using Fura-2 to measure cytosolic Ca^{2+} variations, they showed that Ca^{2+} waves were increased and also the propagation was faster with respect to untreated astrocyte cell cultures. In 2009, Kuchibhotla and co-workers confirmed astrocytic hyperactivity by using multiphoton fluorescence lifetime imaging *in vivo* in the APPswePS1dE9 mouse model of AD. Imaging of cortical astrocytic somata by using Oregon-Green BAPTA1 (OGB) revealed that astrocyte hyperactivity was independent of Aβ plaques proximity and neuronal hyperactivity [94].

Different studies tried to unveil the signaling pathway at the basis of the astrocyte hyperactivity. One of the first hypothesis was related to an involvement of the adenosine triphosphate (ATP)-related pathway. It has been shown that suramin, an antagonist of P2Y receptors, is able to prevent the ability of synthetic Aβ to induce astrocytic Ca^{2+} waves in cell cultures [93]. This hypothesis has been corroborated in the last few years thanks to the *in vivo* work of Petzold's laboratory, in which the role of the P2Y1 receptor has been extensively studied in the SSCx of APPPS1-21 mouse model of AD, that presents a more aggressive form of AD [95]. P2Y1 expression is higher in astrocytes surrounding Aβ plaques as also astrocytic hyperactivity, measured by using OGB. Selective P2Y1 receptor blockade completely normalized astroglial

network dysfunctions [96]. P2Y1 receptor activity is involved in different functions – such as learning and memory [97], inflammation [98], synaptic transmission [99] – that are impaired in AD. Accordingly, chronic treatment with the P2Y1 receptor inhibitor MRS2179 restored synaptic integrity and attenuated cognitive decline without affecting Aβ load and size [100]. Recently, researchers have examined the contribution of TRPA1 channels on astrocytic hyperactivity in APPswePS1dE9 mouse model of AD. It was already known that TRPA1 expression is higher in hippocampal astrocytes of APPswePS1dE9 with respect to wild- type (WT) mice. Ablation of TRPA1 in APPswePS1dE9 mice reduced both behavioural deficits and Aβ deposition [101]. In hippocampal brain slices it has been shown that, after exposure to $A\beta_o$, astrocytic Ca^{2+} activity is higher in both soma and proximal processes and depends on Ca^{2+} influx through TRPA1 channels. The same authors showed that in hippocampal brain slices from APPPS1-21 mouse model, a similar pattern of TRPA1-dependent Ca^{2+} hyperactivity is present at the beginning of $A\beta_o$ accumulation [102].

Overall, overwhelming evidence supports a prominent role of astrocytic Ca^{2+} signaling in AD pathogenesis. In particular, it seems clear that in APPPS1 models astrocytes are characterized by a strong hyperactivity. Astrocytic hyperactivity is related to the *acute phase* of the disease, because it is present together with Aβ plaques. It involves different mechanisms, but the effects of astrocyte altered activity on synaptic plasticity and cognitive functions are still not fully understood. Noteworthy, a large part of these studies has been performed upon cell exposure to synthetic Aβ (see [103] for comments on Aβ toxicity) and only few studies use AD mouse models expressing FAD-linked mutations also in astrocytes (3xTg AD and APPswePS1dE9). Regarding this, a

fundamental aspect that has been neglected is that in AD-patients FAD-linked mutations are present also in astrocytes. How does the astrocytic Ca^{2+} activity change in the presence of a FAD mutation also in astrocytes? Does it always result in astrocyte hyperactivity? Is it mediated by the same signaling pathway?

4. Materials and Methods

4.1 Animal strains

All procedures were conducted in accordance with the Italian and European Communities Council Directive on Animal Care and were approved by the Italian Ministry of Health. Only female mice were used for all the experiments because in the human pathology women are most affected (Alzheimer's Association, 2015; [104]), and PS2APP mice follow this trend [105]. Mice were used at 3 and 6 months of age. C57BL/6J mice were used as WT controls. Instrumental to this project have been three transgenic lines:

1. The single homozygous line expressing PS2-N141I under the prion protein promoter (line PS2.30H) [106] was obtained by embryo revitalization from Charles River Laboratories (Lecco, Italy). We assessed no plaque deposition neither at 3 months nor at 6 months. Cognitive impairments have not been assessed.;

2. The single homozygous line expressing human APP carrying the Swedish mutation under the Thy1 promoter (APPSwe, line BD.AD147.72H) was kindly donated by Hoffmann-La Roche Ltd (Basel Switzerland) [106]. Because of the lack of a mutant presenilin, these mice do not show plaques up to 6 months [107]. They start to

accumulate Aβ at 1 year, with plaque deposition occurring around 18 months (L. Ozmen, personal communication).

3. The double homozygous line expressing the same mutated form of PS2 and the hAPPSwe (PS2APP, line B6.152H) was kindly donated by Hoffmann-La Roche. They present no plaque at 3 months of age, clear amyloid seeding at 6 months and heavy plaque deposition at 10 months. Cognitive impairments have been detected by Morris Water Maze at 8 months [105]. Importantly, PS2APP and APPSwe mice express similar amounts of hAPP [107].

In whisker stimulation experiments we took advantage of CAG-GCaMP3 mice which constitutively express GCaMP3 in different brain cells, mainly in neurons.

4.2 Adeno-associated virus injections

Injections of viral vectors AAV5.GfaABC1D.cyto-tdTomato.SV40 (Penn Vector Core, Addgene 44332) and AAV5.GfaABC1DcytoGCaMP6f.SV40 (Penn Vector Core, Addgene 52925), both carrying the astrocytic promoter GfaABC1D, which induces a sparse expression of the red marker tdTomato and the Ca^{2+} indicator GCaMP6f at the cytosolic level in astrocytes, were performed into the SSCx of P75 or P165 WT, PS2APP, PS2.30H and APPSwe mice. Viral injections were performed under general anesthesia using continuous isoflurane (induction: 4%, maintenance: 1.5%). After inducing anesthesia, mice were injected subcutaneously with Carprofen (5 mg Kg^{-1}) to reduce pain and inflammation following surgery. Depth of anesthesia was assured by monitoring respiration rate, eyelid reflex, vibrissa movements, and reactions to

pinching the tail and toe. Briefly, the skin over the skull was disinfected with Iodopovidone and cut along the sagittal line to expose the bone. Injections of the two viral vectors (60% of the one encoding for GCaMP6f and 40% of the one encoding for tdTomato) were performed after drilling one or two holes (0.5 mm diameter, separated by a distance of 1.5 mm, 1 µl of viral mix into each hole) into the skull over the SSCx (0–1.5 mm posterior to Bregma, 1.5mm lateral to sagittal sinus, and 0.8 mm depth) using a pulled glass pipette in conjunction with a custom-made pressure injection system. Virus injections were performed over a period of 2 to 5 minutes. At the end, the pipette was left in place for 5 more minutes and then gently withdrawn. After injections, the skin was sutured, and mice were revitalized under a heat lamp and returned to their cage. Animals were carefully monitored in the following days for recovery and used for experiments two or three weeks after injections, to give cells enough time to express the fluorescent proteins.

4.3 Brain slice preparation

Coronal SSCx or hippocampal slices of 350 µm were obtained from mice at postnatal days P90-P97 or P180-P187. Animals were anaesthetized with isoflurane and the brain was removed and transferred into an ice-cold artificial cerebrospinal fluid (ACSF, in mM: 125 NaCl, 2.5 KCl, 2 CaCl2, 1 MgCl2, 25 glucose, pH 7.4 with 95% O2 and 5% CO2). Coronal slices were cut with a vibratome (Leica Vibratome VT1000S Mannheim, Germany) in the solution described in [108]. Then, slices were transferred for 1 minute in a solution at room temperature (RT, in mM: 225 D-mannitol, 2.5 KCl, 1.25 NaH2PO4, 26 NaHCO3, 25 glucose, 0.8 CaCl2, 8 MgCl2, 2 kynurenic acid with 95%

O2 and 5% CO2). Finally, slices were transferred in sACSF at 32°C for 20 min and then maintained at RT for the entire experiment.

4.4 Drug applications

Drugs applied to the slice perfusion solution were ATP 100μM (Abcam, Cambridge, UK), Tetrodotoxin (TTX) 1μM (Abcam, Cambridge, UK), Noradrenaline (NA) 10μM (SIGMA Aldrich, Milano, IT).

4.5 Ca^{2+} imaging

To image Ca^{2+} dynamics in GCaMP6f-astrocytes in both *in vivo* and brain slice preparations, we used a two-photon (2P) laser scanning microscope (Multiphoton Imaging System, Scientifica Ltd., UK) equipped with a pulsed IR laser (Chameleon Ultra 2, Coherent, USA) tuned at 920 nm. Power at the sample was kept in the range 5–10 mW to avoid photostimulation and photobleaching. The excitation wavelength used was 920 nm for both GCaMP6f and tdTomato. Images were acquired at 1.53 Hz acquisition frame rate, for 2 minutes in basal conditions or 3 minutes during drug perfusion in brain slices, through a water-immersion objective (Olympus, LUMPlan FI/IR 20×, 1.05 NA). The field of view ranged between 700 × 700 μm and 120 × 120 μm depending on the zoom factor. Ca^{2+} signal recordings were performed in cortical layers II/III in SSCx brain slices or in the CA1 region for hippocampal brain slices. In *in vivo* imaging experiments WT, PS2APP or CAG-GCaMP3 mice were anesthetized with urethane (20% urethane 2 gr Kg^{-1}, ethylcarbamate; SIGMA Aldrich). Animal pinch withdrawal and eyelid reflex were tested to assay the depth of anesthesia. Both eyes were covered with an eye ointment to

prevent corneal desiccation during the experiment and respiration rate, heart rate, and core body temperature were monitored throughout the experiment. The mouse was head-fixed and a craniotomy of 3 mm in diameter was drilled over the SSCx. Craniotomy was covered with a 5 mm diameter coverslip and surrounded by a metal head-post glued to the skull. Mice were mounted under the microscope trough the metal head-post. Imaging was performed in cortical layers II/III (200- 250 μm below the cortical surface) and acquired always at 1.53 Hz. In a subset of experiments performed to investigate astrocytic activity with respect to Aβ plaque proximity mice received an intraperitoneal injection of Methoxy-X04 (5 mg kg^{-1}; 50mM solubilized in DMSO; TOCRIS) 12 h before experiment. Methoxy-X04 was visualized at 920 nm under the 2P microscope.

4.6 Intrinsic optical imaging and whisker stimulation

The specific barrel area activated by single whisker stimulation in the right SSCx was identified by intrinsic optical signal (IOS) imaging through the cranial window (before 2P imaging). A 630 nm led-ring was placed around the objective and images were acquired under 630 nm illumination using a 12-bit CCD camera (Hamamatsu) focused 400 μm below the cortical surface. A single whisker was thread into a needle affixed to a piezo element (Multilayer Piezo Bender Actuator, PI, Milano, IT) and the rostro-caudal whisker stimulus was presented by applying a piezo deflection at 90 Hz for 1s, repeated twice over 20s. The brain region activated by a single whisker deflection was identified by increased light reflection at 630 nm. [109]

4.7 Immunohistochemistry

Three weeks after AAVs injection, mice were deeply anesthetized with Zoletil (30 mg Kg^{-1}) and perfused transcardially with phosphate saline buffer (PBS), followed by 4% PFA in 0.1M PBS, pH 7.4. Brains were PFA fixed overnight, washed and cut in 60-70 μm coronal sections in PBS by vibratome (Leica Vibratome VT1000S). First, floating sections were incubated for 1 h in the Blocking Serum (BS: 1% BSA, 2% goat serum and 1% horse serum in PBS) and 0.2% TritonX-100. Then, primary antibodies were diluted in BS and 0,02% TritonX-100 (16 h at 4°C). Primary antibodies used were: anti-GLT1 antibody (RRID: AB_90949, 1:300 in guinea pig, Millipore AB1783); anti-GFAP (RRID:AB_10013382, 1:300 in rabbit, Dako, Denmark, Z0334); anti β-Amyloid 17-24 (4G8 clone, RRID: AB_2734548 monoclonal in mouse, Biolegend, SanDiego CA, 800712); anti-GFP Alexa Fluo-488 conjugated (RRID: AB_221477, 1:200 rabbit, Invitrogen Thermo Fisher Scientific, A21311). The anti-GFP antibody was used to enhance the GCaMP6f fluorescence which identify infected astrocytes. After washing with PBS, slices were incubated for 2 h at RT with specific secondary antibodies conjugated with Alexa Fluor-488, Alexa Fluor-546 or Cy5 (Invitrogen Thermo Fisher Scientific). Moreover, in 488-546 double staining, nuclei were contrastained by TopRo-3 (1:1000, Invitrogen, Thermo Fisher Scientific). Floating sections were then washed and mounted on glass slides with an Elvanol mounting medium. Negative controls were performed in the absence of the primary antibodies. Immunofluorescence images were obtained with a Leica SP5 confocal microscope with a 20x objective. Single images were taken with an optical thickness of 1 μm and a resolution of 1024x1024. GLT1

immunofluorescence was evaluated on 7 μm z-stacks using an open source ImageJ plugin (GECIquant) and by measuring the Corrected Total Cell Fluorescence (CTCF = Integrated Density – (Total GLT1 ROI Area x Mean Fluorescence of Background)).

4.8 Western Blot analysis

Mouse brains from 6-month-old WT and PS2APP mice were rapidly frozen in liquid nitrogen, minced by cryostat sectioning at -25°C and dissolved in lysis buffer (in mM: 250 sucrose, 10 KCl, 1.5$MgCl_2$ 1EDTA, 1 EGTA, 20 HEPES pH 7.5, 0.2% SDS) [110] supplemented with protease inhibitor cocktail (Sigma-Aldrich). In particular, 25 cortical slices of 40 μm were cut and dissolved in 150 μl of lysis buffer; they were vortex and then centrifugated at 14,000 rpm at 4°C for 10 min; supernatants were collected. Protein concentration was evaluated by the BCA method (Pierce BCA Protein Assay kit, # 23227 Thermo Fisher Scientific). Protein samples were treated with 2x sample buffer (20% glycerol, 1mM DTT, 4% SDS, 0.001% bromophenol blue and 125mM Tris-HCl, pH 6.8) for 10 min at 70°C before loading 20 μg onto 4-12% precast gels (Invitrogen, Thermo Fisher Scientific). For immunoblotting proteins were transferred onto nitrocellulose membrane (Aurogene #11306-41BL) using a wet Invitrogen Trans-Blot equipment (90 min at 400 mA, in ice bath) with transfer buffer (192 mM glycine, 25 mM Tris-HCl pH 8.3 and 20% methanol). After AdvanStain-Ponceau staining (Advansta # R-03021-D50), membranes were blocked in 5% (w/v) milk in T-TBS buffer (150 mM NaCl, 50 mM Tris-HCl pH 7.4, 0.5% Tween20). Filters were then incubated overnight with the guinea-pig antibody anti-GLT1 (1:1000, Millipore Merk) and proteins were visualized with peroxidase-conjugated secondary antibody (1:20,000, Jackson

ImmunoResearch Europe Ltd., Cambridge, UK)) using Clarity Western ECL Substrate (Biorad #1705061) in a UVITEC Mini HD9 system (Cambridge, UK).

4.9 Data Analysis

Detection of astrocyte Region Of Interests (ROIs) displaying Ca^{2+} elevations was performed with ImageJ in a semi-automated manner using the GECIquant plugin [111]. The software was used to identify ROIs corresponding first to the soma (> 30 μm^2; confirmed by visual inspection), then to the proximal processes (> 20 μm^2 and not corresponding to the soma) and finally to the microdomains (between 2 and 20 μm^2 corresponding to neither the soma nor the proximal processes). All pixels within each ROI were averaged to give a single time course of fluorescence values, F(t). Analysis of Ca^{2+} signals was performed with ImageJ (NIH) and a custom software developed in MATLAB 7.6.0 R2008 A (Mathworks, Natick, MA, USA) [112]. To compare relative changes in fluorescence between different cells, we expressed the Ca^{2+} signal for each ROI as $\Delta F/F_0 = (F(t) - F_0)/(F_0)$. F_0 was defined as the 15^{th} percentile of the whole fluorescent trace for each ROI and considered as a global baseline. For each ROI we then defined as baseline trace the points of the $\Delta F/F_0$ trace with absolute values smaller than twice the standard deviation of the overall signal. Significant Ca^{2+} events were then selected with a supervised algorithm as follows. Firstly, a new standard deviation was calculated on the baseline trace, and all local maxima with absolute values exceeding twice this new standard deviation were identified. Secondly, among these events, we considered significant only those associated with local Ca^{2+} dynamics with amplitude larger than fourfold the new standard deviation. The amplitude of each Ca^{2+} event was measured from the

20^{th} percentile of the fluorescent trace interposed between its maximum and the previous significant one. Essentially, this procedure combines a threshold measured from the global baseline with a stricter threshold computed from a local baseline. We adopted this method to reduce artefacts from the recording noise superimposed on the slow astrocytic dynamics and from slow changes in baseline due to physiological or imaging drifts. All Ca^{2+} traces were visually inspected to exclude the ROIs dominated by noise. In the analysis of spontaneous microdomain activity, for each astrocyte we calculated the number of active ROIs, defined as the ROIs displaying at least one significant Ca^{2+} event, the frequency, *i.e.* the total number of Ca^{2+} events per minute and the mean amplitude of the Ca^{2+} events. For each parameter, we then calculated the mean value among all analyzed astrocytes. In the analysis of evoked responses, for each astrocyte we calculated the amplitude of the Ca^{2+} response for soma and the mean amplitude for its proximal processes and microdomains, the mean percentage of responsive proximal processes and the number of active microdomains. We then calculated the percentage of responsive somata and for the other parameters, *i.e.* amplitude, percentage of proximal processes and number of active microdomains, the mean value among all analyzed astrocytes.

4.10 Statistical analysis

Data were tested for normality before statistical analysis, by using Shapiro-Wilk test. For the amplitude, the number of ROIs and the frequency of astrocytic Ca^{2+} events, paired Student's *t*-test was applied on normally distributed data sets and Mann-Whitney test on data sets that were not normally distributed. For comparison between percentages we used Fisher's exact test. Correlation index were computed by using Pearson's (on normal data distribution) and

Spearman's (on non-normal data distribution) correlation coefficient. All results are presented as mean ± SEM. Results were considered statistically significant at $p \leq 0.05$. * $p \leq 0.05$, ** $p \leq 0.01$, *** $p \leq 0.001$.

5. Results

5.1 Astrocytic Ca^{2+} activity in PS2APP mice

To characterize astrocytic activity during the progression of AD, we performed experiments in 3-month-old and 6-month-old PS2APP mice, before and after the appearance of Aβ plaques respectively.

Astrocytic Ca^{2+} signals were evaluated in WT and PS2APP mice, after Adeno-Associated Virus (AAV) injections which induce in astrocytes the selective expression of cytosolic GCaMP6f and tdTomato. Given that GCaMP6f is not fluorescent under basal conditions, injection of tdTomato is performed to help the identification of the infected area and the visualization of infected astrocytes (Fig. 9A). Two weeks after injections, 2P laser-scanning microscopy was used for Ca^{2+} imaging experiments in SSCx brain slices. We studied Ca^{2+} signals in all astrocytic compartments, i.e. soma, proximal and thin processes. All the experiments reported below were performed in ACSF (in mM: 125 NaCl, 2.5 KCl, 2 CaCl2, 1 MgCl2, 25 glucose, pH 7.4 with 95% O2 and 5% CO2 at RT) and in the presence of TTX (1 μM) to block voltage-gated Na^{+} channels thus avoiding the contribution of activity-dependent neuronal signaling.

5.1.1 The amplitude of spontaneous Ca^{2+} microdomain activity is increased in 3-month-old PS2APP mice

We were interested to possible differences in the spontaneous activity of astrocytes from the SSCx of WT and PS2APP mice. We observed a weak spontaneous activity at the level of soma and proximal processes in both WT and PS2APP mice. We then focused our attention on the Ca^{2+} elevations associated to the thin astrocytic processes, the so-called Ca^{2+} microdomains.

These events are spatially confined, often recurrent and exhibit a shorter duration with respect to the global Ca^{2+} signals involving also the thick processes and somata that are typically triggered by GPCRs activation. Examples of Ca^{2+} microdomain activity are represented in Fig. 9.

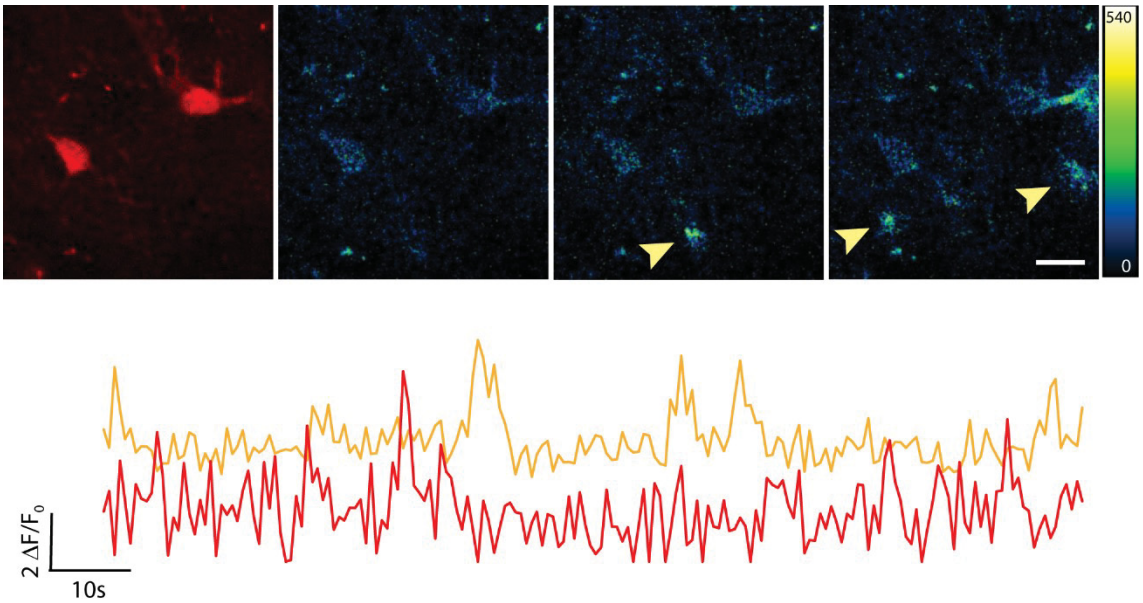

Figure 9. 2P images of tdTomato and GCaMP6f co-infected astrocytes displaying spontaneous Ca^{2+} activity in thin processes. First picture on the left represents the tdTomato signal, whereas the other pictures represent GCaMP6f signal. Arrowheads indicate microdomains of Ca^{2+} elevations while representative traces are shown below. Pseudocolor bar shows LUT applied. Kinetics are reported as $\Delta F/F_0$. Acquisition frame rate is 1.53 Hz. Scale bar, 10 μm.

To quantify spontaneous microdomain activity, in light of the above mentioned features, we measured three different parameters, *i.e.* amplitude, number of active ROIs, and frequency: i) the amplitude of a microdomain represents its change in fluorescence intensity and it is measured as $\Delta F/F_0$; ii) the number of active ROIs, *i.e.* ROIs displaying at least one significant Ca^{2+} event, gives us an indication about the active portion of the astrocyte and iii) the frequency expresses the total number of Ca^{2+} events per minute per astrocyte. Astrocytic Ca^{2+} dynamics at the level of microdomains are frequently characterized by a low signal-to-noise ratio (Fig. 10B), that requires a multistep analysis extensively

explained in the Material and Methods section of this thesis. This analysis revealed that microdomain Ca^{2+} activity shows a significant increase in terms of amplitude in PS2APP with respect to WT mice ($p < 0.05$, Student's *t*-test) (Fig. 10C). Noteworthy, the other two parameters that we analysed, *i.e.* the number of active ROIs and the event frequency, are unchanged in PS2APP mice (Fig. 10D, E).

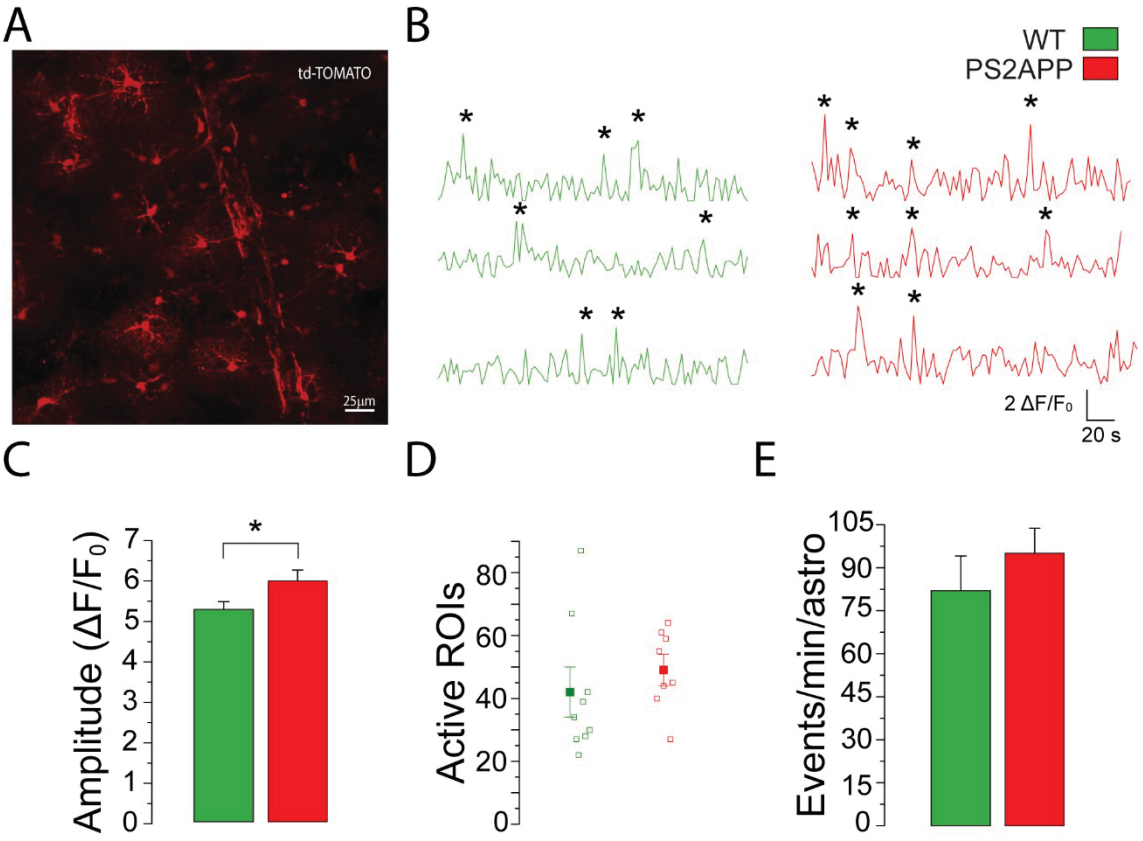

Figure 10. Spontaneous astrocytic microdomain activity in SSCx slices from 3-month-old WT and PS2APP mice. (A) Z-projection of td-Tomato infected astrocytes from the SSCx, scale bar 25 µm. **(B)** Representative traces of microdomain activity from different astrocytes (WT astrocytes, green traces; PS2APP astrocytes, red traces). Asterisks mark significant Ca^{2+} events. **(C, D, E)** Quantification of spontaneous microdomain Ca^{2+} activity in WT (green) and PS2APP (red) mice at 3 months of age (9 astrocytes from 5 WT mice and 8 astrocytes from 5 PS2APP mice). **(C)** Bar histogram reporting the mean amplitude in terms of variation of fluorescence intensity expressed as $\Delta F/F_0$ (mean ± SEM, *$p < 0.05$, Student's *t*-test). **(D)** Scatter plot reporting both the average number of active ROIs (mean ± SEM) for WT and PS2APP astrocytes (full squares) and the number of active ROIs for each single astrocyte (empty squares). **(E)** Bar histogram reporting the mean frequency (mean ± SEM) of microdomain Ca^{2+} activity measured as the total number of events per minute per astrocyte.

5.1.2 Evoked astrocytic Ca^{2+} activity is unchanged in 3-month-old PS2APP mice

To further define the astrocyte Ca^{2+} signaling in 3-month-old PS2APP mice, we studied the Ca^{2+} response to purinergic signaling. This is an important signaling pathway in brain circuits and the release of ATP from both neurons and astrocytes is involved in the modulation of many physiological processes. Furthermore, dysregulations of purinergic signaling have also been suggested to contribute to a variety of brain disorders including AD [113]. To verify whether Ca^{2+} elevations evoked in astrocytes by purinergic signaling are altered in AD, we bath-applied ATP (100 μM), in the presence of TTX (1 μM), and evaluated the amplitude of the Ca^{2+} response – at soma, proximal and thin processes – the number of active ROIs, the mean percentage of active proximal processes and the percentage of active somata. We found no significant differences in 3-month-old PS2APP compared to WT mice (Fig. 11).

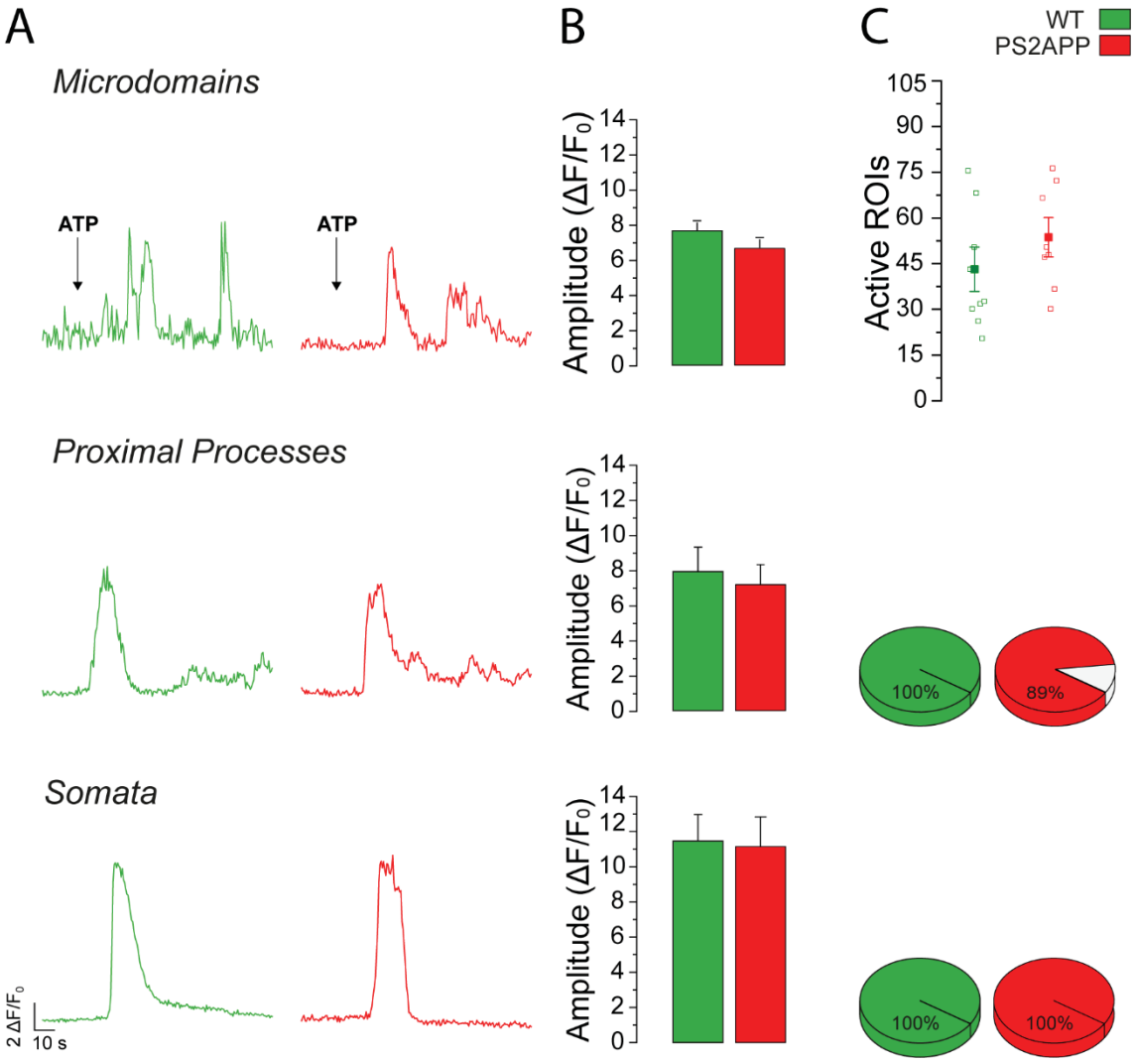

Figure 11. Evoked astrocytic activity in 3-month-old WT and PS2APP mice. Quantification of ATP-evoked Ca^{2+} activity at microdomains, proximal processes and somata from WT (green) and PS2APP (red) mice (8 astrocytes from 5 WT mice and 8 astrocytes from 5 PS2APP mice). **(A)** Representative traces of astrocytic ATP response in the different compartments (WT astrocytes, green traces; PS2APP astrocytes, red traces). **(B)** Bar histograms reporting the Ca^{2+} variation in terms of fluorescence intensity reported as $\Delta F/F_0$. **C)** On the top, scatter plot reporting both the mean values ± S.E.M. of active ROIs for WT and PS2APP astrocytes (full circles) and the number of active ROIs for each single astrocyte (empty circles); in the middle 3D-pie charts reporting the mean percentage of responsive proximal processes, WT (green) and PS2APP (red) mice, respectively, and unresponsive proximal processes (white); on the bottom 3D-pie charts reporting the percentage of responsive somata.

5.1.3 Spontaneous microdomain activity is reduced in 6-month-old PS2APP mice

We also characterized the spontaneous Ca^{2+} activity in astrocytes from 6-month-old mice. In the PS2APP mouse model this time-point corresponds to the onset of plaque deposition. We found that the amplitude of Ca^{2+} microdomains – that was increased in 3-month-old PS2APP mice – is reduced ($p < 0.05$, Student's *t*-test; Fig.12A). We also observed a statistically significant reduction in both the number of active ROIs ($p < 0.01$, Student's *t*-test) and the Ca^{2+} event frequency ($p < 0.05$, Student's *t*-test).

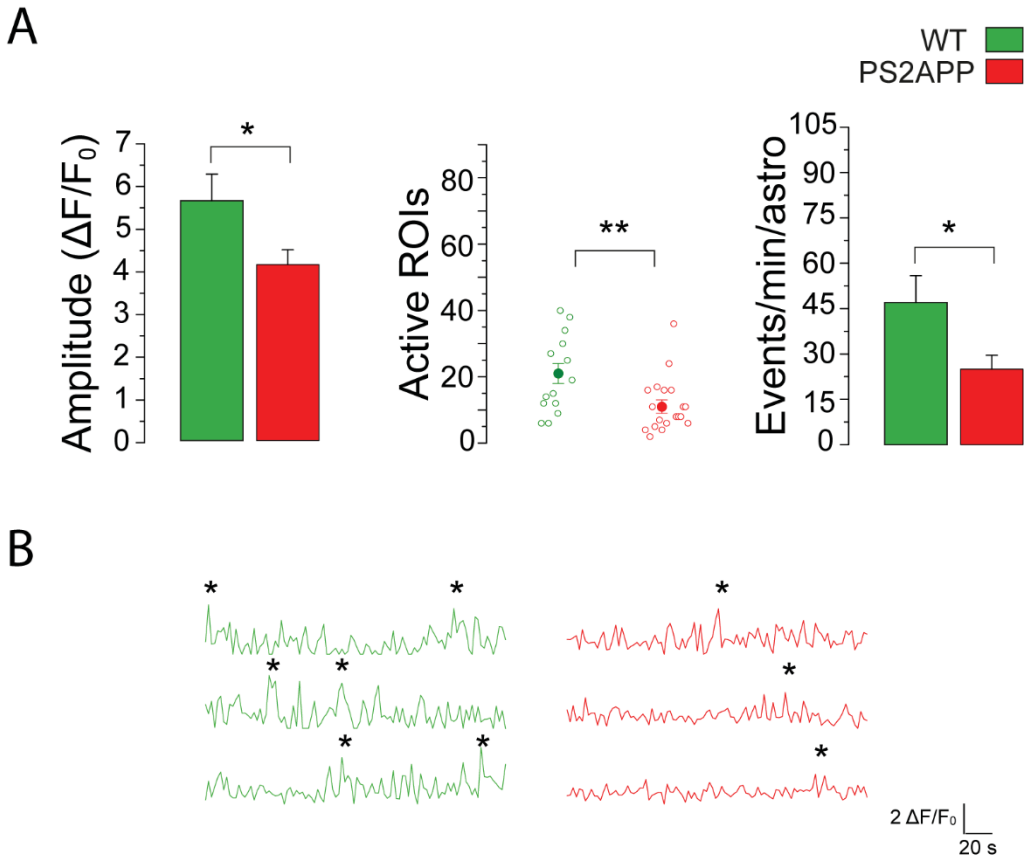

Figure 12. Spontaneous astrocytic activity in 6-month-old WT and PS2APP mice. (A) Quantification of spontaneous microdomain activity in WT (green) and PS2APP (red) mice at 6 months of age (14 astrocytes from 6 WT mice and 21 astrocytes from 7 PS2APP mice). Left panel: *p < 0.05 Student's *t*-test. Middle and right panel: **p < 0.01 and *p < 0.05 Mann-Whitney test. **(B)** Representative traces of microdomain activity from WT astrocytes, green traces and PS2APP astrocytes, red traces. Asterisks mark significant Ca^{2+} events.

Noteworthy, in WT control mice the number of active ROIs and the Ca^{2+} event frequency is also reduced in 6 with respect to 3-month-old mice, indicating that with increasing age the spontaneous activity in astrocytes decreases.

5.1.4 Evoked astrocytic Ca^{2+} activity is reduced in 6-month-old PS2APP mice

In WT mice, all astrocytes respond to ATP challenge (100 μM) with large amplitude Ca^{2+} elevations at soma, proximal processes and microdomains (Fig. 13A, B). In contrast, in PS2APP mice about 40% of the astrocytes respond to ATP at all compartments, with significantly reduced Ca^{2+} elevations ($p < 0.001$ Student's *t*-test). Furthermore, the mean number of active ROIs was also reduced and 60% of the astrocytes were totally unresponsive (Fig. 13C). The overall Ca^{2+} responsiveness of astrocytes is therefore, dramatically impaired in PS2APP mice.

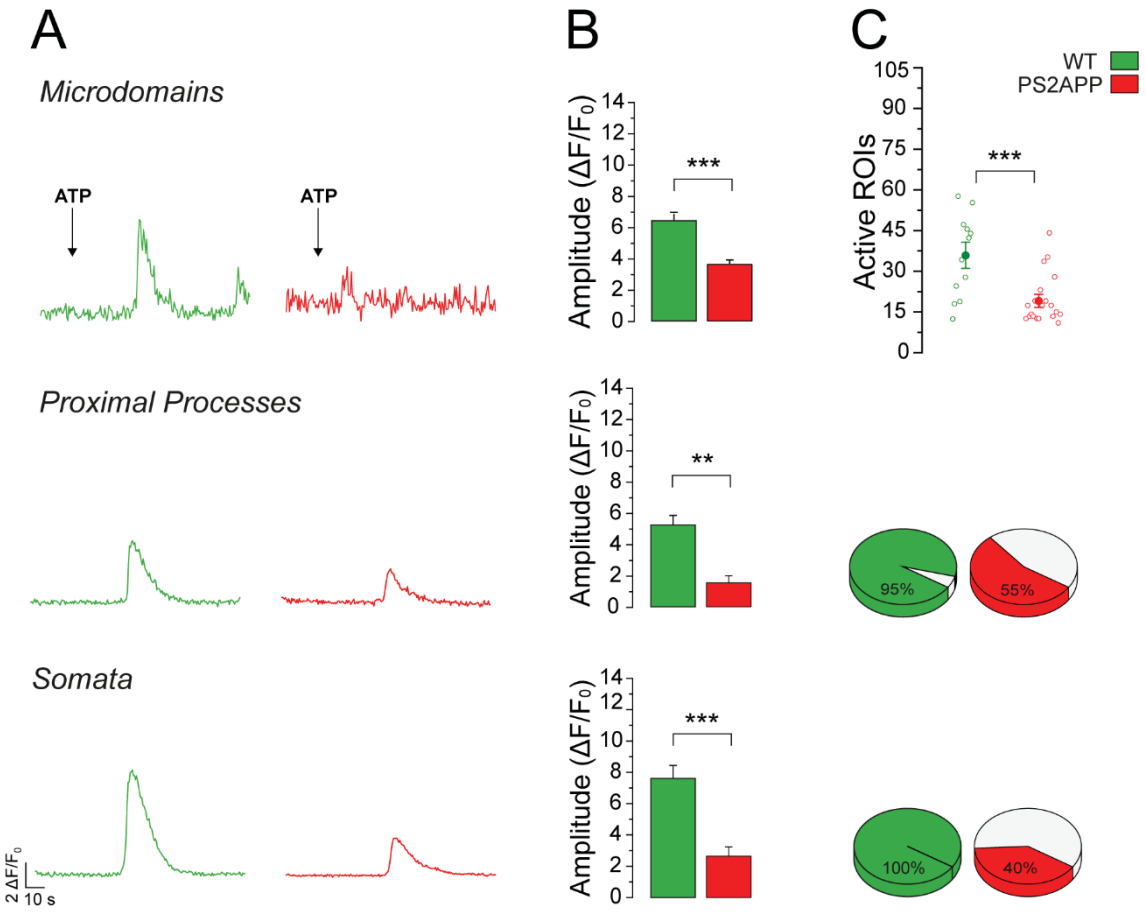

Figure 13. Evoked astrocytic activity in 6-month-old WT and PS2APP mice. Quantification of ATP-evoked Ca^{2+} activity at microdomains, proximal processes and somata from WT (green) and PS2APP (red) mice (14 astrocytes from 6 WT mice and 21 astrocytes from 7 PS2APP mice). **(A)** Representative traces of astrocytic ATP response in the different compartments (WT astrocytes, green traces; PS2APP astrocytes, red traces). **(B)** Bar histograms reporting the Ca^{2+} variation in terms of fluorescence intensity reported as $\Delta F/F_0$, Upper and bottom panel: ***p < 0.001, Student's *t*-test. Middle panel: ** p < 0.01, Mann-Whitney test. **(C)** On the top, scatter plot reporting both the mean values ± S.E.M. of active ROIs for WT and PS2APP astrocytes (full circles) and the number of active ROIs for each single astrocyte (empty circles); in the middle 3D-pie charts reporting the mean percentage of responsive proximal processes, WT (green) and PS2APP (red) mice, respectively, and unresponsive proximal processes (white), ***p < 0.001, Mann-Whitney test; on the bottom 3D-pie charts reporting the percentage of responsive somata, ***p < 0.001 Fisher's exact test.

5.2 Expression of APP or PS2 mutants alone is insufficient to fully replicate astrocytic Ca^{2+} defects

As described in the Material and Methods section of this thesis, the PS2APP mouse model expresses the FAD-linked mutated forms of the human PS2 (PS2-N141I) and the APP carrying the Swedish mutation (APPSwe). To verify whether the alterations present in PS2APP mice were specifically due to one of the two mutants, we took advantage of two single homozygous transgenic lines that express either the PS2 mutant (line PS2.30H) or the APP mutant (APPSwe, line BD.AD147.72H) alone, under the same promoters used for PS2APP mice. In PS2.30H mice, we failed to detect Aβ plaques in SSCx at 6 months of age [107], this is compatible with the fact that murine APP is much less amyloidogenic than human APP. On the other hand, because of the lack of a mutant presenilin and despite the expression of similar amounts of human APP as PS2APP mice, APPSwe mice start to accumulate Aβ at one year of age, with plaque deposition occurring at around 18 months (L. Ozmen, personal communication). Of note, APPSwe and PS2APP mice express similar amounts of hAPP [107].

We carried out experiments in SSCx brain slices of 6-month-old PS2.30H and APPSwe mice and evaluated both spontaneous and evoked activity. No significant differences are present in spontaneous microdomain activity, between the two single transgenic lines compared to WT mice (Fig. 14), although a tendency to a reduction in the microdomain mean frequency is present.

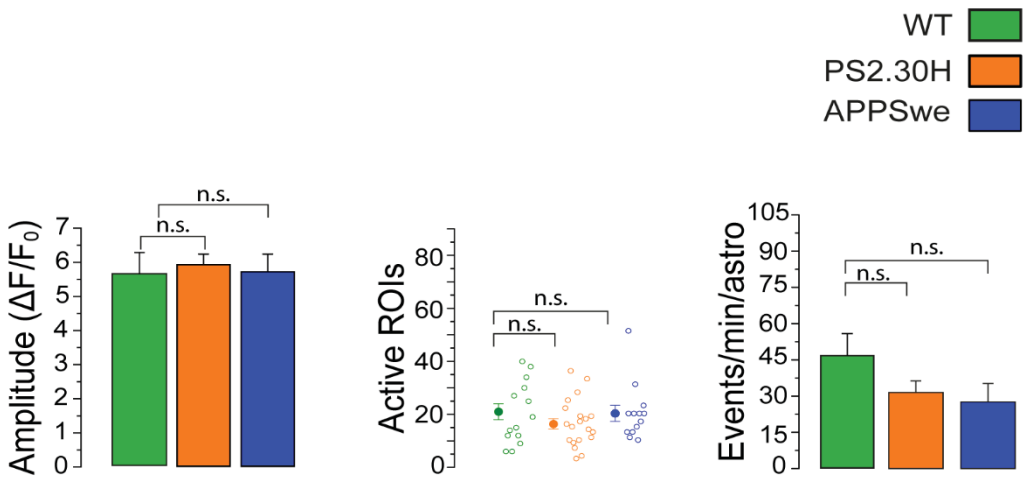

Figure 14. Spontaneous astrocytic activity in 6-month-old WT, PS230.H and APPSwe mice. Quantification of spontaneous microdomain activity in WT (green), PS2.30H (orange) and APPSwe (blue) mice (14 astrocytes from 6 WT mice, 19 astrocytes from 6 PS2.30H mice and 10 astrocytes from 3 APPSwe mice).

As regards the ATP challenge, the amplitude of the response at all compartments was unchanged, but a reduction, albeit not statistically significant, in the microdomain response is present. The percentage of responsive astrocytes also shows a clear tendency to reduction (Fig. 15). We suggest that the expression of PS2 or APP mutants alone is insufficient to cause the full spectrum of astrocytic Ca^{2+} defects.

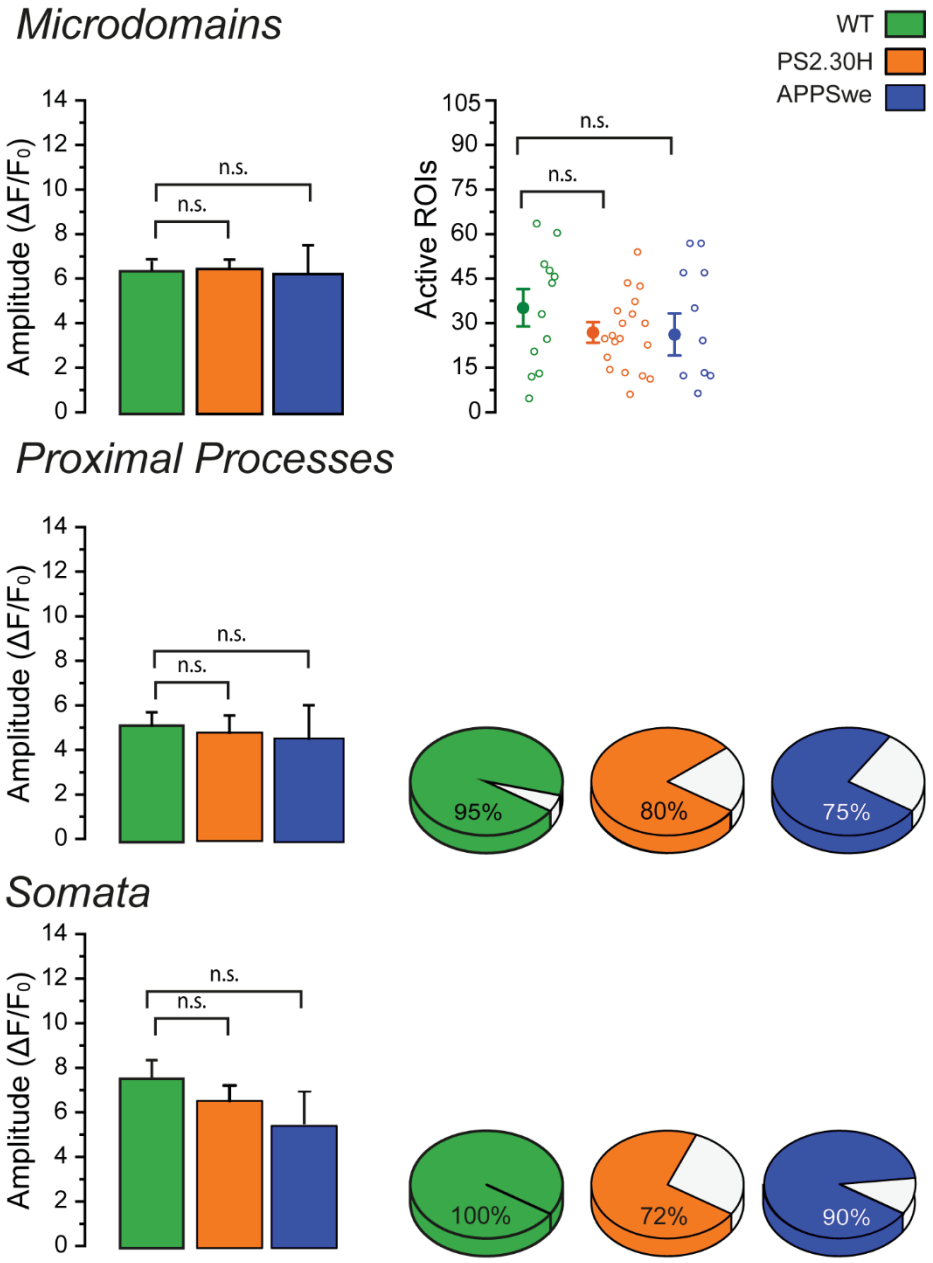

Figure 15. Evoked astrocytic activity in 6-month-old WT, PS2.30H and APPSwe mice. Quantification of ATP-evoked Ca^{2+} activity in all astrocytic compartments: microdomains, proximal processes and somata from WT (green) and PS2.30H (orange) and APPSwe (blue) mice (14 astrocytes from 6 WT mice, 19 astrocytes from 6 PS2.30H mice and 10 astrocytes from 3 APPSwe mice).

5.3 Astrocytic Ca^{2+} alterations are not restricted to purinergic receptor stimulation

The data described above indicate that the co-expression of PS2 and APP mutants, as in the PS2APP model, is required for the astrocytic Ca^{2+} alterations that are observed during AD progression in the PS2APP model. We next asked whether the drastic reduction in the evoked ATP response, that we highlighted in astrocytes from PS2AAP mice, is restricted to purinergic signaling or it rather represents a general mechanism. We thus hypothesized that this dysregulation of astrocytic Ca^{2+} signals is due to a marked reduction in store Ca^{2+} content. To obtain an indirect measurement of ER Ca^{2+} content, we challenged astrocytes with cyclopiazonic acid (CPA, 50µM), an inhibitor of the ER Ca^{2+}-ATPase. Unfortunately, upon CPA perfusion, we failed to observe in both WT (Fig.16) and PS2APP mice, the typical changes of intracellular Ca^{2+} following Ca^{2+} release from the ER.

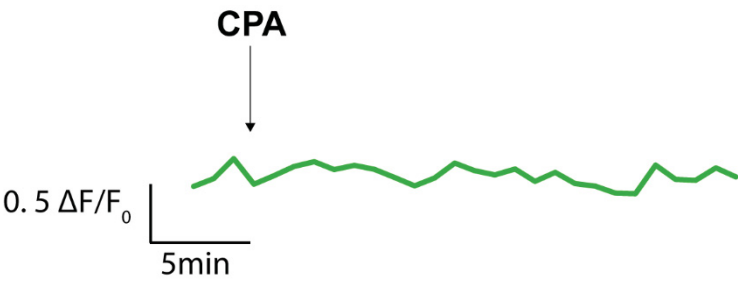

Figure 16. Representative Ca^{2+} trace of typical astrocytic kinetics observed in somata upon CPA perfusion of a slice from a 6-month-old WT mouse.

This failure could be due to a poor penetration of CPA in brain slices of adult mice that are enriched of myelinated fibers with respect to those obtained from juvenile mice. As a consequence, Ca^{2+} ions are slowly released from ER and probably immediately extruded from the astrocytes through plasmalemmal pumps, thus hampering the detection of possible differences between ER Ca^{2+} content in WT and AD mice. Noteworthy, even though we failed to detect

proper cytosolic Ca^{2+} kinetics, the ATP response of astrocytes is abrogated after the CPA treatment, suggesting that the prolonged CPA treatment was efficient. To obtain an alternative indication that the defective Ca^{2+} signaling in astrocytes from PS2APP mice was due to a more general mechanism, we employed another IP3-generating agonist to increase astrocytic Ca^{2+} concentration. It was previously shown that NA promotes a near synchronous Ca^{2+} rise at the level of microdomains, which then results in a global Ca^{2+} response [64]. Experiments in SSCx slice preparations from PS2APP mice with NA (10 µM) were thus conducted in the presence of TTX (1 µM). As observed with ATP stimulation, the response to NA is drastically impaired in PS2APP mice both in terms of amplitude in all astrocytic compartments and percentage of responsive astrocytes (Fig. 17).

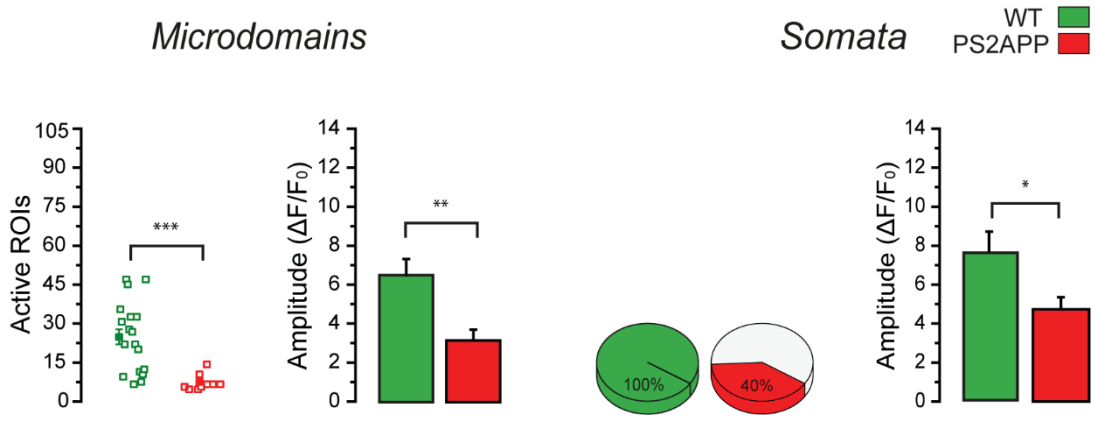

Figure 17. Evoked astrocytic Ca^{2+} activity upon NA perfusion in 6-month-old WT and PS2APP mice. Quantification of NA-evoked Ca^{2+} activity in microdomains and somata from WT (green) and PS2APP (red) mice (15 astrocytes from 3 WT mice, 25 astrocytes from 5 PS2APP mice). For microdomains: ***p < 0.001 Mann-Whitney test, **p < 0.01 Student's *t*-test. For somata: 3D pie-charts, ***p < 0.001 Fisher's exact test; bar histogram, *p < 0.05 Mann-Whitney test.

Given that both NA and ATP responses mainly involve ER Ca^{2+} release, the reduced response can be reasonably caused by either a significant decrease of the ER Ca^{2+} content or a reduced IP_3-R sensitivity. Of note, this impaired Ca^{2+} response requires the co-expression of APPSwe and PS2-N141I and it is timely

defined as it occurs at 6 months of age in concomitance with the surge of $A\beta_{42}$ production, the appearance of Aβ plaques and gliosis in PS2APP mice [107].

5.4 Astrocytic hypoactivity is overall independent of Aβ plaque proximity

Once understood that major astrocytic Ca^{2+} defects are present only in 6-month-old PS2APP mice and that these alterations are reasonably related to a general mechanism involving the IP_3-mediated signaling pathway, we wondered whether astrocytic hypoactivity is also influenced from the proximity to Aβ plaques. Aβ plaque deposition appears in PS2APP mice at 6 months of age [107], therefore we investigated whether Aβ plaques appear at the same time-point in SSCx. We assessed Aβ plaque presence through immunohistochemical analysis by using an anti-Aβ antibody (4G8) that recognizes both Aβ deposition and also intracellular APP accumulation. We found that plaques are clearly detectable also in the SSCx of in 6-month-old PS2APP mice (Fig. 18), suggesting a possible link between astrocytic Ca^{2+} defects and Aβ plaque proximity. Noteworthy, Aβ plaque deposition is associated to an increase in GFAP expression in astrocytes nearby plaques, suggesting that the presence of Aβ plaques causes astrocytic reactivity. Interestingly, astrocytic processes come in close contact also with the plaques as showed in Fig. 18C.

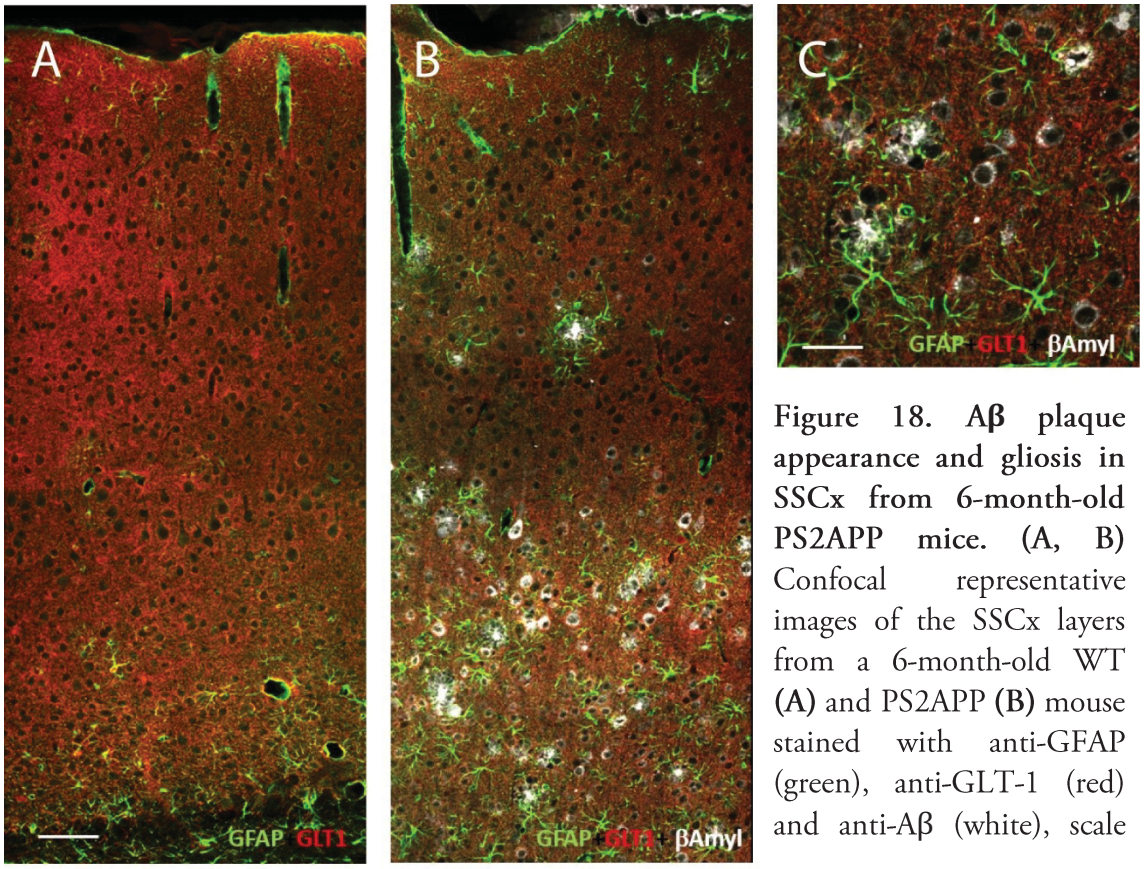

Figure 18. Aβ plaque appearance and gliosis in SSCx from 6-month-old PS2APP mice. (A, B) Confocal representative images of the SSCx layers from a 6-month-old WT **(A)** and PS2APP **(B)** mouse stained with anti-GFAP (green), anti-GLT-1 (red) and anti-Aβ (white), scale bar 75 μm **(C)** Higher magnification image of the SSCx from a 6-month-old PS2APP mouse stained with anti-GFAP (green), anti-GLT1 (red) and anti-Aβ (white), scale bar 32 μm.

To verify in PS2APP mice whether and how astrocytic Ca^{2+} alterations are related to Aβ plaque proximity, 6-month-old PS2APP mice were *i.p.* injected with the Aβ plaque marker methoxy-X04 12 hours before Ca^{2+} imaging experiments. In the analysis, we firstly visualized Aβ plaques and subsequently dichotomized astrocytes in less and more distant than 50 μm from methoxy-X04-positive plaques, as previously described [94, 96] (Fig.19A). Noteworthy, since in brain slices somatic spontaneous activity is almost absent in both WT and AD mice, we essentially evaluated the Ca^{2+} microdomain activity with respect to Aβ plaque proximity. As shown in Fig. 19B, by applying Pearson's correlation analysis we found a negative correlation between the frequency of Ca^{2+} events and the distance from Aβ plaques and a positive correlation when the amplitude of Ca^{2+} events was considered. Therefore, to clarify better if these

differences were statistically significant, we used the Student's *t*-test to quantitively evaluate the difference in two groups of astrocytes, *i.e.* within or outside a distance of 50µm from the border of the plaque, and no statistically significant differences were found (Fig.19C).

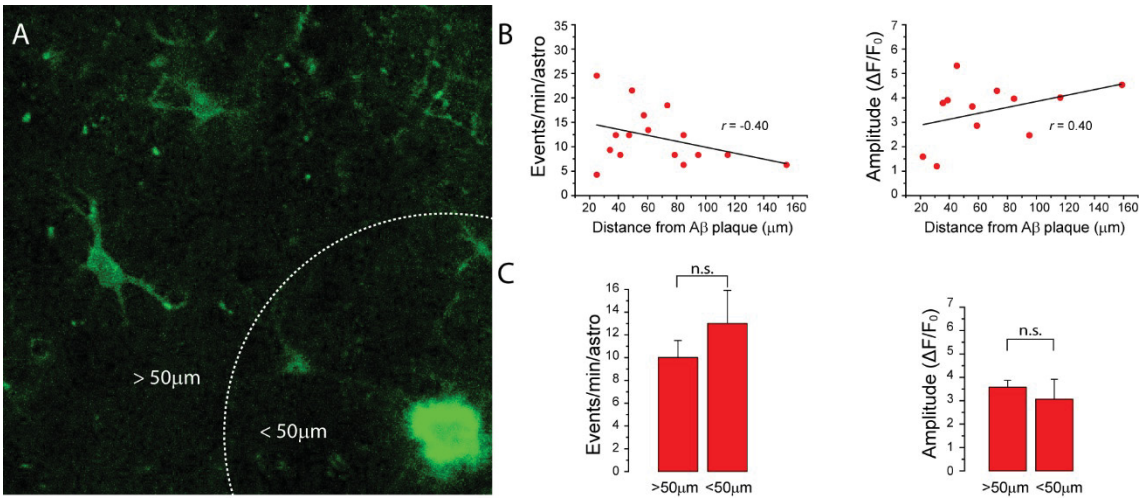

Figure 19. Spontaneous microdomain Ca^{2+} activity in 6-month-old PS2APP mice with respect to Aβ plaque proximity. (A) 2P representative image with an Aβ plaque marked with methoxy-X04 on the right corner. The dashed line divide astrocytes located within or above 50 µm from the plaque. **(B)** Raster plots showing the results of Person's correlation analysis. Left, the frequency of microdomain Ca^{2+} activity shows a negative correlation with respect to Aβ plaque proximity (r = -0.40). Right, the amplitude of microdomain Ca^{2+} activity shows a positive correlation with respect to Aβ plaque proximity. **(C)** Bar histograms reporting the results of Student's *t*-test analysis. Astrocytes that are within (n = 8) or above (n = 8) 50 µm from Aβ plaques exhibit similar Ca^{2+} activity in terms of both frequency (left) and amplitude (right) (N=4 PS2APP mice).

The evoked responses were also not significantly different between the two groups using the Student's *t*-test (data not shown). However, similarly to the spontaneous activity, the correlation analysis between the amplitude of the evoked response and the distance of the responsive astrocytes from plaques revealed a negative correlation, specifically, r = -0.13 for ATP r = -0.34 for NA (data not shown). We concluded that, at the microdomain level, astrocytic Ca^{2+} hypoactivity is poorly influenced from the proximity to Aβ plaques.

5.5 GLT-1 is reduced in PS2APP mice at 6 months of age

To analyze Aβ plaque expression, in a subset of experiments we used as astrocytic marker the antibody against GLT-1. As shown in Fig. 20 in the SSCx from PS2APP mice the total GLT-1 fluorescence in the imaged field is strongly reduced compared to that in the SSCx from WT mice. The reduction in the area covered by the GLT-1 signal is statistically significant, however the loss is mainly due to a reduction in the area covered by the GLT-1 signal even when expressed as corrected total fluorescence (Fig. 20C, left, middle panels), with no change in signal density (Fig. 20C, right panel).

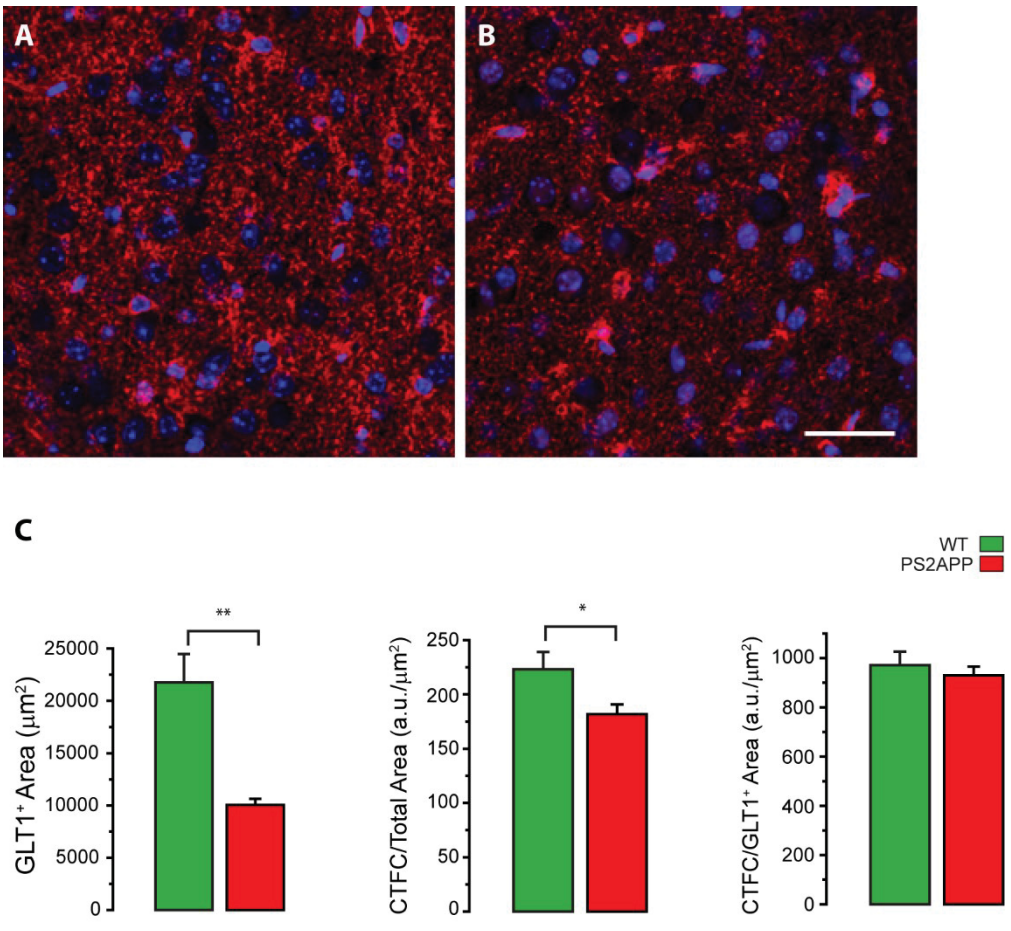

Figure 20. Immunohistochemical analysis showing GLT-1 expression n in the SSCx from WT and PS2APP mice. (A, B) Confocal representative images of the SSCx (L2/3) from a 6-month-old WT (A) and a PS2APP (B) mouse stained with anti-GLT-1 (red signal) and TO-PRO®-3 (blue signal). Scalebar, 40 µm. The two images are captured exactly with

the same parameters. **(C)** GLT-1 immunostaining quantification (n= 29 slices from 3 WT mice, 32 slices from 3 PS2APP mice) *p < 0.05, **p < 0.01 Student's *t*-test. CTFC, Corrected Total Cell Fluorescence.

An additional important feature is the sparse distribution of GLT-1 in PS2APP mice that is revealed at single astrocytes visualized at higher magnification (Fig. 21).

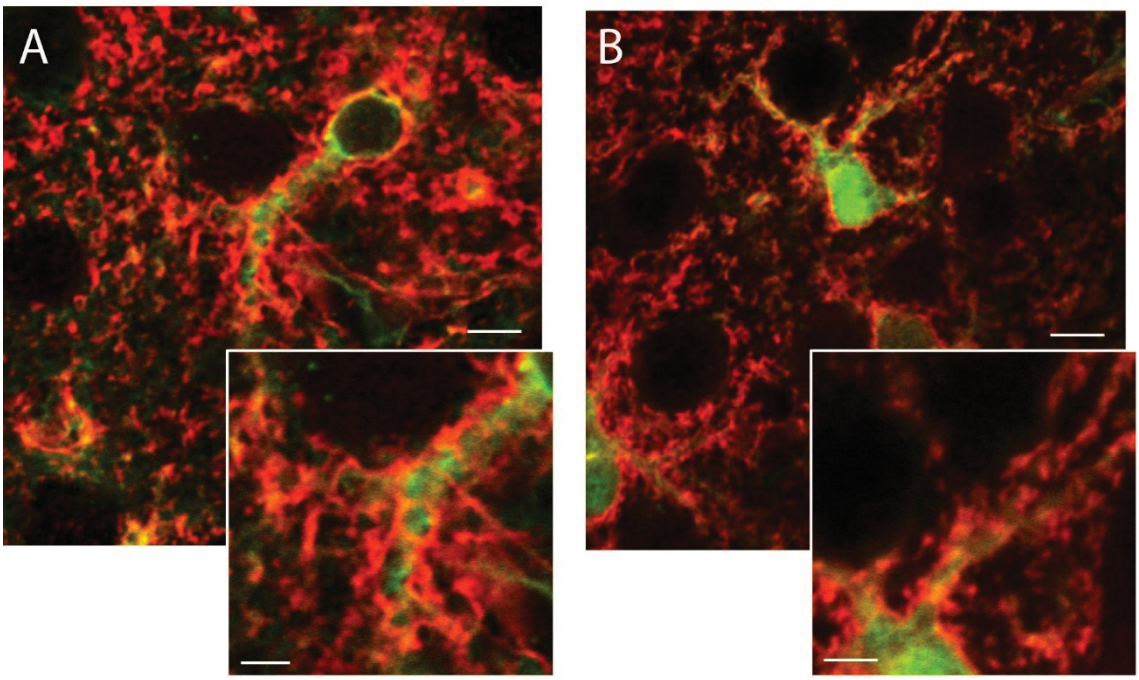

Figure 21. GLT-1 distribution in 6-month-old WT and PS2APP mice. (A,B) Confocal representative images of invidual GCaMP6f expressing astrocytes from SSCx (L2/3) of a WT (A) and a PS2APP (B) mouse after immunostaining with anti-GLT-1 (red signal) and anti-GFP (green signal) that binds to the GFP domain of GCaMP6f. Scale bar, 6 μm). Insets show at high magnification astrocytic proximal processes exhibiting sparse GLT-1 distribution. Scale bar, 4 μm.

Western blot analysis further confirmed the reduced expression of GLT-1 in 6-month-old PS2APP mice (Fig.22). GLT-1 protein appeared as a monomer (62 kD) and multimer (120 kD).

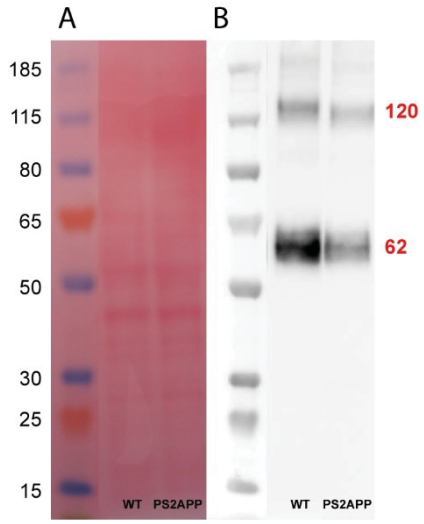

Figure 22. GLT-1 protein expression assessed by western blot analysis. (A) Ponceau and **(B)** GLT-1 western blot of the 4-12% gel; line 1 WT and line 2 PS2APP cortical extracts (20µg/line).

5.6 Spontaneous microdomain Ca^{2+} activity is strongly reduced in SSCx astrocytes from the living intact brain in 6-month-old PS2APP mice

Our results from SSCx brain slices show that astrocytic Ca^{2+} activity is drastically reduced at 6 months of age in PS2APP mice. This reduction is present for both spontaneous and neurotransmitter-evoked activity. Next, we sought to validate in *in vivo* experiments the results obtained in 6-month-old WT and PS2APP mice. Two weeks after GCaMP6f and tdTomato injections, in isoflurane anesthetized mice, we performed 2P Ca^{2+} imaging experiments, focusing on SSCx layer II/III astrocytes. We confirmed that the drastic reduction in microdomain spontaneous activity that we observed in brain slices of PS2APP with respect to WT mice is maintained also *in vivo* (Fig. 23).

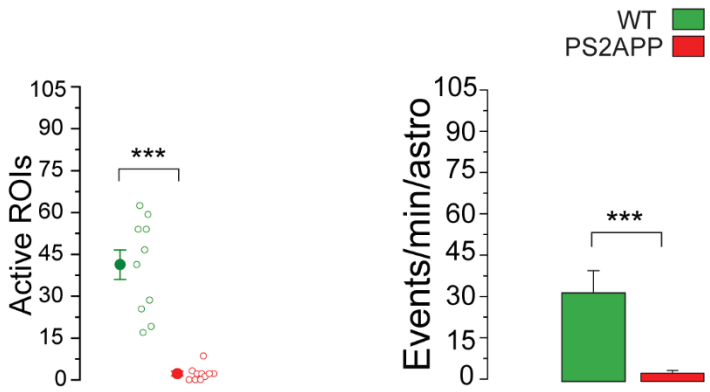

Figure 23. *In vivo* spontaneous microdomain Ca^{2+} activity in the SSCx of 6-month-old WT and PS2APP mice. Quantification of spontaneous microdomain activity in the living intact brain from WT (green) and PS2APP (red) mice (10 astrocytes from 3 WT mice and 10 astrocytes from 3 PS2APP mice), ***p < 0.001 Mann-Whitney test.

5.7 Hippocampal astrocytic Ca^{2+} activity in 3-month-old PS2APP mice follows the same dynamics of cortical astrocytes

Our work is mainly focused on exploring the role of astrocytic Ca^{2+} signaling in the SSCx of AD mice. However, it is well recognized that AD-related dysfunctions affect both cortical and hippocampal-dependent functions including learning and memory processes. Accordingly, we next asked whether the astrocytes of CA1 region from PS2APP mice exhibit the same defects that we observed in cortical astrocytes and, in such a case, whether these astrocytic alterations appear in the hippocampus at an earlier time point with respect to those detected in the SSCx. To address these questions, we first performed Ca^{2+} imaging experiments in hippocampal slices from 3-month-old WT and PS2APP mice. In the hippocampus of PS2APP mice, similarly to what observed in the SSCx, we found a significant increase in the amplitude of spontaneous astrocytic Ca^{2+} activity at the level of microdomains, but also a significant increase in the number of active ROIs (Fig. 24).

Similarly to SSCx astrocytes, in PS2APP mice the evoked ATP response of hippocampal astrocytes is overall unchanged with respect to that in WT astrocytes in all astrocytic compartments (Fig. 25).

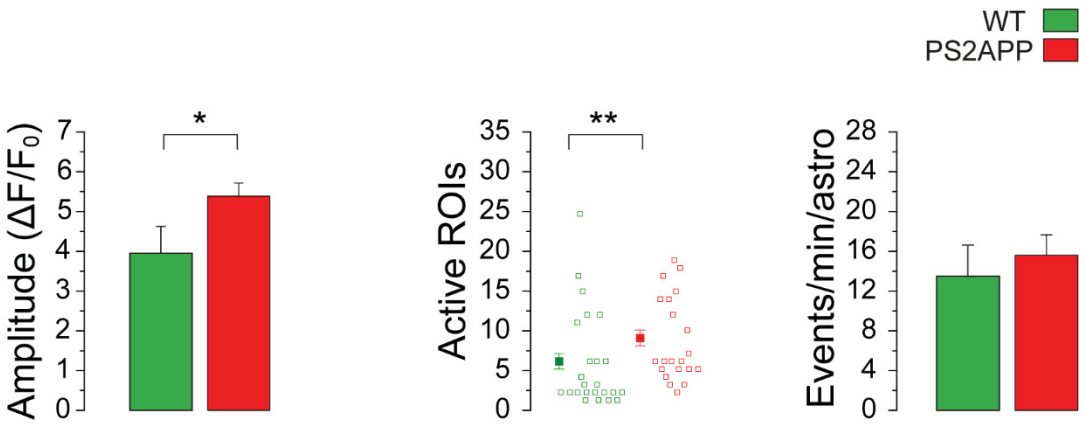

Figure 24. Spontaneous microdomain Ca^{2+} activity in the CA1 of 3-month-old WT and PS2APP mice. Quantification of spontaneous microdomain Ca^{2+} activity in hippocampal astrocytes from WT (green) and PS2APP (red) mice at 3 months of age (25 astrocytes from 3 WT mice and 21 astrocytes from 3 PS2APP mice). Bar histogram on the left reports the Ca^{2+} variations in terms of fluorescence intensity reported as $\Delta F/F_0$, *p < 0.05, Student's *t*-test. Scatter plot reports both the mean values of active ROIs for WT and PS2APP astrocytes (full squares) and the number of active ROIs for each single astrocyte (empty squares), **p < 0.01, Mann-Whitney test. Bar histogram on the right reports the mean frequency of microdomain Ca^{2+} activity measured as total number of events per minute per astrocyte.

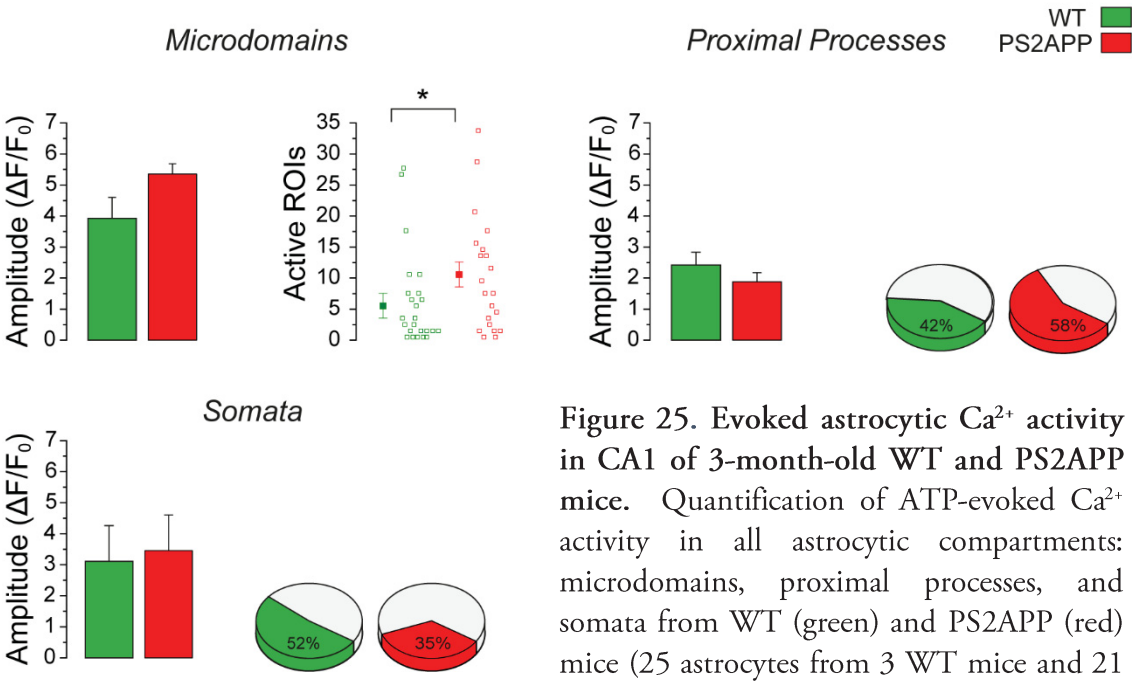

Figure 25. Evoked astrocytic Ca^{2+} activity in CA1 of 3-month-old WT and PS2APP mice. Quantification of ATP-evoked Ca^{2+} activity in all astrocytic compartments: microdomains, proximal processes, and somata from WT (green) and PS2APP (red) mice (25 astrocytes from 3 WT mice and 21 astrocytes from 5 PS2APP mice). *p < 0.05 Mann-Whitney test.

In the next future, we plan to investigate if hippocampal astrocytic activity is altered in 6-month-old AD mice and, in such a case, to assess the consequences on hippocampal-dependent functions.

5.8 Ongoing experiments: astrocytic response to physiological sensory stimulation

To evaluate the astrocytic response to a physiological stimulus, we are currently investigating the response of neurons and astrocytes to whisker stimulation in 6-month-old WT and PS2APP mice co-injected with GCaMP6f, selectively delivered to astrocytes, and RCaMP1.07, selectively delivered to neurons. This approach allows us to evaluate *in vivo* the Ca^{2+} responses in astrocytes and neurons simultaneously [109]. To this aim a single whisker is threaded into a needle fixed to a piezo actuator and stimulated at a specific frequency. An important feature of the SSCx is that each whisker elicits responses only in a specific area, named "barrel" [114]. Therefore, to identify specific whisker barrels, we monitored the IOS. Specifically, we used a 630 nm led ring placed around the bottom of the objective and acquired images with a 16-bit CCD camera focused 400µm below the cortical surface. In preliminary experiments, we took advantage of CAG-GCaMP3 mice that genetically express GCaMP3 mainly in neurons. We combined IOS imaging with manual whisker stimulation (Fig. 26A) or single whisker deflection (90 Hz, 1s; Fig. 26B) to identify the right whisker area by increased light reflectance (due to the decrease in deoxy-haemoglobin accompanying blood flow increase). Interestingly, 2P microscopy allowed to identify the border of each barrel (Fig. 26C). Upon replication of the protocol of single whisker stimulation (see Fig.26B), we

performed Ca^{2+} imaging in neurons of layer II/III in the identified barrel cortex area, and recorded Ca^{2+} increases that are strictly correlated with the stimulus (Fig.26C). In the next future, we will accurately characterize IOS responses and

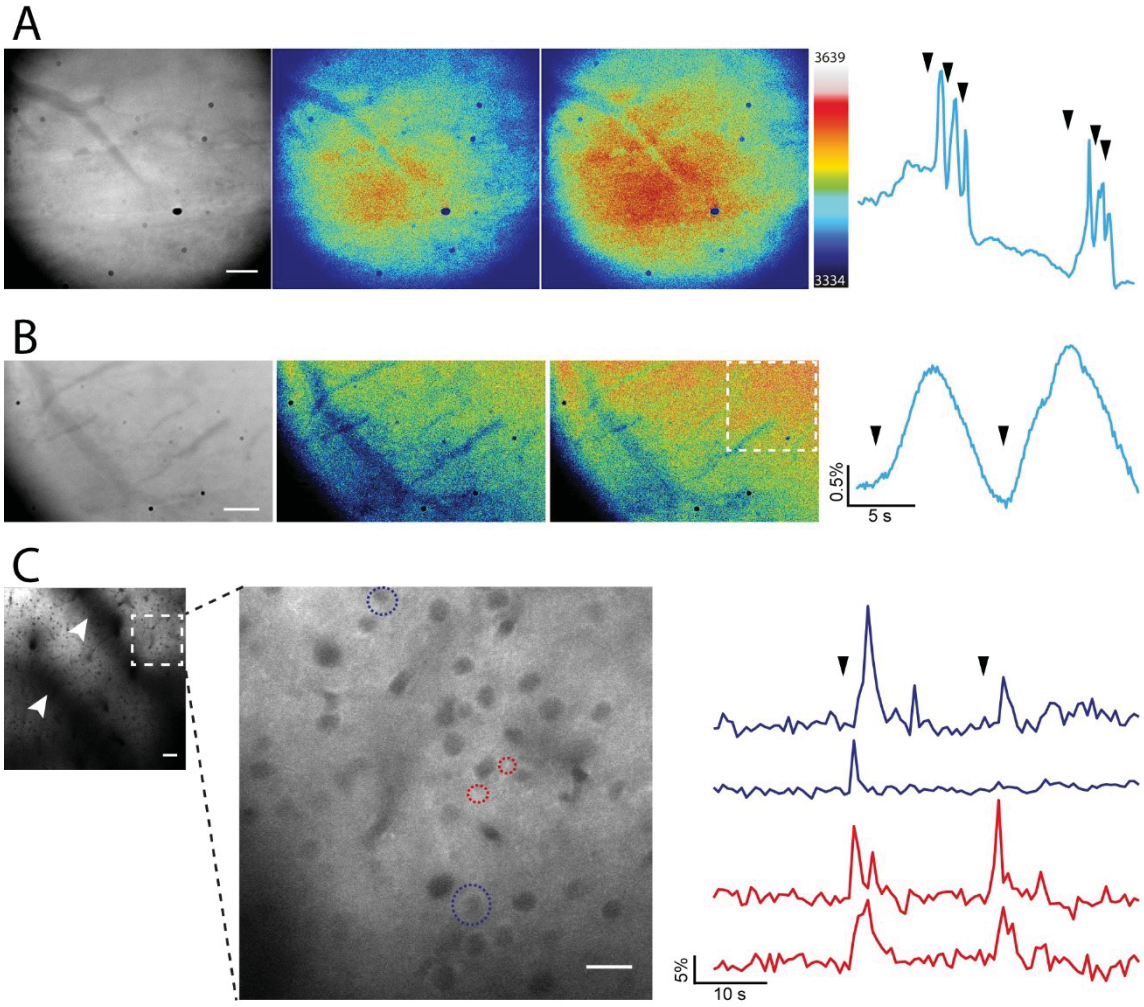

the kinetics of Ca^{2+} impaired in AD with respect to WT mice.

Figure 26. Whisker stimulation: changes in IOS and Ca^{2+} imaging. (A) Representative changes in the IOS after manual whisker stimulations. Left panel, grey scale images of the field. Middle panel, basal intrinsic optic signal imaged at 630nm. Right panel, intrinsic optic signal after manual whisker stimulation. Scale bar, 50 μm. Pseudocolor bar shows the LUT applied. On the right, representative trace showing the change in tissue reflection (R), depicted as $\Delta R/R_0$. Arrowheads mark whisker stimulation time. **(B)** Same as in (A) but after piezo-mediated single whisker stimulation (90Hz, 1s). Dashed box represents the field analysed with 2P microscopy in (C). **(C)** 2P images of GCaMP3 fluorescence in the area corresponding to the dashed box in (B). Arrowheads indicate barrel borders. Scale bar, 100 μm. On the right, higher magnification of the boxed area in the left panel. The nuclei of neuronal cells expressing GCaMP3 are visible as black holes (scale bar, 25 μm). On the bottom, representative traces of Ca^{2+} changes in neuronal cells (blue, dashed circles in blue

on the left) and in putative astrocytes (red, dashed circles in red on the left). Arrowheads mark whisker stimulation time.

6. Discussion and Conclusions

In the present study, we demonstrated that astrocytic Ca^{2+} signaling in the SSCx undergoes a sequence of changes along AD progression, which encompasses both spontaneous and evoked activity. Specifically, with respect to age-matched controls, in 3-month-old PS2APP mice spontaneous Ca^{2+} microdomains are of larger amplitude and shows a general trend for an increased frequency, whereas in 6-month-old PS2APP mice, *i.e.* after the appearance of amyloid plaques, the spontaneous microdomain activity is drastically reduced. As regards the evoked activity, in 3-month-old WT and PS2APP mice all astrocytes respond to ATP and NA with Ca^{2+} elevations at both soma and processes, whereas in 6-month-old PS2APP mice the evoked response is drastically impaired.

6.1 Astrocytic Ca^{2+} activity in PS2APP mice

In the two different AD mouse models based on APP and PS1, the APPPS1-21 [96, 102] and the APPSwe/PS1ΔE9 mouse lines [94] an astrocytic hyperactivity has been observed in relationship to the *acute phase* of the disease, in concomitance with Aβ plaque deposition. In contrast, in the PS2APP mice we detected an astrocytic tendency to hyperactivity when Aβ plaques are still absent at an early phase of the disease, *i.e.* at 3 months of mouse age.

The molecular mechanisms of the astrocyte hyperactivity are unclear. In the APPPS1-21 model, it has been suggested to involve activation of TRPA1 channels [102] or P2Y1Rs [96]. A dysregulation of the astrocyte signaling

mediated by purinergic receptors has been, indeed, proposed to contribute to AD and to possibly represent a therapeutic target [100]. Taking into account this hypothesis and the emerging role of purinergic signaling in neurons and microglia [113], we tested whether the Ca^{2+} responses mediated by purinergic receptor activation are also altered in astrocytes from PS2APP mice. We found no significant differences in ATP-evoked Ca^{2+} responses of SSCx astrocytes between PS2APP and WT mice at 3 months of age, whereas a severe reduction in both the evoked ATP response and the spontaneous activity was recorded at the different compartments of astrocytes in 6-month-old PS2APP mice with respect to age-matched controls. To our knowledge, this is the first study reporting an astrocyte hypoactivity (both spontaneous and evoked) in an AD mouse model which develops in concomitance with Aβ deposition and astrocytic gliosis [107], two phenomena that we confirmed to be present also in the SSCx of 6-month-old PS2APP mice. These data suggest a temporal evolution in astrocytic Ca^{2+} signal changes that is strictly related to the progression of the disease.

Whether and how this defective signaling of astrocytes impacts brain function in PS2APP mice remains to be evaluated. Accumulating evidence supports a direct involvement of astrocytic Ca^{2+} activity in fundamental phenomena in the brain, from the modulation of local synaptic circuitries and neurovascular coupling [58, 115-118] up to behaviour [119-121]. More recently, the consequences of astrocytic Ca^{2+} signaling attenuation have been studied in the striatum, where it causes changes in the functional expression of different genes. For instance, astrocytic Ca^{2+} hypoactivity increases the expression of the astrocytic GABA transporter type 3 (GAT3), leading to increased GABA uptake and a consequent reduction of both ambient GABA level and tonic inhibition

[122]. As reviewed in [123], several studies confirmed the existence of a relationship between GABA and astrocytes in different AD mouse models and describe, conversely, the consequences of abnormal GABA release from astrocytes. These findings raise intriguing questions about the consequence of astrocytic hypoactivity on synaptic transmission in PS2APP mice, which are characterized by hippocampal neuronal hyperexcitability [107]. The role of an astrocytic-mediated mechanism in the excitation/inhibition balance, possibly involving alterations of GABAergic signaling, ought to have proper investigation in the future.

6.2 Expression of APP or PS2 mutants alone is insufficient to fully replicate astrocytic Ca^{2+} defects

We took advantage of APPSwe and PS2.30H mice to clarify whether APP or PS2 mutants alone were sufficient to cause the astrocytic Ca^{2+} deficits that we unveiled in 6-month-old PS2APP mice. Prior studies suggested a prominent role of PS2 on ER Ca^{2+} handling, which leads to a clear reduction of neuronal Ca^{2+} stores and IP_3 responses already in neuronal cultures and hippocampal slices from two-week-old PS2.30H and PS2APP mice [24, 89]. Contrary to the expectations, our analysis failed to reveal a significant difference between astrocytic Ca^{2+} activity in WT and PS2.30H mice, indicating that astrocytic alterations are not caused by PS2 mutant *per* se. Remarkably, these alterations occur in concomitance not only with the appearance of Aβ plaques, but also with astrocytic reactivity. We can speculate that astrocytic Ca^{2+} dysfunctions are linked also to a gliotic condition, influenced by the extracellular environment, and to a consequent global astrocytic rearrangement. The absence of astrocytic Ca^{2+} defects also in APPSwe mice further corroborates the hypothesis that

astrocytic Ca^{2+} alterations in the PS2APP model are not just a matter of human APP overexpression. Of note, a strong relationship between Ca^{2+} dysfunctions and prolonged incubation period of $A\beta_o$ has been reported in the literature [103, 124, 125]. In the study by Lazzari and co-workers [126], the incubation of mouse cortical neurons with soluble $A\beta_o$ is reported to disrupt Ca^{2+} dynamics at the store level, decreasing the response to different IP_3 generating agonists. This mechanism could explain the temporal relationship between the reduced ATP response and a pathological stage in which $A\beta_o$ are abundantly present in PS2APP mice.

6.3 Ca^{2+} alterations affect astrocytic responses to different IP_3 generating agonists

We provided evidence that in 6-month-old PS2APP mice the astrocytic Ca^{2+} response is altered following activation of both purinergic and noradrenergic receptors. These data further support the hypothesis that at the basis of this defective astrocytic response is a general mechanism involving the disruption of intracellular Ca^{2+} signal dynamics at the Ca^{2+} store level. In such a case, astrocytic Ca^{2+}-dependent functions can be critically compromised. Among the different processes that involve Ca^{2+} signaling, a prominent position is occupied by the astrocyte modulation of synaptic transmission. Indeed, astrocytes display intracellular Ca^{2+} elevations in response to synaptic activity and, in a variety of cases, signal back to neurons by releasing gliotransmitters via a Ca^{2+} dependent mechanism [38]. Further research should be undertaken to investigate the consequence of these astrocytic Ca^{2+} signal alterations on astrocyte-to-neuron communication.

6.4 Aβ plaque deposition and astrocytic Ca^{2+} activity

Taking in account the temporal correlation between Aβ plaque appearance and astrocytic Ca^{2+} alterations, we investigated whether Aβ plaque proximity influences astrocytic Ca^{2+} activity. In APPPS1 mouse models, this relationship has been investigated at the *in vivo* level in anesthetized mice by two different groups with contrasting results, possibly linked to different mouse models and analytic strategies used in these studies. In 6-8-month-old APPswe-PS1ΔE9 mice, Kuchibhotla and co-workers found that cortical astrocytic hyperactivity is independent of Aβ plaque proximity [94]. In this work, the authors analysed the differences between astrocytes positioned at less, or more, than 20 μm from plaques and they concluded that astrocytic activity was independent from plaque proximity. However, in the same mouse strain, they also reported an increase in intercellular Ca^{2+} waves and synchrony between distant astrocytes. In contrast, by using Pearson's correlation analysis Delekate and colleagues found that the relative fraction of hyperactive astrocytes in the SSCx of APPPS1-21 mice closer to plaques (< 50 μm) was significantly larger than those farther away [96]. Considering these controversial results, we decided to apply two different types of analytical approaches on our data. Specifically, by using Pearson's correlation analysis, we obtained different types and degrees of correlation for the different parameters that we analysed, thus preventing to drive from our data a clear conclusion. Conversely, by comparing the two groups of astrocytes with Student's *t*-test we obtained no significant differences between astrocytes with respect to proximity to Aβ plaques. This controversy will probably be resolved by performing more experiments in order to clarify whether or not the absence of significant differences is only a matter of number

of experiments. Altogether, our data can only suggest that Aβ plaque proximity poorly influences astrocytic Ca^{2+} activity in the SSCx of PS2APP mice.

6.5 GLT-1 reduction in 6-month-old PS2APP astrocytes

The activity of the astrocyte-specific glutamate transporter GLT-1 provides a fundamental contribution to the excitatory/inhibitory balance in brain circuits. To characterize the expression and distribution of GLT-1, we carried out immunohistochemical experiments in the mouse SSCx. We found that in 6-month-old PS2APP mice GLT-1 is significantly reduced. Furthermore, the distribution of GLT-1 in the astrocytic membrane appears fragmented in PS2APP mice and this is in marked contrast with the homogeneous GLT-1 expression in astrocytes from WT mice. Chen and co-workers proposed that IP_3R-mediated increases in the cytosolic Ca^{2+} may contribute to GLT-1 trafficking [127]. Therefore, astrocytic Ca^{2+} alterations and GLT-1 alterations, unexpectedly, could be unexpectedly related. GLT-1 action assures a rapid glutamate uptake at the synaptic cleft, contributing to a precise and fast synaptic transmission. On the other hand, the impairment of glutamate clearance could strongly impact brain network excitability favouring excitotoxicity and ultimately cell death. Noteworthy, in human patients the excitatory amino-acid transporter 2 (the human homologue of GLT-1) is significantly reduced in early stages of AD [128]. At variance with the contrasting results obtained in Ca^{2+} imaging experiments, GLT-1 alterations are a shared feature between PS2APP and APPP/S1-21 model [129].

6.6 Whisker stimulation, IOS and Ca^{2+} imaging: joining different techniques to deeply understand the brain

"Life is like a jigsaw puzzle, you have to see the whole picture then put it together piece by piece"

Terry McMillan, A day late and a dollar short (2000)

Brain, as life, is a puzzle and neuroscientists give it their best shots to fix the pieces in the right position. As for a puzzle, also for the brain it is important to see *the whole picture*, so that, by understanding how the brain works in physiological conditions, we can infer which are the consequences of pathological states on brain concerted actions. We took in account only a few pieces of the puzzle, *i.e.* the astrocytic Ca^{2+} alterations and their different features along the progression of the disease, but at this point we want to look at a wider picture that comprises brain response to physiological stimuli. In this way we can clarify whether also a physiological sensory stimulation fails to evoke a proper astrocytic Ca^{2+} response. As explained in the results section, to address this point we set up an approach that takes advantage of different techniques. We combined single whisker stimulation, IOS and Ca^{2+} imaging to perform experiments in mice expressing GCaMP3 in different brain cells. Different interesting questions emerged from the results obtained in these preliminary experiments. For example, using different modes of whisker stimulation we noticed different kinetics in the IOS changes after single whisker deflection and after repetitive manual whisker displacement. IOS kinetics after single whisker stimulation are slow similarly to those reported in different studies [130-132], whereas the kinetics of manual whisker stimulation are extremely fast. This aspect could depend on the unprecise type of stimulus that we presented, being it larger and less precise, or to other collateral mechanisms that shapes this type

of kinetics. Further investigations are needed to clarify this issue. More relevant for the aims of this study, Ca^{2+} imaging *in vivo* experiments inspired a variety of possible meaningful *pieces*. We identified clear responses of the neuropil, but also of different neuronal bodies, which were in some cases highly correlated with the stimulus onset and in others were more delayed. Furthermore, we distinguished other types of cellular elements, possibly astrocytes, responding with a clear Ca^{2+} increase correlated with the onset of the stimulus. In future experiments we will combine RCaMP1.07 expression in neurons with GCaMP6f expression in astrocytes in order to simultaneously monitor Ca^{2+} responses in neurons and astrocytes. Our final goal is to verify whether astrocytic responses to whisker stimulation are impaired in PS2APP mice.

6.7 Conclusions

In this thesis we shed light, for the first time, onto astrocytic Ca^{2+} signaling in an AD mouse model based on PS2, unveiling an opposite tendency with respect to the Ca^{2+} dynamics observed in astrocytes from PS1-based AD models. Whereas in APPPS1 mice astrocytic Ca^{2+} activity is characterized by a marked hyperactivity [94, 96], in PS2APP mice we found a strong reduction of astrocytic Ca^{2+} activity. An additional innovative and significant aspect in this thesis is the evaluation of astrocytic Ca^{2+} signaling not only at the level of the soma, as reported in previous works related to Ca^{2+} signaling in AD, but also at the level of the processes, including Ca^{2+} microdomains, accordingly to the emerging role of these structures as fundamental elements in astrocytic contribution to different physiological processes [65]. A natural progression of this work is to clarify the mechanisms responsible of the alterations in spontaneous Ca^{2+} microdomain activity and the consequences of astrocytic

hypoactivity on synaptic transmission and, ultimately, behavior. Considering the crucial roles of astrocytes in synaptic transmission and behavioural functions, as reviewed by Araque *et al.* [38] and Oliveira *et al.* [133] respectively, it is reasonably to hypothesize that the consequences of astrocytic hypoactivity can be highly relevant for AD pathogenesis. Hopefully, future research will benefit of astrocytic Ca^{2+} signaling rescue as a possible therapeutic approach.

7. Bibliography

[1] M. Navarrete, A. Araque, The Cajal school and the physiological role of astrocytes: a way of thinking, Frontiers in neuroanatomy 8 (2014) 33.

[2] C. Patterson, J.W. Feightner, A. Garcia, G.Y. Hsiung, C. MacKnight, A.D. Sadovnick, Diagnosis and treatment of dementia: 1. Risk assessment and primary prevention of Alzheimer disease, CMAJ : Canadian Medical Association journal = journal de l'Association medicale canadienne 178 (2008) 548-556.

[3] A. Verkhratsky, M. Nedergaard, Physiology of Astroglia, Physiological reviews 98 (2018) 239-389.

[4] K. Maurer, S. Volk, H. Gerbaldo, Auguste D and Alzheimer's disease, Lancet (London, England) 349 (1997) 1546-1549.

[5] M. Bielschowsky, Die Silberimprägnation der Neurofibrillen: einige Bemerkungen zu der von mir angegebenen Methode und den von mir gelieferten Bildern, Journal für Psychologie und Neurologie 3 (1904) 169-189.

[6] A. Alzheimer, Über einen eigenartigen schweren Erkrankungsprozeß der Hirnrinde, Neurologisches Centralblatt 23 (1906) 1129-1136.

[7] A. Alzheimer, Über eigenartige Krankheitsfälle des späteren Alters, Zeitschrift für die Gesamte Neurologie und Psychiatrie 4 (1911) 356–385.

[8] M. Goedert, C.M. Wischik, R.A. Crowther, J.E. Walker, A. Klug, Cloning and sequencing of the cDNA encoding a core protein of the paired helical filament of Alzheimer disease: identification as the microtubule-associated protein tau, Proceedings of the National Academy of Sciences of the United States of America 85 (1988) 4051-4055.

[9] G.G. Glenner, C.W. Wong, Alzheimer's disease: initial report of the purification and characterization of a novel cerebrovascular amyloid protein, Biochemical and biophysical research communications 120 (1984) 885-890.

[10] D. Goldgaber, M.I. Lerman, O.W. McBride, U. Saffiotti, D.C. Gajdusek, Characterization and chromosomal localization of a cDNA encoding brain amyloid of Alzheimer's disease, Science (New York, N.Y.) 235 (1987) 877-880.

[11] T. Tokuda, T. Fukushima, S. Ikeda, Y. Sekijima, S. Shoji, N. Yanagisawa, A. Tamaoka, Plasma levels of amyloid beta proteins Abeta1-40 and Abeta1-42(43) are elevated in Down's syndrome, Annals of neurology 41 (1997) 271-273.

[12] R. Sherrington, E.I. Rogaev, Y. Liang, E.A. Rogaeva, G. Levesque, M. Ikeda, H. Chi, C. Lin, G. Li, K. Holman, T. Tsuda, L. Mar, J.F. Foncin, A.C. Bruni, M.P. Montesi, S. Sorbi, I. Rainero, L. Pinessi, L. Nee, I. Chumakov, D. Pollen, A. Brookes, P. Sanseau, R.J. Polinsky, W. Wasco, H.A. Da Silva, J.L. Haines, M.A. Perkicak-Vance, R.E. Tanzi, A.D. Roses, P.E. Fraser, J.M. Rommens, P.H. St George-Hyslop, Cloning of a gene bearing missense mutations in early-onset familial Alzheimer's disease, Nature 375 (1995) 754-760.

[13] E. Levy-Lahad, W. Wasco, P. Poorkaj, D.M. Romano, J. Oshima, W.H. Pettingell, C.E. Yu, P.D. Jondro, S.D. Schmidt, K. Wang, et al., Candidate gene for the chromosome 1 familial Alzheimer's disease locus, Science (New York, N.Y.) 269 (1995) 973-977.

[14] W.J. Strittmatter, A.M. Saunders, D. Schmechel, M. Pericak-Vance, J. Enghild, G.S. Salvesen, A.D. Roses, Apolipoprotein E: high-avidity binding to beta-amyloid and increased frequency of type 4 allele in late-onset familial Alzheimer disease, Proceedings of the National Academy of Sciences of the United States of America 90 (1993) 1977-1981.

[15] E.H. Corder, A.M. Saunders, N.J. Risch, W.J. Strittmatter, D.E. Schmechel, P.C. Gaskell, Jr., J.B. Rimmler, P.A. Locke, P.M. Conneally, K.E. Schmader, et al., Protective effect of

apolipoprotein E type 2 allele for late onset Alzheimer disease, Nature genetics 7 (1994) 180-184.
[16] Y. Zhao, X. Wu, X. Li, L.L. Jiang, X. Gui, Y. Liu, Y. Sun, B. Zhu, J.C. Pina-Crespo, M. Zhang, N. Zhang, X. Chen, G. Bu, Z. An, T.Y. Huang, H. Xu, TREM2 Is a Receptor for beta-Amyloid that Mediates Microglial Function, Neuron 97 (2018) 1023-1031 e1027.
[17] C.Y.D. Lee, A. Daggett, X. Gu, L.L. Jiang, P. Langfelder, X. Li, N. Wang, Y. Zhao, C.S. Park, Y. Cooper, I. Ferando, I. Mody, G. Coppola, H. Xu, X.W. Yang, Elevated TREM2 Gene Dosage Reprograms Microglia Responsivity and Ameliorates Pathological Phenotypes in Alzheimer's Disease Models, Neuron 97 (2018) 1032-1048 e1035.
[18] J.A. Hardy, G.A. Higgins, Alzheimer's disease: the amyloid cascade hypothesis, Science (New York, N.Y.) 256 (1992) 184-185.
[19] C. Haass, D.J. Selkoe, Soluble protein oligomers in neurodegeneration: lessons from the Alzheimer's amyloid beta-peptide, Nature reviews. Molecular cell biology 8 (2007) 101-112.
[20] S.G. Younkin, Evidence that A beta 42 is the real culprit in Alzheimer's disease, Annals of neurology 37 (1995) 287-288.
[21] S. Lesne, M.T. Koh, L. Kotilinek, R. Kayed, C.G. Glabe, A. Yang, M. Gallagher, K.H. Ashe, A specific amyloid-beta protein assembly in the brain impairs memory, Nature 440 (2006) 352-357.
[22] G.M. Shankar, S. Li, T.H. Mehta, A. Garcia-Munoz, N.E. Shepardson, I. Smith, F.M. Brett, M.A. Farrell, M.J. Rowan, C.A. Lemere, C.M. Regan, D.M. Walsh, B.L. Sabatini, D.J. Selkoe, Amyloid-beta protein dimers isolated directly from Alzheimer's brains impair synaptic plasticity and memory, Nature medicine 14 (2008) 837-842.
[23] Z.S. Khachaturian, Hypothesis on the regulation of cytosol calcium concentration and the aging brain, Neurobiology of aging 8 (1987) 345-346.
[24] E. Zampese, C. Fasolato, T. Pozzan, P. Pizzo, Presenilin-2 modulation of ER-mitochondria interactions: FAD mutations, mechanisms and pathological consequences, Communicative & integrative biology 4 (2011) 357-360.
[25] K. Herrup, The case for rejecting the amyloid cascade hypothesis, Nature neuroscience 18 (2015) 794-799.
[26] J. Sevigny, P. Chiao, T. Bussiere, P.H. Weinreb, L. Williams, M. Maier, R. Dunstan, S. Salloway, T. Chen, Y. Ling, J. O'Gorman, F. Qian, M. Arastu, M. Li, S. Chollate, M.S. Brennan, O. Quintero-Monzon, R.H. Scannevin, H.M. Arnold, T. Engber, K. Rhodes, J. Ferrero, Y. Hang, A. Mikulskis, J. Grimm, C. Hock, R.M. Nitsch, A. Sandrock, The antibody aducanumab reduces Abeta plaques in Alzheimer's disease, Nature 537 (2016) 50-56.
[27] W.A. Eimer, D.K. Vijaya Kumar, N.K. Navalpur Shanmugam, A.S. Rodriguez, T. Mitchell, K.J. Washicosky, B. Gyorgy, X.O. Breakefield, R.E. Tanzi, R.D. Moir, Alzheimer's Disease-Associated beta-Amyloid Is Rapidly Seeded by Herpesviridae to Protect against Brain Infection, Neuron 99 (2018) 56-63 e53.
[28] C.R. Jack, Jr., D.S. Knopman, W.J. Jagust, R.C. Petersen, M.W. Weiner, P.S. Aisen, L.M. Shaw, P. Vemuri, H.J. Wiste, S.D. Weigand, T.G. Lesnick, V.S. Pankratz, M.C. Donohue, J.Q. Trojanowski, Tracking pathophysiological processes in Alzheimer's disease: an updated hypothetical model of dynamic biomarkers, The Lancet. Neurology 12 (2013) 207-216.
[29] R.C. Petersen, How early can we diagnose Alzheimer disease (and is it sufficient)? The 2017 Wartenberg lecture, Neurology (2018).
[30] K. Blennow, H. Hampel, M. Weiner, H. Zetterberg, Cerebrospinal fluid and plasma biomarkers in Alzheimer disease, Nature reviews. Neurology 6 (2010) 131-144.
[31] J. Dumurgier, S. Schraen, A. Gabelle, O. Vercruysse, S. Bombois, J.L. Laplanche, K. Peoc'h, B. Sablonniere, K.V. Kastanenka, C. Delaby, F. Pasquier, J. Touchon, J. Hugon, C.

Paquet, S. Lehmann, Cerebrospinal fluid amyloid-beta 42/40 ratio in clinical setting of memory centers: a multicentric study, Alzheimer's research & therapy 7 (2015) 30.
[32] H. Zetterberg, K. Tullhog, O. Hansson, L. Minthon, E. Londos, K. Blennow, Low incidence of post-lumbar puncture headache in 1,089 consecutive memory clinic patients, European neurology 63 (2010) 326-330.
[33] A.G. Vlassenko, T.L. Benzinger, J.C. Morris, PET amyloid-beta imaging in preclinical Alzheimer's disease, Biochimica et biophysica acta 1822 (2012) 370-379.
[34] Y. Cui, B. Liu, S. Luo, X. Zhen, M. Fan, T. Liu, W. Zhu, M. Park, T. Jiang, J.S. Jin, Identification of conversion from mild cognitive impairment to Alzheimer's disease using multivariate predictors, PloS one 6 (2011) e21896.
[35] S. Makin, The amyloid hypothesis on trial, Nature 559 (2018) S4-S7.
[36] C. Golgi, Sulla sostanza connettiva del cervello (nevroglia). Rendiconti del R Instituto Lombardo di Scienze e Lettere Vol. 3, 1870, pp. 275-277.
[37] M. Lenhossék, Der feinere Bau des Nervensystems im Lichte neuester Forschung Berlin, 1893.
[38] A. Araque, G. Carmignoto, P.G. Haydon, S.H. Oliet, R. Robitaille, A. Volterra, Gliotransmitters travel in time and space, Neuron 81 (2014) 728-739.
[39] C.C. John Lin, K. Yu, A. Hatcher, T.W. Huang, H.K. Lee, J. Carlson, M.C. Weston, F. Chen, Y. Zhang, W. Zhu, C.A. Mohila, N. Ahmed, A.J. Patel, B.R. Arenkiel, J.L. Noebels, C.J. Creighton, B. Deneen, Identification of diverse astrocyte populations and their malignant analogs, Nature neuroscience 20 (2017) 396-405.
[40] N.J. Abbott, L. Ronnback, E. Hansson, Astrocyte-endothelial interactions at the blood-brain barrier, Nature reviews. Neuroscience 7 (2006) 41-53.
[41] W.S. Chung, N.J. Allen, C. Eroglu, Astrocytes Control Synapse Formation, Function, and Elimination, Cold Spring Harbor perspectives in biology 7 (2015) a020370.
[42] E.A. Bushong, M.E. Martone, Y.Z. Jones, M.H. Ellisman, Protoplasmic astrocytes in CA1 stratum radiatum occupy separate anatomical domains, The Journal of neuroscience : the official journal of the Society for Neuroscience 22 (2002) 183-192.
[43] M.M. Halassa, T. Fellin, H. Takano, J.H. Dong, P.G. Haydon, Synaptic islands defined by the territory of a single astrocyte, The Journal of neuroscience : the official journal of the Society for Neuroscience 27 (2007) 6473-6477.
[44] T. Fellin, O. Pascual, S. Gobbo, T. Pozzan, P.G. Haydon, G. Carmignoto, Neuronal synchrony mediated by astrocytic glutamate through activation of extrasynaptic NMDA receptors, Neuron 43 (2004) 729-743.
[45] P. Jourdain, L.H. Bergersen, K. Bhaukaurally, P. Bezzi, M. Santello, M. Domercq, C. Matute, F. Tonello, V. Gundersen, A. Volterra, Glutamate exocytosis from astrocytes controls synaptic strength, Nature neuroscience 10 (2007) 331-339.
[46] G. Perea, A. Araque, Astrocytes potentiate transmitter release at single hippocampal synapses, Science (New York, N.Y.) 317 (2007) 1083-1086.
[47] R. Min, T. Nevian, Astrocyte signaling controls spike timing-dependent depression at neocortical synapses, Nature neuroscience 15 (2012) 746-753.
[48] D.P. Schafer, E.K. Lehrman, B. Stevens, The "quad-partite" synapse: microglia-synapse interactions in the developing and mature CNS, Glia 61 (2013) 24-36.
[49] A. Mishra, Binaural blood flow control by astrocytes: listening to synapses and the vasculature, The Journal of physiology 595 (2017) 1885-1902.
[50] A.H. Cornell-Bell, S.M. Finkbeiner, M.S. Cooper, S.J. Smith, Glutamate induces calcium waves in cultured astrocytes: long-range glial signaling, Science (New York, N.Y.) 247 (1990) 470-473.
[51] A. Volterra, J. Meldolesi, Astrocytes, from brain glue to communication elements: the revolution continues, Nature reviews. Neuroscience 6 (2005) 626-640.
[52] A. Verkhratsky, R.K. Orkand, H. Kettenmann, Glial calcium: homeostasis and signaling function, Physiological reviews 78 (1998) 99-141.

[53] D.A. Rusakov, Disentangling calcium-driven astrocyte physiology, Nature reviews. Neuroscience 16 (2015) 226-233.
[54] R. Zorec, V. Parpura, A. Verkhratsky, Astroglial Vesicular Trafficking in Neurodegenerative Diseases, Neurochemical research 42 (2017) 905-917.
[55] I. Allaman, M. Belanger, P.J. Magistretti, Astrocyte-neuron metabolic relationships: for better and for worse, Trends in neurosciences 34 (2011) 76-87.
[56] L. Pasti, A. Volterra, T. Pozzan, G. Carmignoto, Intracellular calcium oscillations in astrocytes: a highly plastic, bidirectional form of communication between neurons and astrocytes in situ, The Journal of neuroscience : the official journal of the Society for Neuroscience 17 (1997) 7817-7830.
[57] D.A. Rusakov, K. Zheng, C. Henneberger, Astrocytes as regulators of synaptic function: a quest for the Ca2+ master key, The Neuroscientist : a review journal bringing neurobiology, neurology and psychiatry 17 (2011) 513-523.
[58] M.A. Di Castro, J. Chuquet, N. Liaudet, K. Bhaukaurally, M. Santello, D. Bouvier, P. Tiret, A. Volterra, Local Ca2+ detection and modulation of synaptic release by astrocytes, Nature neuroscience 14 (2011) 1276-1284.
[59] A. Panatier, J. Vallee, M. Haber, K.K. Murai, J.C. Lacaille, R. Robitaille, Astrocytes are endogenous regulators of basal transmission at central synapses, Cell 146 (2011) 785-798.
[60] E. Shigetomi, E.A. Bushong, M.D. Haustein, X. Tong, O. Jackson-Weaver, S. Kracun, J. Xu, M.V. Sofroniew, M.H. Ellisman, B.S. Khakh, Imaging calcium microdomains within entire astrocyte territories and endfeet with GCaMPs expressed using adeno-associated viruses, The Journal of general physiology 141 (2013) 633-647.
[61] R.L. Rungta, L.P. Bernier, L. Dissing-Olesen, C.J. Groten, J.M. LeDue, R. Ko, S. Drissler, B.A. MacVicar, Ca(2+) transients in astrocyte fine processes occur via Ca(2+) influx in the adult mouse hippocampus, Glia 64 (2016) 2093-2103.
[62] E. Shigetomi, X. Tong, K.Y. Kwan, D.P. Corey, B.S. Khakh, TRPA1 channels regulate astrocyte resting calcium and inhibitory synapse efficacy through GAT-3, Nature neuroscience 15 (2011) 70-80.
[63] E. Shigetomi, O. Jackson-Weaver, R.T. Huckstepp, T.J. O'Dell, B.S. Khakh, TRPA1 channels are regulators of astrocyte basal calcium levels and long-term potentiation via constitutive D-serine release, The Journal of neuroscience : the official journal of the Society for Neuroscience 33 (2013) 10143-10153.
[64] A. Agarwal, P.H. Wu, E.G. Hughes, M. Fukaya, M.A. Tischfield, A.J. Langseth, D. Wirtz, D.E. Bergles, Transient Opening of the Mitochondrial Permeability Transition Pore Induces Microdomain Calcium Transients in Astrocyte Processes, Neuron 93 (2017) 587-605 e587.
[65] N. Bazargani, D. Attwell, Astrocyte calcium signaling: the third wave, Nature neuroscience 19 (2016) 182-189.
[66] M.V. Sofroniew, Molecular dissection of reactive astrogliosis and glial scar formation, Trends in neurosciences 32 (2009) 638-647.
[67] E.M. Hol, M. Pekny, Glial fibrillary acidic protein (GFAP) and the astrocyte intermediate filament system in diseases of the central nervous system, Current opinion in cell biology 32 (2015) 121-130.
[68] S. Okada, M. Nakamura, H. Katoh, T. Miyao, T. Shimazaki, K. Ishii, J. Yamane, A. Yoshimura, Y. Iwamoto, Y. Toyama, H. Okano, Conditional ablation of Stat3 or Socs3 discloses a dual role for reactive astrocytes after spinal cord injury, Nature medicine 12 (2006) 829-834.
[69] R.G. Nagele, M.R. D'Andrea, H. Lee, V. Venkataraman, H.Y. Wang, Astrocytes accumulate A beta 42 and give rise to astrocytic amyloid plaques in Alzheimer disease brains, Brain research 971 (2003) 197-209.

[70] M. Olabarria, H.N. Noristani, A. Verkhratsky, J.J. Rodriguez, Concomitant astroglial atrophy and astrogliosis in a triple transgenic animal model of Alzheimer's disease, Glia 58 (2010) 831-838.
[71] J.E. Simpson, P.G. Ince, G. Lace, G. Forster, P.J. Shaw, F. Matthews, G. Savva, C. Brayne, S.B. Wharton, Astrocyte phenotype in relation to Alzheimer-type pathology in the ageing brain, Neurobiology of aging 31 (2010) 578-590.
[72] C. Finsterwald, P.J. Magistretti, S. Lengacher, Astrocytes: New Targets for the Treatment of Neurodegenerative Diseases, Current pharmaceutical design 21 (2015) 3570-3581.
[73] A. Verkhratsky, R. Zorec, J.J. Rodriguez, V. Parpura, Pathobiology of Neurodegeneration: The Role for Astroglia, Opera medica et physiologica 1 (2016) 13-22.
[74] U. Wilhelmsson, E.A. Bushong, D.L. Price, B.L. Smarr, V. Phung, M. Terada, M.H. Ellisman, M. Pekny, Redefining the concept of reactive astrocytes as cells that remain within their unique domains upon reaction to injury, Proceedings of the National Academy of Sciences of the United States of America 103 (2006) 17513-17518.
[75] S.A. Liddelow, K.A. Guttenplan, L.E. Clarke, F.C. Bennett, C.J. Bohlen, L. Schirmer, M.L. Bennett, A.E. Munch, W.S. Chung, T.C. Peterson, D.K. Wilton, A. Frouin, B.A. Napier, N. Panicker, M. Kumar, M.S. Buckwalter, D.H. Rowitch, V.L. Dawson, T.M. Dawson, B. Stevens, B.A. Barres, Neurotoxic reactive astrocytes are induced by activated microglia, Nature 541 (2017) 481-487.
[76] H. Chun, H. An, J. Lim, J. Woo, J. Lee, H. Ryu, C.J. Lee, Astrocytic proBDNF and Tonic GABA Distinguish Active versus Reactive Astrocytes in Hippocampus, Experimental neurobiology 27 (2018) 155-170.
[77] S. Jo, O. Yarishkin, Y.J. Hwang, Y.E. Chun, M. Park, D.H. Woo, J.Y. Bae, T. Kim, J. Lee, H. Chun, H.J. Park, D.Y. Lee, J. Hong, H.Y. Kim, S.J. Oh, S.J. Park, H. Lee, B.E. Yoon, Y. Kim, Y. Jeong, I. Shim, Y.C. Bae, J. Cho, N.W. Kowall, H. Ryu, E. Hwang, D. Kim, C.J. Lee, GABA from reactive astrocytes impairs memory in mouse models of Alzheimer's disease, Nature medicine 20 (2014) 886-896.
[78] S.F. Carter, M. Scholl, O. Almkvist, A. Wall, H. Engler, B. Langstrom, A. Nordberg, Evidence for astrocytosis in prodromal Alzheimer disease provided by 11C-deuterium-L-deprenyl: a multitracer PET paradigm combining 11C-Pittsburgh compound B and 18F-FDG, Journal of nuclear medicine : official publication, Society of Nuclear Medicine 53 (2012) 37-46.
[79] B. Vignoli, G. Battistini, R. Melani, R. Blum, S. Santi, N. Berardi, M. Canossa, Peri-Synaptic Glia Recycles Brain-Derived Neurotrophic Factor for LTP Stabilization and Memory Retention, Neuron 92 (2016) 873-887.
[80] D.J. Selkoe, M.S. Wolfe, Presenilin: running with scissors in the membrane, Cell 131 (2007) 215-221.
[81] A.S. Yoo, I. Cheng, S. Chung, T.Z. Grenfell, H. Lee, E. Pack-Chung, M. Handler, J. Shen, W. Xia, G. Tesco, A.J. Saunders, K. Ding, M.P. Frosch, R.E. Tanzi, T.W. Kim, Presenilin-mediated modulation of capacitative calcium entry, Neuron 27 (2000) 561-572.
[82] G. Zatti, R. Ghidoni, L. Barbiero, G. Binetti, T. Pozzan, C. Fasolato, P. Pizzo, The presenilin 2 M239I mutation associated with familial Alzheimer's disease reduces Ca2+ release from intracellular stores, Neurobiology of disease 15 (2004) 269-278.
[83] R. Filadi, E. Greotti, G. Turacchio, A. Luini, T. Pozzan, P. Pizzo, Presenilin 2 Modulates Endoplasmic Reticulum-Mitochondria Coupling by Tuning the Antagonistic Effect of Mitofusin 2, Cell reports 15 (2016) 2226-2238.
[84] H. Tu, O. Nelson, A. Bezprozvanny, Z. Wang, S.F. Lee, Y.H. Hao, L. Serneels, B. De Strooper, G. Yu, I. Bezprozvanny, Presenilins form ER Ca2+ leak channels, a function disrupted by familial Alzheimer's disease-linked mutations, Cell 126 (2006) 981-993.

[85] D. Shilling, D.O. Mak, D.E. Kang, J.K. Foskett, Lack of evidence for presenilins as endoplasmic reticulum Ca2+ leak channels, The Journal of biological chemistry 287 (2012) 10933-10944.
[86] M. Brini, T. Cali, D. Ottolini, E. Carafoli, Calcium pumps: why so many?, Comprehensive Physiology 2 (2012) 1045-1060.
[87] J. Shen, Function and dysfunction of presenilin, Neuro-degenerative diseases 13 (2014) 61-63.
[88] G. Zatti, A. Burgo, M. Giacomello, L. Barbiero, R. Ghidoni, G. Sinigaglia, C. Florean, S. Bagnoli, G. Binetti, S. Sorbi, P. Pizzo, C. Fasolato, Presenilin mutations linked to familial Alzheimer's disease reduce endoplasmic reticulum and Golgi apparatus calcium levels, Cell calcium 39 (2006) 539-550.
[89] M.J. Kipanyula, L. Contreras, E. Zampese, C. Lazzari, A.K. Wong, P. Pizzo, C. Fasolato, T. Pozzan, Ca2+ dysregulation in neurons from transgenic mice expressing mutant presenilin 2, Aging cell 11 (2012) 885-893.
[90] S. Chakroborty, C. Briggs, M.B. Miller, I. Goussakov, C. Schneider, J. Kim, J. Wicks, J.C. Richardson, V. Conklin, B.G. Cameransi, G.E. Stutzmann, Stabilizing ER Ca2+ channel function as an early preventative strategy for Alzheimer's disease, PloS one 7 (2012) e52056.
[91] D. Del Prete, F. Checler, M. Chami, Ryanodine receptors: physiological function and deregulation in Alzheimer disease, Molecular neurodegeneration 9 (2014) 21.
[92] M.P. Mattson, Cellular actions of beta-amyloid precursor protein and its soluble and fibrillogenic derivatives, Physiological reviews 77 (1997) 1081-1132.
[93] N.J. Haughey, M.P. Mattson, Alzheimer's amyloid beta-peptide enhances ATP/gap junction-mediated calcium-wave propagation in astrocytes, Neuromolecular medicine 3 (2003) 173-180.
[94] K.V. Kuchibhotla, C.R. Lattarulo, B.T. Hyman, B.J. Bacskai, Synchronous hyperactivity and intercellular calcium waves in astrocytes in Alzheimer mice, Science (New York, N.Y.) 323 (2009) 1211-1215.
[95] R. Radde, T. Bolmont, S.A. Kaeser, J. Coomaraswamy, D. Lindau, L. Stoltze, M.E. Calhoun, F. Jaggi, H. Wolburg, S. Gengler, C. Haass, B. Ghetti, C. Czech, C. Holscher, P.M. Mathews, M. Jucker, Abeta42-driven cerebral amyloidosis in transgenic mice reveals early and robust pathology, EMBO reports 7 (2006) 940-946.
[96] A. Delekate, M. Fuchtemeier, T. Schumacher, C. Ulbrich, M. Foddis, G.C. Petzold, Metabotropic P2Y1 receptor signalling mediates astrocytic hyperactivity in vivo in an Alzheimer's disease mouse model, Nature communications 5 (2014) 5422.
[97] G. Burnstock, U. Krugel, M.P. Abbracchio, P. Illes, Purinergic signalling: from normal behaviour to pathological brain function, Progress in neurobiology 95 (2011) 229-274.
[98] C. Agulhon, M.Y. Sun, T. Murphy, T. Myers, K. Lauderdale, T.A. Fiacco, Calcium Signaling and Gliotransmission in Normal vs. Reactive Astrocytes, Frontiers in pharmacology 3 (2012) 139.
[99] O. Pascual, K.B. Casper, C. Kubera, J. Zhang, R. Revilla-Sanchez, J.Y. Sul, H. Takano, S.J. Moss, K. McCarthy, P.G. Haydon, Astrocytic purinergic signaling coordinates synaptic networks, Science (New York, N.Y.) 310 (2005) 113-116.
[100] N. Reichenbach, A. Delekate, B. Breithausen, K. Keppler, S. Poll, T. Schulte, J. Peter, M. Plescher, J.N. Hansen, N. Blank, A. Keller, M. Fuhrmann, C. Henneberger, A. Halle, G.C. Petzold, P2Y1 receptor blockade normalizes network dysfunction and cognition in an Alzheimer's disease model, The Journal of experimental medicine 215 (2018) 1649-1663.
[101] K.I. Lee, H.T. Lee, H.C. Lin, H.J. Tsay, F.C. Tsai, S.K. Shyue, T.S. Lee, Role of transient receptor potential ankyrin 1 channels in Alzheimer's disease, Journal of neuroinflammation 13 (2016) 92.

[102] A. Bosson, A. Paumier, S. Boisseau, M. Jacquier-Sarlin, A. Buisson, M. Albrieux, TRPA1 channels promote astrocytic Ca(2+) hyperactivity and synaptic dysfunction mediated by oligomeric forms of amyloid-beta peptide, Molecular neurodegeneration 12 (2017) 53.
[103] M. Agostini, C. Fasolato, When, where and how? Focus on neuronal calcium dysfunctions in Alzheimer's Disease, Cell calcium 60 (2016) 289-298.
[104] R. Schmidt, E. Kienbacher, T. Benke, P. Dal-Bianco, M. Delazer, G. Ladurner, K. Jellinger, J. Marksteiner, G. Ransmayr, H. Schmidt, E. Stogmann, J. Friedrich, C. Wehringer, [Sex differences in Alzheimer's disease], Neuropsychiatrie : Klinik, Diagnostik, Therapie und Rehabilitation : Organ der Gesellschaft Osterreichischer Nervenarzte und Psychiater 22 (2008) 1-15.
[105] L. Ozmen, A. Albientz, C. Czech, H. Jacobsen, Expression of transgenic APP mRNA is the key determinant for beta-amyloid deposition in PS2APP transgenic mice, Neuro-degenerative diseases 6 (2009) 29-36.
[106] J.G. Richards, G.A. Higgins, A.M. Ouagazzal, L. Ozmen, J.N. Kew, B. Bohrmann, P. Malherbe, M. Brockhaus, H. Loetscher, C. Czech, G. Huber, H. Bluethmann, H. Jacobsen, J.A. Kemp, PS2APP transgenic mice, coexpressing hPS2mut and hAPPswe, show age-related cognitive deficits associated with discrete brain amyloid deposition and inflammation, The Journal of neuroscience : the official journal of the Society for Neuroscience 23 (2003) 8989-9003.
[107] R. Fontana, M. Agostini, E. Murana, M. Mahmud, E. Scremin, M. Rubega, G. Sparacino, S. Vassanelli, C. Fasolato, Early hippocampal hyperexcitability in PS2APP mice: role of mutant PS2 and APP, Neurobiology of aging 50 (2017) 64-76.
[108] G.P. Dugue, A. Dumoulin, A. Triller, S. Dieudonne, Target-dependent use of co-released inhibitory transmitters at central synapses, The Journal of neuroscience : the official journal of the Society for Neuroscience 25 (2005) 6490-6498.
[109] J.L. Stobart, K.D. Ferrari, M.J.P. Barrett, C. Gluck, M.J. Stobart, M. Zuend, B. Weber, Cortical Circuit Activity Evokes Rapid Astrocyte Calcium Signals on a Similar Timescale to Neurons, Neuron 98 (2018) 726-735 e724.
[110] F. Boscia, A. Pannaccione, R. Ciccone, A. Casamassa, C. Franco, I. Piccialli, V. de Rosa, A. Vinciguerra, G. Di Renzo, L. Annunziato, The expression and activity of KV3.4 channel subunits are precociously upregulated in astrocytes exposed to Abeta oligomers and in astrocytes of Alzheimer's disease Tg2576 mice, Neurobiology of aging 54 (2017) 187-198.
[111] R. Srinivasan, B.S. Huang, S. Venugopal, A.D. Johnston, H. Chai, H. Zeng, P. Golshani, B.S. Khakh, Ca(2+) signaling in astrocytes from Ip3r2(-/-) mice in brain slices and during startle responses in vivo, Nature neuroscience 18 (2015) 708-717.
[112] L. Mariotti, G. Losi, A. Lia, M. Melone, A. Chiavegato, M. Gomez-Gonzalo, M. Sessolo, S. Bovetti, A. Forli, M. Zonta, L.M. Requie, I. Marcon, A. Pugliese, C. Viollet, B. Bettler, T. Fellin, F. Conti, G. Carmignoto, Interneuron-specific signaling evokes distinctive somatostatin-mediated responses in adult cortical astrocytes, Nature communications 9 (2018) 82.
[113] L.T. Woods, D. Ajit, J.M. Camden, L. Erb, G.A. Weisman, Purinergic receptors as potential therapeutic targets in Alzheimer's disease, Neuropharmacology 104 (2016) 169-179.
[114] T.A. Woolsey, H. Van der Loos, The structural organization of layer IV in the somatosensory region (SI) of mouse cerebral cortex. The description of a cortical field composed of discrete cytoarchitectonic units, Brain research 17 (1970) 205-242.
[115] C. Henneberger, T. Papouin, S.H. Oliet, D.A. Rusakov, Long-term potentiation depends on release of D-serine from astrocytes, Nature 463 (2010) 232-236.

[116] L. Mariotti, G. Losi, M. Sessolo, I. Marcon, G. Carmignoto, The inhibitory neurotransmitter GABA evokes long-lasting Ca(2+) oscillations in cortical astrocytes, Glia 64 (2016) 363-373.
[117] M. Navarrete, G. Perea, L. Maglio, J. Pastor, R. Garcia de Sola, A. Araque, Astrocyte calcium signal and gliotransmission in human brain tissue, Cerebral cortex (New York, N.Y. : 1991) 23 (2013) 1240-1246.
[118] N. Takata, T. Mishima, C. Hisatsune, T. Nagai, E. Ebisui, K. Mikoshiba, H. Hirase, Astrocyte calcium signaling transforms cholinergic modulation to cortical plasticity in vivo, The Journal of neuroscience : the official journal of the Society for Neuroscience 31 (2011) 18155-18165.
[119] M.M. Halassa, C. Florian, T. Fellin, J.R. Munoz, S.Y. Lee, T. Abel, P.G. Haydon, M.G. Frank, Astrocytic modulation of sleep homeostasis and cognitive consequences of sleep loss, Neuron 61 (2009) 213-219.
[120] J. Han, P. Kesner, M. Metna-Laurent, T. Duan, L. Xu, F. Georges, M. Koehl, D.N. Abrous, J. Mendizabal-Zubiaga, P. Grandes, Q. Liu, G. Bai, W. Wang, L. Xiong, W. Ren, G. Marsicano, X. Zhang, Acute cannabinoids impair working memory through astroglial CB1 receptor modulation of hippocampal LTD, Cell 148 (2012) 1039-1050.
[121] M. Tanaka, P.Y. Shih, H. Gomi, T. Yoshida, J. Nakai, R. Ando, T. Furuichi, K. Mikoshiba, A. Semyanov, S. Itohara, Astrocytic Ca2+ signals are required for the functional integrity of tripartite synapses, Molecular brain 6 (2013) 6.
[122] X. Yu, A.M.W. Taylor, J. Nagai, P. Golshani, C.J. Evans, G. Coppola, B.S. Khakh, Reducing Astrocyte Calcium Signaling In Vivo Alters Striatal Microcircuits and Causes Repetitive Behavior, Neuron (2018).
[123] A. Lia, M. Zonta, L.M. Requie, G. Carmignoto, Dynamic interactions between GABAergic and astrocytic networks, Neuroscience letters (2018).
[124] S. Camandola, M.P. Mattson, Aberrant subcellular neuronal calcium regulation in aging and Alzheimer's disease, Biochimica et biophysica acta 1813 (2011) 965-973.
[125] K.N. Green, F.M. LaFerla, Linking calcium to Abeta and Alzheimer's disease, Neuron 59 (2008) 190-194.
[126] C. Lazzari, M.J. Kipanyula, M. Agostini, T. Pozzan, C. Fasolato, Abeta42 oligomers selectively disrupt neuronal calcium release, Neurobiology of aging 36 (2015) 877-885.
[127] T. Chen, M. Tanaka, Y. Wang, S. Sha, K. Furuya, L. Chen, M. Sokabe, Neurosteroid dehydroepiandrosterone enhances activity and trafficking of astrocytic GLT-1 via sigma1 receptor-mediated PKC activation in the hippocampal dentate gyrus of rats, Glia 65 (2017) 1491-1503.
[128] E. Masliah, M. Alford, R. DeTeresa, M. Mallory, L. Hansen, Deficient glutamate transport is associated with neurodegeneration in Alzheimer's disease, Annals of neurology 40 (1996) 759-766.
[129] J.K. Hefendehl, J. LeDue, R.W. Ko, J. Mahler, T.H. Murphy, B.A. MacVicar, Mapping synaptic glutamate transporter dysfunction in vivo to regions surrounding Abeta plaques by iGluSnFR two-photon imaging, Nature communications 7 (2016) 13441.
[130] A. Grinvald, E. Lieke, R.D. Frostig, C.D. Gilbert, T.N. Wiesel, Functional architecture of cortex revealed by optical imaging of intrinsic signals, Nature 324 (1986) 361-364.
[131] S. Sheth, M. Nemoto, M. Guiou, M. Walker, N. Pouratian, A.W. Toga, Evaluation of coupling between optical intrinsic signals and neuronal activity in rat somatosensory cortex, NeuroImage 19 (2003) 884-894.
[132] M. Sintsov, D. Suchkov, R. Khazipov, M. Minlebaev, Developmental Changes in Sensory-Evoked Optical Intrinsic Signals in the Rat Barrel Cortex, Frontiers in cellular neuroscience 11 (2017) 392.
[133] J.F. Oliveira, V.M. Sardinha, S. Guerra-Gomes, A. Araque, N. Sousa, Do stars govern our actions? Astrocyte involvement in rodent behavior, Trends in neurosciences 38 (2015) 535-549.

Acknowledgments

We acknowledge L. Ozmen and F. Hoffmann-La Roche Ltd (Basel, Switzerland) for kindly donating the transgenic mice used in this study and the Cariparo Foundation for funding the PhD fellowship.

Publications

1. Letizia Mariotti*, Gabriele Losi*, Annamaria Lia, Marcello Melone, Angela Chiavegato, Marta Gómez-Gonzalo, Michele Sessolo, Serena Bovetti, Angelo Forli, Micaela Zonta, Linda Maria Requie, Iacopo Marcon, Arianna Pugliese, Cécile Viollet, Bernhard Bettler, Tommaso Fellin, Fiorenzo Conti & Giorgio Carmignoto (2018) Interneuron-specific signaling evokes distinctive somatostatin-mediated responses in adult cortical astrocytes. *Nature Communication* 9:82

2. Annamaria Lia, Micaela Zonta, Linda Maria Requie & Giorgio Carmignoto (2018) Dynamic interactions between GABAergic and astrocytic networks. *Neuroscience Letters*

nature COMMUNICATIONS

ARTICLE

DOI: 10.1038/s41467-017-02642-6 OPEN

Interneuron-specific signaling evokes distinctive somatostatin-mediated responses in adult cortical astrocytes

Letizia Mariotti[1,2], Gabriele Losi[1,2], Annamaria Lia[1,2], Marcello Melone[3,4], Angela Chiavegato[2], Marta Gómez-Gonzalo[1,2], Michele Sessolo[1,2], Serena Bovetti[5], Angelo Forli[5], Micaela Zonta[1,2], Linda Maria Requie[1,2], Iacopo Marcon[1,2], Arianna Pugliese[3], Cécile Viollet[6], Bernhard Bettler[7], Tommaso Fellin[5], Fiorenzo Conti[3,4,8] & Giorgio Carmignoto[1,2]

The signaling diversity of GABAergic interneurons to post-synaptic neurons is crucial to generate the functional heterogeneity that characterizes brain circuits. Whether this diversity applies to other brain cells, such as the glial cells astrocytes, remains unexplored. Using optogenetics and two-photon functional imaging in the adult mouse neocortex, we here reveal that parvalbumin- and somatostatin-expressing interneurons, two key interneuron classes in the brain, differentially signal to astrocytes inducing weak and robust $GABA_B$ receptor-mediated Ca^{2+} elevations, respectively. Furthermore, the astrocyte response depresses upon parvalbumin interneuron repetitive stimulations and potentiates upon somatostatin interneuron repetitive stimulations, revealing a distinguished astrocyte plasticity. Remarkably, the potentiated response crucially depends on the neuropeptide somatostatin, released by somatostatin interneurons, which activates somatostatin receptors at astrocytic processes. Our study unveils, in the living brain, a hitherto unidentified signaling specificity between interneuron subtypes and astrocytes opening a new perspective into the role of astrocytes as non-neuronal components of inhibitory circuits.

[1] Neuroscience Institute, National Research Council (CNR), 35121 Padova, Italy. [2] Department of Biomedical Sciences, Università degli Studi di Padova, 35121 Padova, Italy. [3] Department of Experimental and Clinical Medicine, Università Politecnica delle Marche, 60126 Ancona, Italy. [4] Center for Neurobiology of Aging, INRCA IRCCS, 60121 Ancona, Italy. [5] Optical Approches to Brain Function Laboratory, Department of Neuroscience and Brain Technologies, Istituto Italiano di Tecnologia, 16163 Genova, Italy. [6] Inserm UMR894, Center for Psychiatry and Neuroscience, Université Paris-Descartes, 75014 Paris, France. [7] Departement of Biomedicine, University of Basel, 4031 Basel, Switzerland. [8] Foundation for Molecular Medicine, Università Politecnica delle Marche, 60126 Ancona, Italy. Letizia Mariotti and Gabriele Losi contributed equally to this work. Correspondence and requests for materials should be addressed to G.C. (email: giorgio.carmignoto@bio.unipd.it)

Inhibition is a fundamental operational mechanism in the brain that is governed by GABAergic interneurons[1,2]. A large diversity of interneurons in terms of morphology, connectivity, molecular and functional properties ensures a signaling specificity to surrounding neurons. These unique features allow the different GABAergic interneurons to strictly control local network excitability and modulate synaptic transmission[1,2]. Among key interneurons in the neocortex are parvalbumin (PV)- and somatostatin (SST)-expressing interneurons. The former regulate the spike-timing and the gain of pyramidal neurons by targeting soma and proximal dendrites, while the latter control signal integration and synaptic plasticity by targeting the distal dendrites of pyramidal neurons[1–4].

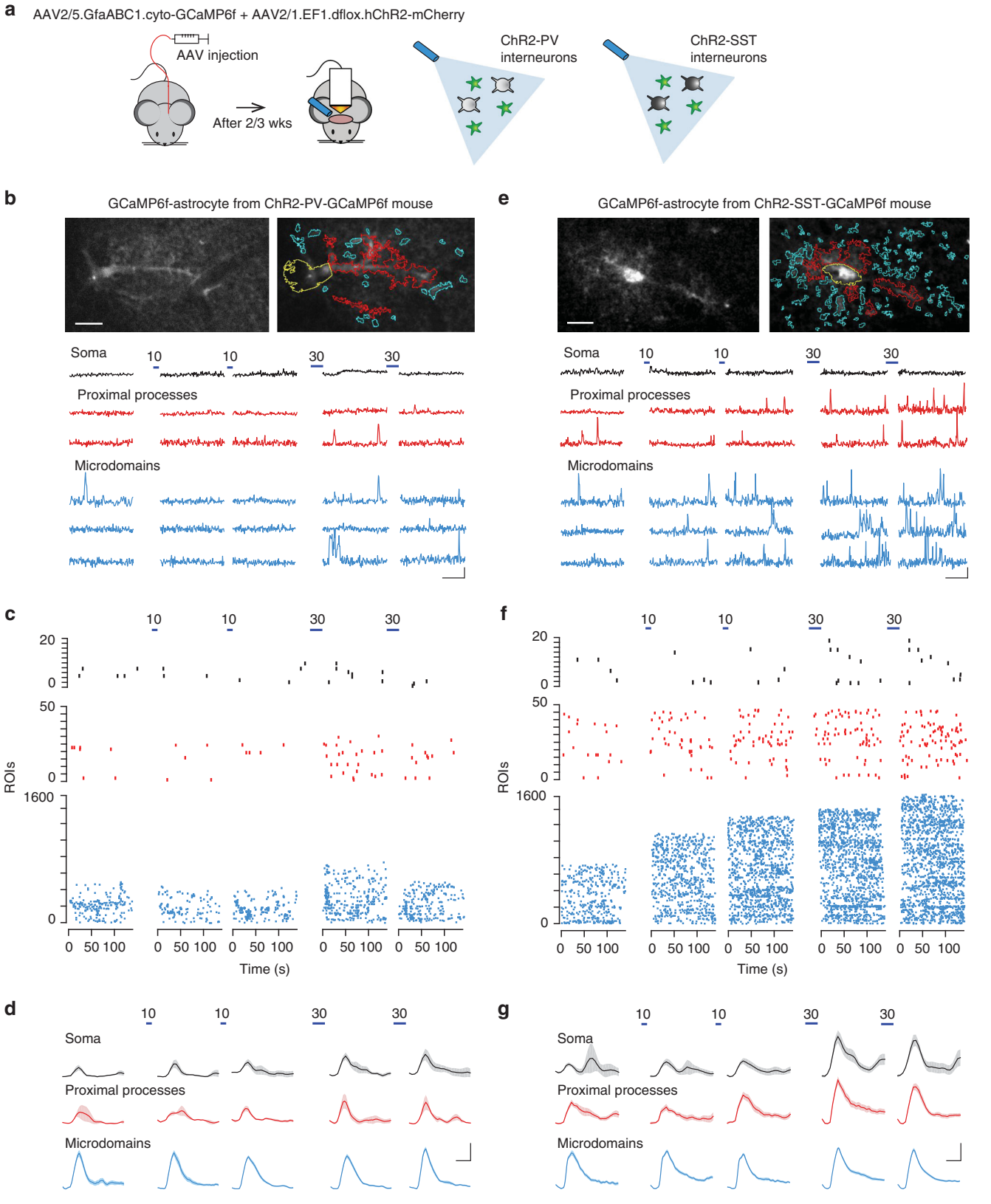

The glial cells astrocytes are additional modulatory elements of local network excitability and synaptic transmission[5,6]. In vivo studies revealed that different neurotransmitter systems, including glutamatergic, acetylcholinergic, and noradrenergic pathways[7–10], signal to astrocytes inducing in these cells complex cytosolic Ca^{2+} changes that represent a key event in the action of astrocytes in local brain circuits[5,6,11–13]. Astrocytes have been proposed to crucially affect GABAergic synaptic transmission[14–16], but whether the various interneuron classes, which warrant the specificity of GABAergic signaling to postsynaptic neurons, also specifically signal to astrocytes is a question that remains completely unexplored. We here address this issue in the mouse somatosensory cortex (SSCx) and study the signaling to astrocytes of PV and SST interneurons by combining optogenetics with 2-photon Ca^{2+} imaging in in vivo and in situ slice experiments.

Results

Experimental set-up. To selectively stimulate PV or SST interneurons and evaluate potential Ca^{2+} responses of astrocytes, we used an adeno-associated virus (AAV)-based strategy (Fig. 1a). Through this approach, we induced in PV interneurons of adult PV-Cre mice or SST interneurons of adult SST-Cre mice, the selective expression of the light-gated cation channel channelrhodopsin-2 (ChR2)[17] (Supplementary Fig. 1a–d) and in astrocytes the sparse expression of GCaMP6f (Supplementary Fig. 2a, b), a genetically encoded Ca^{2+} indicator (GECI)[18–20] (ChR2-PV-GCaMP6f or ChR2-SST-GCaMP6f mice, see Methods).

Parvalbumin interneurons evoke depressing Ca^{2+} responses. We first studied Ca^{2+} signal dynamics in different compartments of GCaMP6f-expressing astrocytes including the soma, the proximal processes and the fine processes exhibiting spatially restricted Ca^{2+} transients, i.e., Ca^{2+} microdomains[19,21,22], in the SSCx of ChR2-PV-GCaMP6f mice (Fig. 1) and quantified their basic properties (Fig. 2). We applied 10 light pulses ($\lambda = 473$ nm, 150 ms duration, 1 Hz) that induced in ChR2-expressing PV interneurons firing activity (mean firing rate, 40.8 ± 5.75 Hz; Supplementary Fig. 3) comparable to that exhibited by these interneurons in awake mice[3]. No Ca^{2+} elevations were observed in GCaMP6f-astrocytes either during (Supplementary Fig. 4a, b) or after (Fig. 1b, c) the 10 pulse stimulation. Equally ineffective was a second episode of this type of PV interneuron stimulation applied with a 5-min interval. Only a more prolonged activation by 30 pulses induced at both proximal processes and microdomains, an increase in the mean number of active sites (regions of interest, ROIs) and the frequency of Ca^{2+} transients, whereas Ca^{2+} event amplitude was increased in the proximal processes and remained unchanged in the microdomains (Fig. 1b–d; Fig. 2b, c, open bars, Supplementary Movie 1). As revealed by both the raster plots reporting the Ca^{2+} events from all the monitored GCaMP6f-astrocytes (Fig. 1c) and the quantification of Ca^{2+} response properties (Fig. 2), a second 30 pulse stimulation evoked reduced Ca^{2+} elevations suggesting a depression of the astrocyte response to successive episodes of PV interneuron activity.

Somatostatin interneurons evoke potentiating Ca^{2+} responses. We then studied the Ca^{2+} dynamics in GCaMP6f-expressing astrocytes from ChR2-SST-GCaMP6f mice. Optogenetic stimulation by 10 light pulses (150 ms duration, 1 Hz) induced in ChR2-expressing SST interneurons in vivo a firing activity (mean firing rate, 13.4 ± 2.4 Hz; Supplementary Fig. 3) comparable to that exhibited by these interneurons in awake mice[23,24]. To support this finding, we performed fluorescence-guided juxtasomal recordings in layer 2 of the somatosensory cortex of awake head-fixed mice, trained to remain still under the microscope (Supplementary Fig. 5a). Compatibly with previous studies, SST interneurons exhibited periods of spontaneous firing containing brief bursts of high instantaneous activity (Supplementary Fig. 5b–d) similar to that induced in these neurons by our optogenetic stimulation. In contrast to PV interneurons, 10 light pulse stimulation of SST interneurons was sufficient to activate GCaMP6f-astrocytes (Fig. 1e, f) inducing an increase in the mean number of active ROIs and the mean frequency of Ca^{2+} events in both proximal processes and microdomains (Fig. 2b, c, closed bars; Supplementary Movie 2). As in the astrocyte response to PV stimulation, the amplitude of Ca^{2+} events increased only in the proximal processes. These data indicate that astrocytes are more sensitive to SST than PV interneuron activity. Interestingly, with respect to the first, a second episode of SST interneuron activation by 10 pulses applied with a 5-min interval induced a greater Ca^{2+} response in astrocytes and a similar potentiation was observed following the two successive 30 pulse stimulations. The raster plots (Fig. 1f) and the quantification of Ca^{2+} response in the proximal processes and microdomains (Fig. 2b, c) confirm that, with respect to the first, a second episode of SST interneuron stimulation (by either 10 or 30 pulses) was significantly more effective, rather than less effective as in the case of PV interneuron stimulation, indicating a potentiation of the astrocyte response to SST interneuron signaling. The response depression to PV interneurons and the response potentiation to SST interneurons are confirmed by the significant leftward and rightward shift, respectively, in the cumulative distributions of Ca^{2+} event frequency (Fig. 2d). These in vivo results were fully replicated in SSCx slices obtained from young ChR2-PV- and ChR2-SST-GCaMP6f mice (Supplementary Figs. 6 and 7).

Integration of Ca^{2+} microdomain responses. With respect to spontaneous events, the mean amplitude of evoked Ca^{2+} elevations in the proximal processes was significantly increased in response to activation of PV or SST interneurons (Fig. 1d, g, red traces and Fig. 2b, right panel), whereas that of evoked Ca^{2+} microdomains was unchanged (Fig. 1d, g, blue traces; Fig. 2c, right panel; see also Supplementary Figs. 6 and 7). These data suggest that the interneuron signaling is essentially encoded into an increased microdomain frequency in the astrocytic fine processes and subsequently integrated in the proximal processes into larger amplitude Ca^{2+} elevations. Whether this signal integration

Fig. 1 Calcium signal dynamics reveal differential astrocyte responses to PV and SST interneuron activation. **a** Schematic of the in vivo experimental approach (left) and of the optogenetic stimulation of ChR2-PV or ChR2-SST interneurons (right). **b** Top, images of a representative GCaMP6f-astrocyte in layer 2/3 SSCx from an adult ChR2-PV-GCaMP6f mouse with the ROIs defined by GECIquant software for the Ca^{2+} response to the first 30 light pulse stimulation (blue lines) of PV interneurons at the soma (yellow), proximal processes (red), and microdomains (blue), scale bar, 20 μm (see Supplementary Movie 3). Bottom, Ca^{2+} signal dynamics at different astrocytic compartments before and after successive 10 and 30 light pulse PV interneuron activations. Scale bars, 50 s, 20% dF/F_0. **c**, **d** Raster plots of Ca^{2+} peaks (**c**) and mean time course of Ca^{2+} transients (**d**) from all in vivo monitored GCaMP6f-astrocytes, at rest and following PV interneuron stimulations. Scale bar, 5 s, 20% dF/F_0. **e**–**g** Same as in **b**–**d**, but for ChR2-SST-GCaMP6f mice and SST interneuron stimulation

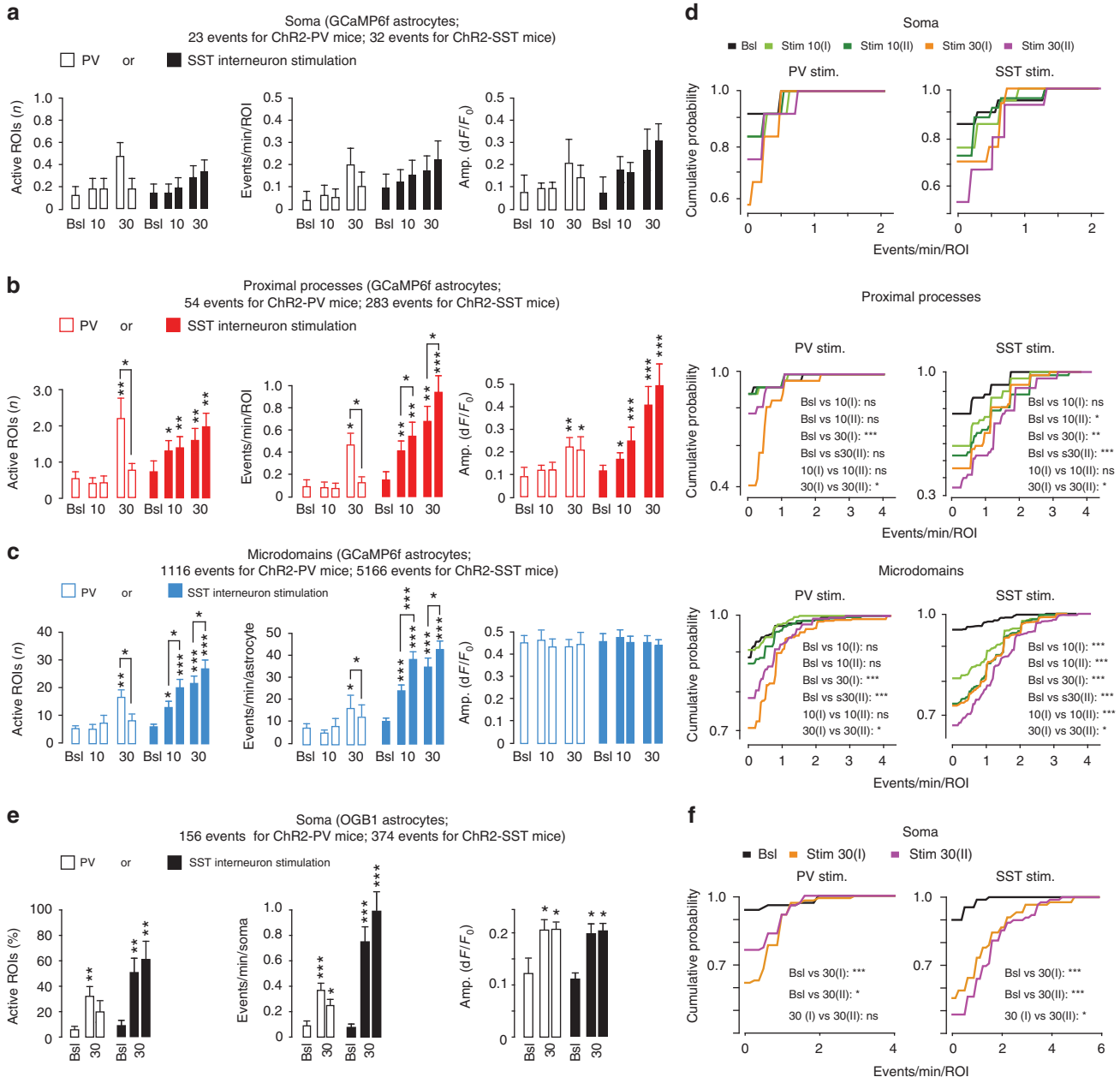

Fig. 2 Properties of the astrocyte response to PV and SST interneurons in vivo. **a**–**c** Average data of Ca^{2+} signal dynamics at different compartments of GCaMP6f-astrocytes from ChR2-PV- or ChR2-SST-GCaMP6f mice in response to PV interneuron (14 astrocytes, 7 mice) and SST interneuron signaling (20 astrocytes, 8 mice). **d**, **f** Cumulative distributions of astrocytic Ca^{2+} events confirming significant response depression to successive PV interneuron stimulations and significant response potentiation to successive SST interneuron stimulations. $^{*}p \leq 0.05$, $^{**}p \leq 0.01$; $^{***}p \leq 0.001$, Kolmogorov–Smirnov test. Exact *p*-values for the data reported in this as well as all the other figures are reported in the Supplementary Table 4e. Mean percentage of responsive astrocytes, mean frequency and amplitude of somatic Ca^{2+} events in response to PV interneuron (white bars, 100 astrocytes, 6 ChR2-PV mice) or SST interneuron (black bars, 90 astrocytes, 7 ChR2-SST mice) optogenetic activation in the SSCx in vivo after loading with OGB-1 and the specific astrocytic marker SR101. Data are represented as mean ± SEM

involves also the astrocytic soma is, however, unclear. Indeed, due to the documented sparse nature of GCaMP6f expression in astrocytes[20], somatic Ca^{2+} events in ChR2-PV- and ChR2-SST-GCaMP6f mice were analyzed from a limited number of cells. We therefore addressed this issue in ChR2-PV or ChR2-SST mice after loading a large number of astrocytes with chemical Ca^{2+} indicators, such as Oregon Green BAPTA-1 or Fluo-4-AM, and SR101, a specific astrocytic marker[25]. By evaluating Ca^{2+} signals in vivo (Fig. 2e; Supplementary Fig. 8) and in slice preparations (Supplementary Fig. 9), we observed somatic Ca^{2+} response of astrocytes to both PV and SST interneurons. These results suggest that the integration of microdomain Ca^{2+} signals involve, in addition to the proximal processes, also the astrocytic soma. The cumulative distributions of event frequency also revealed a significant potentiation of somatic Ca^{2+} signals in response to SST interneurons and a tendency to depression in response to PV interneurons (Fig. 2f; Supplementary Fig. 9f).

Altogether, these data demonstrate that astrocytes differently respond to PV and SST interneurons and change their Ca^{2+} response as a function of the previous history of activity in the surrounding GABAergic interneuron type-specific network.

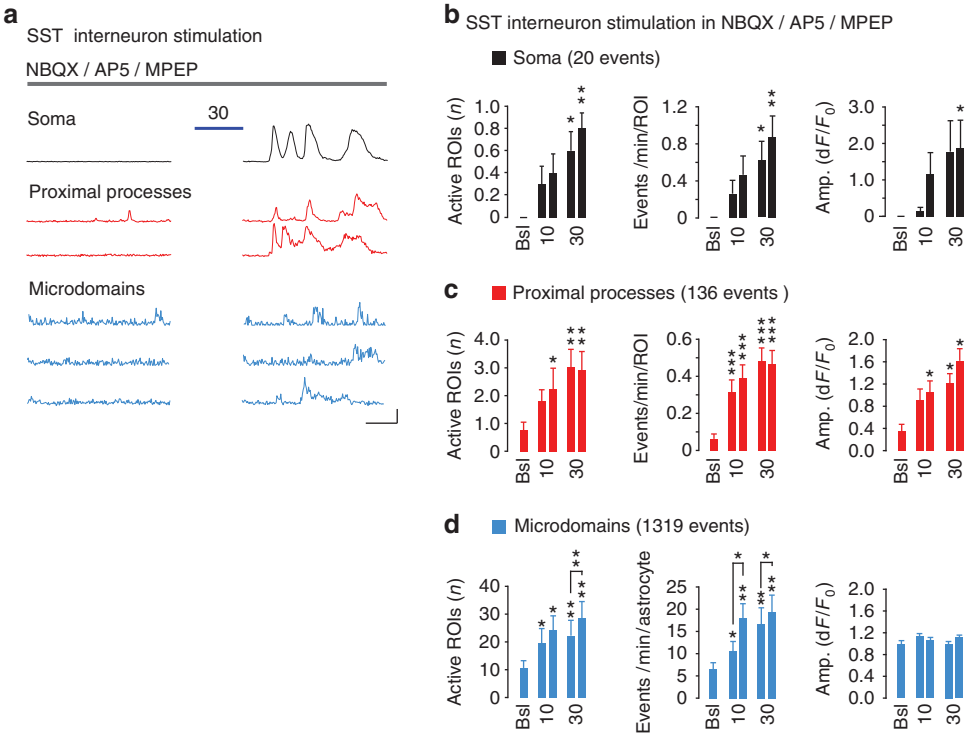

Fig. 3 Astrocyte response to SST interneurons does not depend on glutamatergic transmission. **a** Representative traces and **b**–**d** quantitative evaluation of GCaMP6f-astrocyte responses to SST interneuron activation (10 or 30 light pulses) in SSCx slice preparations (9 astrocytes, 9 slices, 3 mice) in the presence of NBQX (10 μM), D-AP5 (50 μM), and MPEP (50 μM). Scale bars, 20 s, 50% dF/F_0. Data are means ± SEM

We next performed additional in vivo and brain slice experiments to obtain further insights into PV and SST interneuron signaling and to control the specificity of the astrocyte response. In SSCx slice preparations, we found that the increased Ca^{2+} elevations induced by interneuron signaling in the different astrocytic compartments, including microdomains, were mediated by activation of $GABA_B$ receptors ($GABA_BRs$) because they were abolished by the specific $GABA_BR$ antagonist SCH50911 (Supplementary Figs. 7 and 9). These responses were independent on TRPA1 channel activation (Supplementary Fig. 10), a channel that has been previously proposed to modulate spontaneous microdomain activity[26]. The microdomain responses were detected with a delay of 14.93 ± 1.34 s from the onset of 10 pulse activation of SST interneurons and with longer delays in the proximal processes and soma, which may reflect slow intracellular $GABA_BR$-mediated signaling pathways. A similar delay (14.97 ± 1.30 s; $p = 0.949$) of the microdomain response was measured following the onset of 30 pulse activation of SST interneurons (Supplementary Fig. 4c, d) suggesting that the duration of interneuron stimulation does not affect the delay of the astrocyte response. Altogether, these results suggest that astrocytes do not respond rapidly to synaptically released GABA and accompany a sustained interneuron activity with multiple, slowly developing $GABA_BR$-mediated Ca^{2+} elevations.

We also evaluated the time window of the astrocyte response potentiation to SST interneuron signaling by increasing the interval between the first and the second SST interneuron stimulation. We found that the potentiation is a transient phenomenon as it was absent with 20-min intervals ($p = 0.688$) and observed with 10-min intervals only as a small, albeit significant ($p = 0.031$), increase in the mean number of active microdomains (Supplementary Fig. 11).

To rule out the possibility of unspecific effects produced on astrocytes by prolonged illumination with the imaging laser[27], we monitored Ca^{2+} signals in astrocytes from ChR2-SST- or ChR2-PV-GCaMP6f mice without optogenetic stimulation. We failed to detect during the imaging sessions any significant change in the frequency or the amplitude of Ca^{2+} peaks in the different astrocytic compartments, in both in vivo (Supplementary Fig. 12a–c) and SSCx slice experiments (Supplementary Fig. 12d–f).

The results obtained with the specific $GABA_BR$ antagonist SCH50911 indicate a direct effect of synaptic GABA on astrocytes. The astrocyte response to interneurons might, however, be due, at least in part, to an increased local network excitability deriving from the inhibition exerted by SST interneurons on PV interneuron firing that, in turn, reduces the inhibition of PV interneurons to pyramidal neurons, ultimately enhancing glutamatergic signaling[28,29]. To address this hypothesis, we stimulated SST interneurons in the presence of different glutamate receptor selective blockers, i.e., NBQX (10 μM, 2,3-dihydroxy-6-nitro-7-sulfamoyl-benzo(F)quinoxaline) for AMPARs, D-AP5 (50 μM, D-2-amino-5-phosphonopentanoate) for NMDARs and MPEP (50 μM, Methyl-6-(phenylethynyl) pyridine) for the metabotropic glutamate type 5 receptor. Under these conditions, the overall Ca^{2+} response of astrocytes to SST interneuron signaling was unchanged (Fig. 3) suggesting that glutamatergic signaling does not contribute to the astrocyte response to SST interneuron activity.

The depression of astrocytic Ca^{2+} elevations in response to PV interneurons and the potentiation in response to SST interneurons could be due to a change in the synaptic release of GABA rather than to an intrinsic astrocytic property. To address this hypothesis, we measured the firing rate from PV and SST interneurons and the amplitude of evoked inhibitory post-synaptic currents (IPSCs) from pyramidal neurons, at each light pulse in the two sets of 10 and in the two sets of 30 light pulses applied with a 5-min interval. In the case of PV interneurons,

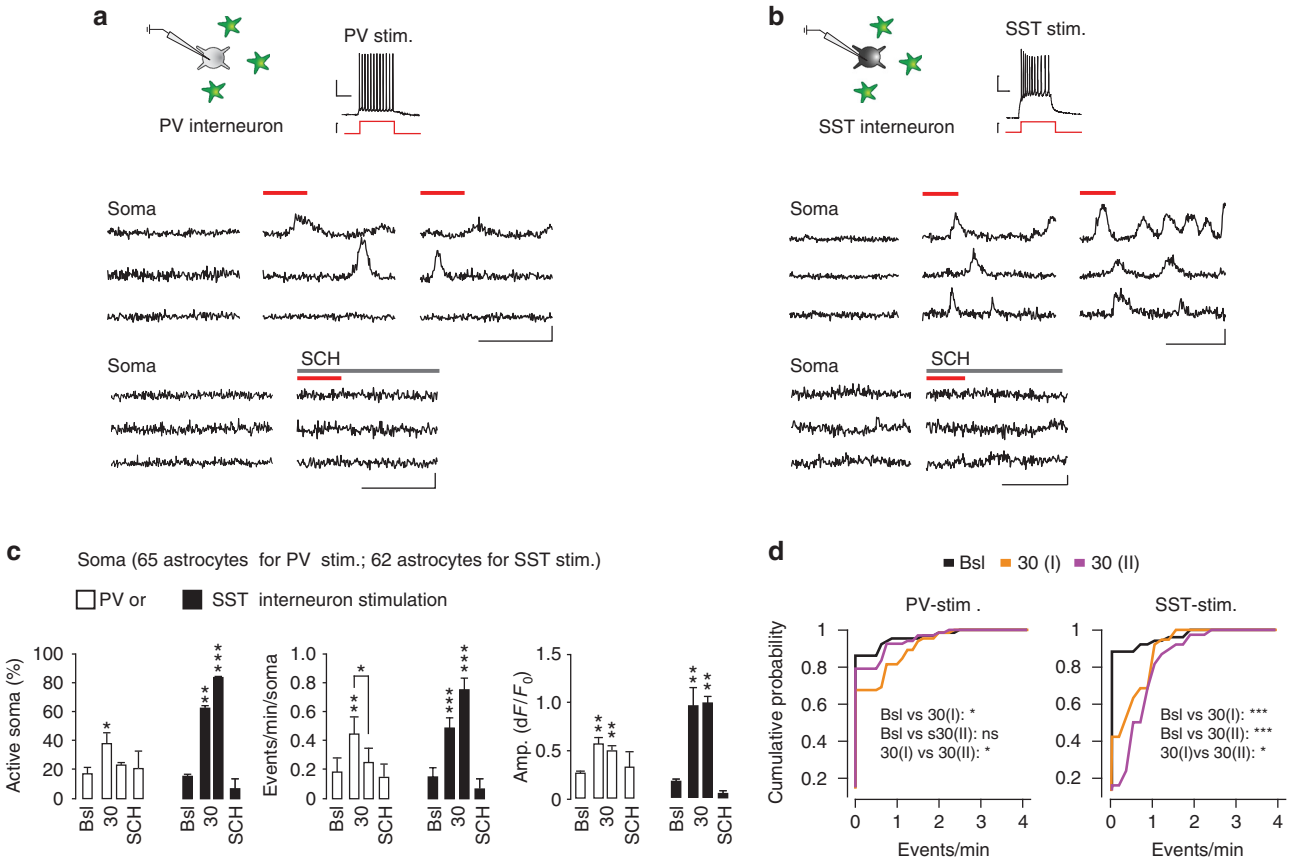

Fig. 4 GABAergic signaling from individual PV or SST interneurons in SSCx slices is sufficient to recruit neighboring astrocytes. **a**, **b** Top, schematics of patch-clamp experiments and representative AP firing induced by intracellular depolarizing current pulse injections into a PV (mean firing rate, 11.8 ± 2.1 Hz) or a SST interneuron (mean firing rate 9.0 ± 1.44 Hz; burst firing rate, 30 ± 4.8 Hz). Scale bars, 100 ms, 20 mV, 200 pA. Bottom: somatic Ca^{2+} signal dynamics from representative astrocytes before and after two sequences of 30 current pulses (red lines) delivered to PV or SST interneurons in absence or presence of SCH50911 (SCH, 50 µM). Astrocytes from an area within 100 µm from the patched interneuron were considered. Scale bars, 50 s, 20% dF/F_0. **c** Mean percentage of responsive astrocytes and mean Ca^{2+} oscillation frequency in response to individual PV (65 astrocytes, 4 slices, 4 mice) or SST interneuron (62 astrocytes, 4 slices, 4 mice) stimulation. Data are represented as mean ± SEM. **d** Cumulative distributions of Ca^{2+} event frequency after two subsequent 30 current pulse injections. With respect to the first stimulation, the astrocyte response to the second PV interneuron stimulation was significantly depressed, whereas that to the second SST interneuron stimulation was significantly potentiated (Kolmogorov–Smirnov test, $^{*}p \leq 0.05$, $^{**}p \leq 0.01$, $^{***}p \leq 0.001$)

besides an unchanged firing rate during each set of light pulses, we observed a reduction in IPSC amplitude (Supplementary Fig. 13e) that can be indicative of a $GABA_A$ receptor desensitization[30] and/or a decrease in synaptic GABA release. The IPSC reduction during the two sets of 30 pulse PV interneuron stimulation was, however, similar, in terms of both its time course ($p = 0.66$ and $p = 0.83$ for the fast and the slow time decay component, respectively) and amplitude ($p = 0.55$; Supplementary Fig. 13e, f) suggesting that a decrease in GABA release cannot explain the impairment of the astrocyte response to the second PV interneuron stimulation. In the case of SST interneurons, both the firing rate (Supplementary Fig. 13g–i) and the evoked IPSC amplitude (Supplementary Fig. 13j–l) were unchanged suggesting that the astrocyte response potentiation to SST interneurons is unlikely due to an increase in the amount of synaptically released GABA. However, direct measurements of GABA concentrations would be necessary to validate this conclusion.

Individual PV or SST interneurons recruit nearby astrocytes. The optogenetic activation induces synaptic GABA release from a large number of ChR2-expressing interneurons. We asked whether a more restricted release of GABA, such as that deriving from activation of a single interneuron, also recruits neighboring astrocytes. To address this question, we used SSCx slices from tdTomato-floxed::PV- and SST-Cre mice as well as G42 and GIN mice expressing the enhanced green fluorescence protein (GFP) in a subset of PV- or SST-positive interneurons, respectively, after astrocyte loading with Fluo-4-AM and SR101. We found that astrocytes from an area within 100 µm from the patched interneuron were effectively recruited by individual PV or SST interneuron activation (30 depolarizing current pulses, 300-ms duration, 1 Hz) and they exhibited potentiated Ca^{2+} elevations in response to SST interneuron and depressed Ca^{2+} elevations in response to PV interneuron stimulation (Fig. 4d). Both responses were sensitive to the $GABA_BR$ antagonist SCH50911 (Fig. 4a–c). A localized synaptic GABA release from a single interneuron is, therefore, sufficient to recruit nearby astrocytes evoking a response with the same properties as those of the response observed in the optogenetic experiments.

Crucial role of the neuropeptide somatostatin. To clarify whether the mechanism of the higher sensitivity of astrocytes to SST than PV interneurons derives from a closer position of

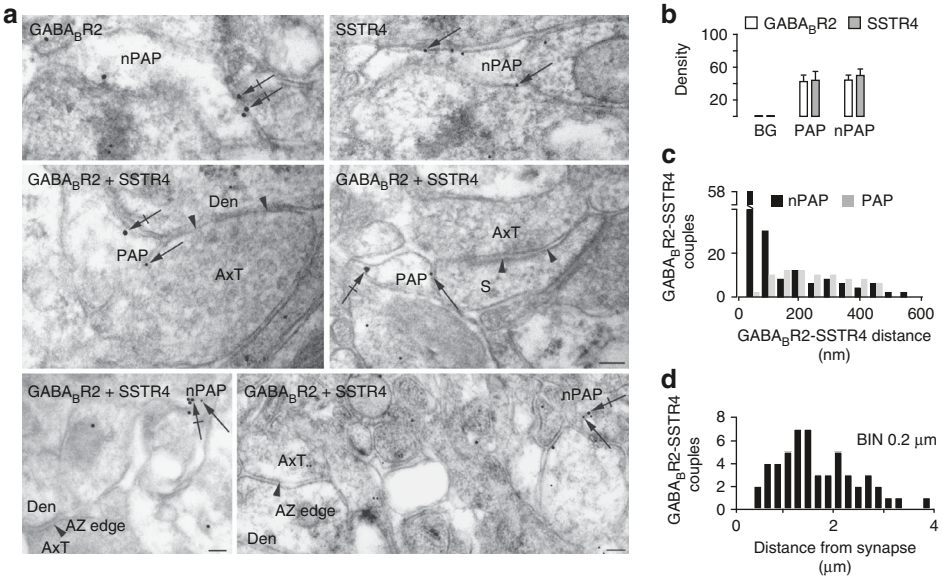

Fig. 5 GABA$_B$Rs and SST4Rs colocalize at non perisynaptic astrocytic processes (nPAPs). **a** Upper row, GABA$_{B2}$ and SSTR4 immunogold EM single-labeled nPAPs (arrows point to 18 and 12 nm membrane-associated gold particles, respectively). Middle row, GABA$_{B2}$-SSTR4 double-labeled PAPs nearby to an axo-dendritic shaft (left) and an axo-spinous (right) symmetric synapse (arrowheads point to edges of active zones). Lower row, double-labeled nPAPs not in the proximity of symmetric synapses (arrowheads). **b** GABA$_{B2}$ and SSTR4 relative density (particles/µm^2) in double-labeled PAPs ($n = 40$) and nPAPs ($n = 77$) is higher than background (BG; $p < 0.0001$, Mann–Whitney test), whereas it is similar between PAPs and nPAPs. **c** Distance distribution of immunogold GABA$_{B2}$ and SSTR4 pairs at PAP membranes (40 pairs from 37 PAPs) and nPAPs (100 pairs from 97 nPAPs). **d** Lateral position of GABA$_{B2}$ and SSTR4 pairs with an edge-to-edge distance within 50 nm with respect to the closest AZ margin of a symmetric synapse (53 couples from 53 nPAPs). Axt, axon terminal; Den, dendrite; s, spine. Scale bars, 100 nm

astrocytic processes to SST than PV interneuron synapses, we performed electron microscope (EM) immunocytochemical experiments. Obtained data revealed, however, similar structural relationships between astrocytic processes and PV/SST interneuron synapses (Supplementary Fig. 14; Table 1).

The different astrocytic response to PV and SST interneurons may be due to a different molecular signaling between these interneuron classes and astrocytes. To address this hypothesis, we studied whether the neuropeptide SST, that is released in addition to GABA by SST interneurons[31], contributes to the response of astrocytes. In double-immunogold EM experiments, we first investigated whether astrocytes express SST receptors, focusing on the SST type 4 receptor (SSTR4), which was previously described in astrocytes from cell culture and hippocampal slice preparations[32,33]. Post-embedding EM experiments revealed that astrocytic processes express both GABA$_{B2}$ and SSTR4 with similar densities at perisynaptic astrocytic processes (PAPs) and at processes not contacting symmetric synapses (nPAPs; Fig. 5a, b). Most interestingly, pairs of GABA$_{B2}$-SSTR4 gold particles exhibiting an edge-to-edge separation distance within 50 nm, were found almost exclusively at nPAPs (Fig. 5c) suggesting functional interactions between the two receptors. Notably, the GABA$_{B2}$-SSTR4 couples (<50 nm) were found at nPAPs at a mean distance of 1.79 ± 0.10 µm from symmetric synapses (Fig. 5d).

The specificity of the anti-GABA$_{B2}$ and anti-SSTR4 antibodies used in our EM immunocytochemical study was validated in experiments on GABA$_{B2}$[34] and SSTR4[35] knockout mice (Supplementary Figs. 15 and 16; Supplementary Tables 2 and 3).

We then asked whether activation of astrocytic SSTRs could induce per se Ca^{2+} signal changes. We found that application of the neuropeptide SST (1–2 µM) induced a weak, albeit significant, increase of Ca^{2+} event frequency in GCaMP6f-astrocytes from SSCx slices (Fig. 6a, b). In the presence of tetrodotoxin (TTX, 1 µM) and a cocktail of different neurotransmitter receptor antagonists, such as SCH (50 µM, for GABA$_B$R), MPEP (50 µM, for mGluR5), and PPADS (100 µM, for P2YR), the response of astrocytes to SST was unchanged suggesting a direct action of SST on astrocytic SSTRs (Fig. 6c).

These observations prompted us to directly investigate whether a synergistic action of SST may occur on GABA-mediated Ca^{2+} response of astrocytes to SST interneuron signaling. First, we found that in the presence of CYN 154806 (20 µM), a SSTR antagonist, SST interneuron activation by 10 light pulses was ineffective and only following 30 pulses were Ca^{2+} changes observed (Fig. 6d; Supplementary Movie 3). Second, in the presence of CYN 154806, the astrocyte Ca^{2+} response induced by a second episode of 30 pulse stimulation was not potentiated and it rather exhibited a significant reduction in the mean number of microdomains ($p = 0.007$) and the mean event frequency ($p = 0.003$, Fig. 6d, e, lower panels). Therefore, astrocytic Ca^{2+} responses to SST interneurons in the presence of CYN 154806 become comparable to those evoked by PV interneurons. We next asked whether bath perfusion of the neuropeptide SST (1–2 µM) could result in an astrocyte response to PV interneurons similar to that induced by SST interneurons. We found that under these conditions, astrocytes did not exhibit the response depression upon the second episode of 30 pulse activation of PV interneurons, albeit they failed to respond to 10 pulse stimulation (Fig. 7a–d). It appears, therefore, that PV interneuron activation coupled with exogenous SST peptide can mimic, at least in part, the astrocyte response to SST interneurons.

The results reported above suggest an important role of the neuropeptide SST in the astrocyte response to SST interneurons. To evaluate the degree of astrocytic response facilitation or depression, we calculated the mean ratio of the second to the first response of the astrocytes to the two successive activations of SST interneurons (RR, see Methods), comprehensive of both Ca^{2+} elevations at proximal processes and microdomains, in the absence or presence of the SSTR blocker, and of PV interneurons

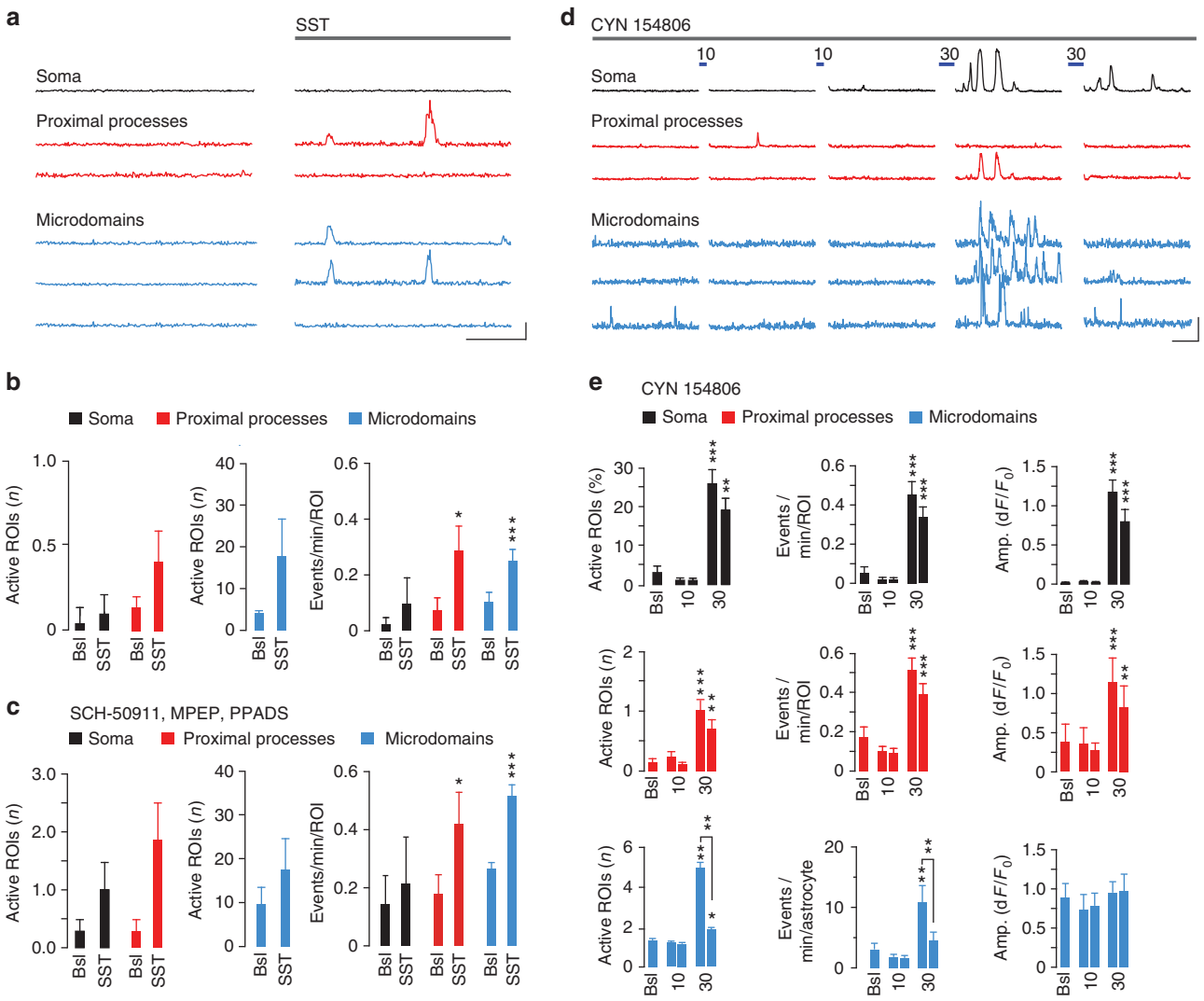

Fig. 6 SST interneuron signaling specificity to astrocytes depends on the neuropeptide somastostatin. **a** Representative traces and **b**, **c** quantitative evaluation of GCaMP6f-astrocyte responses to the neuropeptide SST in SSCx slices in the absence (28 astrocytes, 8 slices, 3 mice) or the presence (9 astrocytes, 9 slices, 3 mice) of antagonists of $GABA_B$ (SCH50911, 50 µM), mGlu5 (MPEP, 50 µM) and purinergic (PPADS, 100 µM) receptor antagonists and in the continuous presence of TTX (1 µM). Scale bars, 50 s, 20% dF/F_0. The response of GCaMP6f-astrocytes is not affected by the mix of receptor antagonists. **d** Representative Ca^{2+} traces of a GCaMP6f-astrocyte before and after subsequent 10 and 30 pulse SST interneuron activations in the presence of 20 µM CYN 154806. Scale bars, 50 s, 20% dF/F_0. **e** Mean number of active ROIs, event frequency and amplitude at soma, proximal processes and microdomains of GCaMP6f-astrocytes (57 astrocytes, 10 slices, 5 mice). Data are represented as mean ± SEM

in the presence or absence of the neuropeptide SST (Fig. 8a). Obtained values confirmed that the astrocyte response was significantly depressed upon the 30 pulse successive stimulations of PV interneurons and it was significantly facilitated upon both 10 and 30 pulse successive stimulations of SST interneurons. When the activation of SSTRs was prevented, the astrocyte response to SST interneuron stimulations was depressed and became undistinguishable from that to PV interneurons. Furthermore, when the PV interneuron stimulations were applied in the presence of the neuropeptide SST, no depression of the astrocyte response was observed (Fig. 8a).

Discussion

We analyzed the GABAergic signaling to astrocytes of PV- and SST-expressing interneurons in the mouse somatosensory cortex in vivo and in situ. Our work provides evidence for the following main findings. First, astrocytes are more sensitive to SST than PV interneuron signaling. Second, astrocytic Ca^{2+} responses weaken or strengthen upon successive episodes of activity in PV and SST interneuron circuit, respectively. Third, both the high sensitivity and the potentiated Ca^{2+} response to SST interneurons crucially depend on the neuropeptide Somastostatin, released by these interneurons, and the following activation of SST receptors expressed at astrocytic processes in close association with $GABA_B$ receptors.

The higher sensitivity of astrocytes to SST than PV interneuron signaling was revealed by the observation that a prolonged activity in the PV interneuron circuit was necessary to evoke astrocytic $GABA_BR$-mediated Ca^{2+} elevations, whereas a short episode of activity in the SST interneuron circuit was sufficient to activate astrocytes. These results provide indication of a signaling specificity to the astrocytic network of GABAergic interneuron subtypes. As a further support to this, we observed that astrocytes activated by a first episode of activity in the PV interneuron circuit, either failed to respond or exhibited a response depression upon a successive episode of similar activity, both in terms of frequency and amplitude of evoked Ca^{2+} elevations. In contrast,

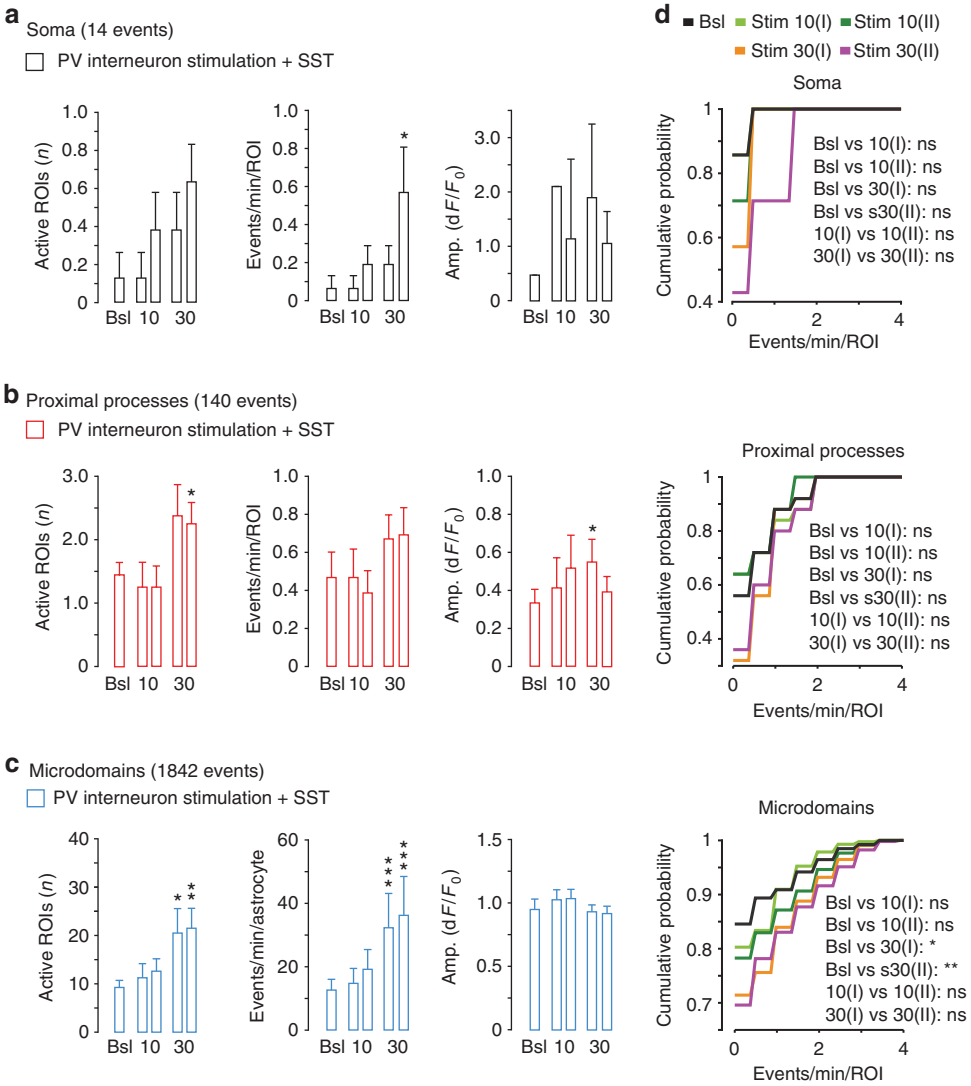

Fig. 7 The neuropeptide somatostatin prevents the depression of the astrocyte response to PV interneurons. **a**–**c** Average data of GCaMP6f-astrocyte Ca^{2+} response to PV interneuron activation (10 or 30 light pulses) from SSCx slice preparations (8 astrocytes, 8 slices, 3 mice) in the presence of somatostatin (1–2 µM). **d** Cumulative distributions of Ca^{2+} events show no response depression to successive 30 pulse stimulations of PV interneurons (for proximal processes, $p = 0.694$; for microdomains, $p = 0.957$, Kolmogorov–Smirnov test)

the robust long-lasting astrocytic Ca^{2+} oscillations evoked by an initial SST interneuron activation were further strengthened by successive episodes of activity and almost all astrocytes from the SSCx layer 2–3 were ultimately recruited indicating that a sustained activity in the SST interneuron circuit is complemented by a sustained activity in the astrocytic network. Notably, evoked $GABA_BR$-mediated Ca^{2+} elevations in astrocytes weaken or strengthen when surrounding PV or SST interneurons are repetitively activated demonstrating a distinguished plasticity of the astrocyte response to these two interneuron subtypes.

Clues for a modulation of the astrocytic Ca^{2+} elevations evoked by neuronal signals have been previously obtained in cell cultures[36] and slice preparations[37–40], but totally unexplored was this property of astrocytes in the real functioning in vivo context. Our study unveils that astrocytes in the adult mouse somatosensory cortex modulate their Ca^{2+} responses as a function of previous states of activity in the surrounding interneuronal network suggesting the existence in these glial cells of a form of cellular memory. This remarkable plasticity of the astrocyte response and the signaling specificity of GABAergic interneuron subtypes suggest that astrocytes are functionally associated to inhibitory circuits. Accordingly, the sustained recruitment of a large astrocytic network to SST interneuron circuit, coupled with the typically slow neuromodulatory action of gliotransmission[5], may contribute to the homeostatic regulation of dendritic inputs and signal integration in pyramidal neurons that is a primary role of SST interneurons[4,23,41–43]. Consistent with this hypothesis, $GABA_BR$-mediated Ca^{2+} elevations in astrocytes has been recently reported to evoke a release of the gliotransmitter glutamate[44] that significantly potentiates synaptic transmission in the hippocampus[45].

The differential properties of the astrocyte response to PV and SST interneurons were observed following both optogenetic light pulses, that activate a large number of ChR2-expressing interneurons, and intracellular current pulse activation of individual interneurons. A synaptic GABA release from a single interneuron is, therefore, sufficient to recruit neighboring astrocytes indicating that each interneuron is in extensive and efficient functional contacts with the surrounding astrocytic network.

The mechanism governing the dynamics of Ca^{2+} microdomains is poorly defined. We here report that Ca^{2+} elevations evoked by synaptic GABA in different astrocytic compartments,

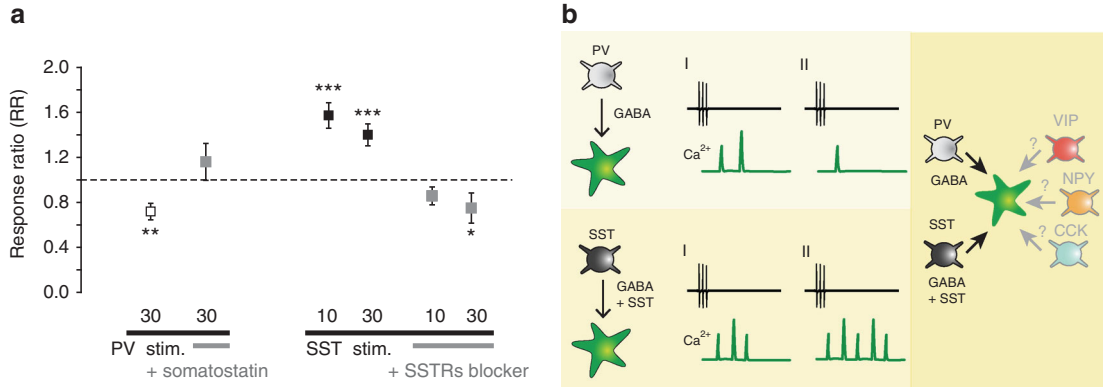

Fig. 8 Specificity of neuropeptide-releasing interneuron signaling to astrocytes. **a** Astrocyte response ratio (RR, see Methods) of the second versus the first 10 or 30 light pulse stimulation of PV or SST interneurons in the absence or presence of the neuropeptide SST or of a somatostatin receptors (SSTRs) blocker. $*p \leq 0.05$, $**p \leq 0.01$, $***p \leq 0.001$. Data are represented as mean ± SEM. **b** Schematic of the signaling specificity to astrocytes of SST and PV interneurons (left) and of the potential recruitment of the astrocytic network by different neuropeptide-releasing interneurons (right)

including microdomains, were mediated by activation of the $GABA_BR$ that previous studies reported to be functionally expressed in astrocytes[44–49]. We also evaluated the possible contribution of Ca^{2+} influx through TRPA1 channels that a recent study using plasma membrane-targeted GCaMP3 proposed to modulate spontaneous microdomain activity[26]. In our study, we found that both spontaneous and evoked microdomains were not affected in the presence of the TRPA1 antagonist HC030031 (Supplementary Fig. 8). These findings should, however, be interpreted with caution as cytosolic GCaMP6f signal may understate near plasma membrane Ca^{2+} microdomain activity. The signaling pathways mediating the Ca^{2+} microdomain activity remain, therefore, to be clarified. The contribution of IP3 signaling pathway in the Ca^{2+} elevations induced by PV and SST interneuron signaling also remains to be defined. Future analyses on $IP_3R2^{-/-}$ mice expressing ChR2 on PV or SST interneurons and GCaMP6f on astrocytes will help clarifying this important issue. It will be also important to validate the GABAergic interneuron type-specific response of astrocytes in awake non-anesthetized animals, given that astrocyte Ca^{2+} signaling can be affected by anesthetics[50,51].

The unique properties of the astrocyte response to SST interneurons, i.e., the high sensitivity to synaptic GABA and the potentiated Ca^{2+} elevations, were mediated by the neuropeptide somatostatin that is co-released with GABA by SST, but not PV interneurons[31]. Consistently, the astrocyte response was observed after an intense activation of Somatostatin interneurons that triggers somatostatin release[52,53]. As a further support to this signaling mode of SST interneurons, our immunogold experiments revealed a close association between SSTRs and $GABA_BRs$ at astrocytic processes that is consistent with functional interactions occurring between the two receptors. $GABA_BR$-SSTR4 couples (<50 nm) were fundamentally found at processes not contacting symmetric synapses, rather than at perisynaptic astrocytic processes suggesting that once released from SST interneurons, GABA and SST travel a certain distance before reaching $GABA_B$-SSTR4R couples. Therefore, a possible synergistic action between the two astrocytic receptors, which may account for the enhanced Ca^{2+} elevations in response to SST interneurons, would eventually occur with a certain delay after intense firing in these interneurons, as we observed in our experiments. All together, our results suggest that astrocytes do not respond rapidly to synaptically released GABA. Rather, they sense GABA tonic elevations and accompany a sustained interneuron activity with multiple, slowly developing Ca^{2+} elevations.

The mechanism of the Ca^{2+} response depression induced by PV interneuron signaling to astrocytes remains to be defined. Desensitization and internalization of $GABA_B$ receptors have been reported to occur in neurons[30,54], but whether similar mechanisms also occur in astrocytes and account for the reduction of the astrocytic response to PV interneurons is unknown. If this were the case, a prevention of $GABA_B$ receptor desensitization or internalization by a concomitant activation of astrocytic SST and $GABA_B$ receptors might account for the powerful recruitment of astrocytes by SST interneuron signaling. Consistent with this hypothesis, we found that exogeneous neuropeptide SST applications prevented the depression of the astrocyte response, otherwise, occurring after the second episode of PV interneuron stimulation, whereas it was not sufficient to induce a response potentiation. A low SST concentration, possibly due to poor penetration of the neuropeptide into the brain tissue, might account for such a partial effect.

Subtypes of SSTRs have been reported to interact and form heterodimers with other G-protein-coupled receptors generating receptor oligomers that can have different desensitization and internalization properties as well as unique pharmacological profiles[33,55–58]. In support of this view, SSTR activation in cultured astrocytes has been reported to synergistically potentiate the Ca^{2+} response to α1 adrenergic receptor-mediated signaling[55].

Different SSTRs are also expressed on neuronal axon terminals and they are proposed to cooperate with pre-synaptic GABARs in the control of glutamate release[31]. We cannot, therefore, exclude that a change in the network activity mediated by neuronal SSTR activation may contribute to modulate the astrocyte response to SST interneuron signaling.

Besides SST, various neuropeptides, such as neuropeptide Y (NPY), vasointestinal polypeptide (VIP), colecystokinin (CCK), neurokinin B and enkephalins, are synthesized with GABA by distinct interneuron classes and their release has been proposed to contribute to interneuron-specific actions by targeting neuronal receptors[31]. Our results suggest that neuropeptides are also used by interneurons to target astrocytic receptors. Besides SSTRs, astrocytes express, indeed, different receptors for neuropeptides that are released by interneurons including NPY, VIP, CCK, and opioids[31,33,55,59]. Based on these observations, we postulate that the mode of the SST interneuron signaling that we describe here may represent a general mechanism in brain networks by which neuropeptide-releasing interneurons recruit to their specific circuits neighboring astrocytes inducing Ca^{2+} elevations with unique spatial-temporal properties (Fig. 8b).

In the somatosensory cortex of adult mice, we identified a novel signaling mode of GABAergic interneurons that revealed the presence of cell-specific interneuronal-astrocytic networks. Our study opens a new perspective into the role of astrocytes as distinct functional components of interneuron type-specific neocortical circuits.

Methods

Mouse strains and adeno-associated virus injections. We used C57BL/6 wild type (WT) mice and the following transgenic mice: *Tg(GadGFP)45704Swn* (GIN), (*CB6-Tg(Gad1-EGFP)G42Zjh/J*) (G42), *Pvalb<tm1(cre)Arbr>*(PV-Cre) and *Sst* < tm2.1(cre)Zjh>(SST-Cre), and tdTomato reporter line B6;129S6-*Gt(ROSA)26Sor*$^{tm14(CAG-tdTomato)Hze}$/J. All procedures were conducted in accordance with the Italian and European Community Council Directive on Animal Care and approved by the Italian Ministry of Health. Injections of viral vectors AAV2/1.EF1.dflox.hChR2(H134R)-mCherry.WPRE.hGH (Penn Vector Core, Addgene 20297) or AAV1.EF1a.DIO.hChR2(H134R)-eYFP.WPRE.hGH, Addgene 20298), carrying the doublefloxed ChR2 sequence, and AAV5.GfaABC1DcytoGCaMP6f.SV40, carrying the astrocytic promoter GfaABC1D, which induces a sparse expression of the Ca^{2+} indicator GCaMP6f in astrocytes, were performed into the SSCx of postnatal day 35–50 (P35-P50) PV-Cre or SST-Cre mice anesthetized with Zoletil (30 mg/kg) and Xylazine (20 mg/kg). Depth of anesthesia was assured by monitoring respiration rate, eyelid reflex, vibrissae movements, and reactions to pinching the tail and toe. Injections of the two viral vectors were performed after drilling one or two holes (0.5 mm dia) into the skull over the SSCx at a distance of 1.5 mm (1.5 µl to each hole, 0–1.5 mm posterior to Bregma, 1.5 mm lateral to sagittal sinus, and 150 µm depth) using a pulled glass pipette in conjunction with a custom-made pressure injection system. After injections, the skin was sutured and mice were revitalized under a heat lamp and returned to their cage. Optogenetic and imaging in vivo experiments were performed in P50-P65 mice, 2 weeks after injections. For slice experiments, PV-Cre and SST-Cre pups (P0–P2) anesthetized by hypothermia and secured into a modeled platform were injected. Optogenetic and imaging experiments were carried out on SSCx slices from P15-P25 mice.

Slice preparation, dye loading and patch-clamp recordings. Coronal SSCx slices of 350 µm were obtained from mice at postnatal days P15-25. Animals were anesthetized as reported above, the brain removed and transferred into an ice-cold solution (ACSF, in mM: 125 NaCl, 2.5 KCl, 2 $CaCl_2$, 1 $MgCl_2$, 25 glucose, pH 7.4 with 95% O_2, and 5% CO_2). Slices were cut in the solution reported in Dugue et al.[60] and then kept for 1 min in the solution (in mM): 225 D-mannitol, 2.5 KCl, 1.25 NaH_2PO_4, 26 $NaHCO_3$, 25 glucose, 0.8 $CaCl_2$, 8 $MgCl_2$, 2 kynurenic acid with 95% O_2, and 5% CO_2. Finally, slices were kept in ACSF at 30 °C for 20 min and then maintained between 19 and 22 °C for the entire experiment. In a set of experiments, SSCx slices were incubated with the Ca^{2+} sensitive dye Fluo-4 AM (10 µM; Life Technologies) and the selective astrocyte dye Sulforhodamine 101[25] (SR101, 0.2 µM, Sigma Aldrich, Italy), as previously described[44]. For the in vivo experiments, the bulk loading of cortical astrocytes was performed with the dye OGB-1 AM (final concentration 1 mM, Thermo Fisher Scientific, USA) and SR101 (final concentration 0.5 mM). For whole-cell patch-clamp recordings, slices were perfused in a submerged chamber at a rate of 3–4 ml/min with (in mM): 120 NaCl, 2.5 KCl, 1 NaH_2PO_4, 26 $NaHCO_3$, 1 $MgCl_2$, 2 $CaCl_2$, 10 glucose, pH 7.4 (with 95% O_2 and 5% CO_2). Neurons were visualized under a confocal microscope (TCS-SP5-RS, Leica Microsystems, Germany) or a Multiphoton Imaging System (Scientifica Ltd, UK) equipped with a CCD camera for differential interference contrast (DIC) image acquisition. Single-cell recordings were performed in voltage- or current-clamp configuration using a multiclamp 700B amplifier (Molecular Devices, USA). Signals were filtered at 1 kHz and sampled at 10 kHz with a Digidata 1440 s interface and pClamp 10 software (Molecular Devices). The pipette resistance was 3–4 MΩ. Access resistance was monitored throughout the recordings and was between 8.4 and 24.2 MΩ. Neurons that had a >15% change in access resistance were discarded. Whole-cell intracellular pipette solution was (in mM): 145 K-gluconate, 5 $MgCl_2$, 0.5 EGTA, 2 Na_2ATP, 0.2 Na_2GTP, 10 HEPES, to pH 7.2 with KOH, osmolarity, 280 ÷ 290 mOsm. Data were not corrected for the liquid junction potential. Recordings were analyzed with Clampfit 10.3.

Drug applications. Drugs applied to the slice perfusion solution were: SCH50911 (20–50 µM), CYN 154806 (20 µM), and somatostatin (SST, 1–2 µM) from Tocris (UK), Tetrodotoxin (1 µM), CGP52432 (20 µM), HC030031 (80 µM), NBQX (10 µM), APV (50 µM), MPEP (50 µM), PPADS (100 µM) from Abcam (UK).

Ca^{2+} imaging. To image Ca^{2+} dynamics in GCaMP6f-astrocytes, we used 2-photon laser scanning microscope in both in vivo (Ultima IV, Bruker) and brain slice (Multiphoton Imaging System, Scientifica Ltd., UK) preparations equipped with a pulsed red laser (Chameleon Ultra 2, Coherent, USA) tuned at 920 nm. Power at sample was controlled in the range 5–10 mW. The excitation wavelengths used were 920 nm for GCaMP6f, 740 nm for Fluo-4 and 830 nm for OGB-1. SR101 is visible at both 740 and 920 nm. Images were acquired with a water-immersion lens (Olympus, LUMPlan FI/IR 20×, 1.05 NA), with a field of view between 700 × 700 µm and 120 × 120 µm at 1–3.5 Hz acquisition frame rate. Each Ca^{2+} signal recording was performed in cortical layers 2–3 for about 2 min and 30 s with 5 min interval between the first and the second stimulation of interneurons by 10 or 30 light pulses, whereas a longer interval of about 10 min was applied before initiating the first 30 pulse stimulation. In control experiments, the same imaging protocol was applied without optogenetic stimulation. A confocal laser scanning microscope (TCS-SP5-RS, Leica Microsystems, Germany) equipped with two lasers tuned at 488 nm and 543 nm was used only in a subset of experiments to continuously monitor Ca^{2+} signals from GCaMP6f-astrocytes during optogenetic light activation of PV or SST interneurons in SSCx slices (Supplementary Fig. 4), an unfeasible condition in our 2-photon experiments. In in vivo imaging experiments, P55-P65 ChR2-PV-GCaMP6f or ChR2-SST-GCaMP6f mice were anesthetized with urethane (20% urethane, ethylcarbamate; SIGMA Aldrich). Animal pinch withdrawal and eyelid reflex were tested to assay the depth of anesthesia. Dexamethasone sodium phosphate (2 mg/kg body weight) was injected intramuscularly to reduce cortical stress response during surgery and prevent cerebral edema. Atropine (0.05 mg/kg body weight) was injected subcutaneously to avoid saliva accumulation. Both eyes were covered with an eye ointment to prevent corneal desiccation during the experiment. We monitored the respiration rate, heart rate, and core body temperature throughout the experiment. The mouse was head-fixed and a craniotomy of 2–3 mm in diameter was drilled over the SSCx. Mice were mounted under the microscope with a metal head-post glued to the skull. Imaging was performed through a water-immersion lens (Olympus, LUMPlan FL/N 20×, 1.05 NA) at a resolution of 512 × 512 pixels with zoom 4, leading to a field of 50.7 × 50.7 µm in superficial layers (50–150 µm below the cortical surface) and acquired at 1–2 Hz. Imaging session lasted up to 2 h.

Optogenetic stimulation. Full-field photo-stimulation of ChR2-expressing interneurons consisted of 150 ms light pulses ($\lambda = 473$ nm) delivered by a blue module laser diode (MLD, COBOLT, Solna, SE), which was collimated and coupled under the objective with an optic fiber (ThorLabs, NJ, USA) held at 26° angle above the brain tissue. The optic fiber was 300 µm in diameter with a 0.22 NA. The resulting illuminated ellipse was 550 µm long and 150 µm wide.

Two-photon-targeted juxtasomal recordings in vivo. Experimental procedures followed what previously described[61]. In brief, for recordings in anesthetized mice, PV-Cre/tdTomato and SST-Cre/tdTomato double-transgenic mice were injected at P0 with AV2/1.EF1.dflox.hChR2(H134R)-mCherry.WPRE.hGH (Addgene 20297). Four to five weeks after virus injections mice were anesthetized with urethane (2 g/kg) and a small craniotomy (~1 mm × 1 mm) was opened onto the mouse skull. The patch pipette (resistance: 4–9 MΩ) was filled with ACSF solution mixed with Alexa Fluor-488 (20 µM, Invitrogen Thermo Fisher, USA) and lowered to cortical layer 2/3 (110–300 µm from the brain surface). tdTomato-positive neurons were targeted by imaging their fluorescence with the two-photon microscope ($\lambda = 920$ nm or 730 nm). Full-field optogenetic stimulation of interneurons was performed as in Zucca et al.[61] Light intensity was 0.2–6 mW at the fiber tip. For recordings in non-anesthetized mice, 2 weeks before the experiment mice were anesthetized with 2% isoflurane/0.8% oxygen and a custom metal plate was mounted with dental cement on the skull. Habituation sessions were performed on each day (starting 2–3 days after plate implantation) with a gradually increasing duration (from 15 to 60 min, for 7–10 days). The day of the recording, mice were anesthetized with isofluorane and a small craniotomy was opened on the somatosensory cortex as described above. After the surgery, mice recovered for at least 30 min before the beginning of the experimental session. Electrical signals were amplified by a Multiclamp 700B, low-pass filtered at 10 kHz, digitized at 50 kHz with a Digidata 1440 and acquired with pClamp 10 (Axon instruments, USA). Electrophysiological traces were analyzed using Clampfit 10 software.

Pre-embedding electron microscopy. Three C57BL/6 (P21) mice were anesthetized with chloral hydrate (12% i.p., 300 mg/kg) and perfused through the ascending aorta with physiological saline solution followed by a mixture of 4% paraformaldehyde (PFA) and 0.2% glutaraldheyde in PBS. Brains were post-fixed in the same fixative used for perfusion for 3 days and parietal cortex was cut serially in the coronal plane (40 µm sections) with a vibratome and immediately processed for immunoperoxidase according to previous pre-embedding electron microscopy protocols[62]. For antibody specificity on the SSTR4, two 9-month-old mice (WT and SSTR4 KO[35]) were perfused through the ascending aorta with a flush of physiological saline solution followed by 4% PFA in PBS. Brains were post-fixed in the same fixative for 1 h, cryopreserved and then frozen until cutting by a vibratome. For antibody specificity on the $GABA_{B2}$ two 7-week-old WT BALB/c JR1 mice and two $GABA_{B2}$ KO BALB/c JR1 mice[34] were perfused through the ascending aorta with physiological saline solution followed by 4% PFA in PBS. Brains were post-fixed in the same fixative used for perfusion for 7 days until cutting by a vibratome. For PV and SST visualization sections were incubated in a solution containing rabbit polyclonal anti-PV (1:500; raised against rat muscle PV; PV28, RRID:AB_10013386, Swant, Switzerland) or rat monoclonal anti-SST primary antibodies (1:80; raised against synthetic 1–14 cyclic SST, MAB 354; RRID: AB_2255365 EMD Millipore, Germany; 2 h at room temperature and overnight at 4 °C)[63]. The following day, sections were incubated in a solution containing the

appropriate biotinylated secondary antibodies (1:200; Jackson ImmunoResearch, USA; 1 h at room temperature). Antibody bindings sites were visualized by avidin–biotin peroxidase complex, 3,3 diaminobenzidinetetrahydrochloride and H_2O_2[62]. Method specificity was verified by substituting primary antibodies with phosphate buffer (PB) or non immune serum. Subsequently, embedding procedure of immunoperoxidase processed sections was performed as described[62]. Small blocks of embedded tissue containing layers 2/3 of the SSCx were selected, glued to blank epoxy and sectioned with an ultramicrotome (MTX; Research and Manufacturing Company Inc., USA). The most superficial ultrathin sections (60 nm) were collected and mounted on 200 mesh copper grids, stained with Sato's lead and examined with a Philips EM 208 and CM10 electron microscope (Eindhoven, The Netherlands) coupled to a MegaView-II high resolution CCD camera (Soft Imaging System, Germany). Identification of labeled and unlabeled profiles was based on established morphological criteria[64]. Microscopic fields were selected and captured at original magnifications of 30,000 or ×50,000. According to the different postsynaptic targets of PV and SST interneurons, PV interneuron immunopositive terminals were sampled at axo-somatic, proximal axo-dendritic, and axo-axonic synapses, and SST interneuron immunopositive terminals at axo-dendritic shaft and axo-spinous synapses PAPs were then identified and quantification at symmetric synapses of PV and SST interneurons performed.

Post-embedding electron microscopy. Three C57BL/6 (P21) were anesthetized with chloral hydrate (12% i.p.; 300 mg/kg) and perfused through the ascending aorta with a flush of physiological saline solution followed by 4% PFA in PBS. Brains were post-fixed in the same fixative for 7 days and parietal cortex was cut serially in the coronal plane in 50 µm thick sections with a vibratome. Sections were processed for an osmium-free embedding method[62,65,66]. Chips including layers 2/3 of SSCx, were selected, glued to blank resin blocks and sectioned with an ultramicrotome. Thin sections (60–80 nm) were cut and mounted on 300 mesh nickel grids and processed for immunogold post-embedding labeling[62,65,66]. For $GABA_{B2}$ and SSTR4 visualization, grids were incubated overnight (26 °C) in a solution containing anti-$GABA_{B2}$ mouse monoclonal antibody (1:50; raised against amino acids 183–482 mapping within an extracellular domain of $GABA_{B2}$ of human origin, specific for detection of $GABA_{B2}$ of mouse, rat and human; H10; sc-393270, Santa Cruz Biotechnology Inc., USA) and anti-SSTR4 rabbit polyclonal antibody (1:50; raised against amino acids 171–220 of SSTR4 of human origin, specific for detection of SSTR4 of mouse, rat and human; H50; sc-25678, RRID: AB_2196360, Santa Cruz Biotechnology), and then incubated for 2 h (26 °C) in a solution containing anti-mouse and anti-rabbit secondary antibodies conjugated to 18 and 12 nm gold particles (1:20; 115–215–068, 111–205–144, Jackson ImmunoResearch, USA). Grids were finally stained with uranyl acetate and Sato's lead. The optimal concentration of antibodies to $GABA_{B2}$ and SSTR4 was sought by testing several dilutions; the concentration yielding the lowest level of background labeling and still immunopositive elements was used to perform the final studies. Gold particles were not detected when primary antiserum was omitted. When normal serum was substituted for immune serum, sparse and scattered gold particles were observed, but they did not show any specific relationship to subcellular compartments. Ultrathin sections (15 ultrathin sections/animal) were examined at ×50,000–85,000 and fields that included at least 1 immunolabeled astrocytic profile and/or perisynaptic astrocytic process associated with a symmetric synapse exhibiting a clear pre-synaptic (AZ) and post-synaptic specialization were selected[64,67]. For determining the relative density of $GABA_{B2}$ and SSTR4 double-labeled astrocytic profiles, pyramidal cell nuclei were also identified: gold particles within labeled structures counted and areas calculated using ImageJ (NIH, Bethesda, MD, USA). Background was calculated by estimating labeling density over pyramidal cell nuclei (0.54 ± 0.05, $n = 12$ for $GABA_{B2}$ and 0.57 ± 0.02, $n = 12$ for SSTR4)[62,68]. Particle densities were counted in perisynaptic (PAPs; 42.43 ± 7.27 for $GABA_{B2}$ and 44.02 ± 10.66, $n = 40$ for SSTR4) and non perisynaptic astrocytic processes (nPAPs; 44.26 ± 6.07 for $GABA_{B2}$ and 49.88 ± 7.87 for SSTR4) and compared with background labeling. Gold particles were considered associated with plasma membrane if they were within 15 nm of the extracellular side of the membrane, and cytoplasmic if they were 25 nm from the extracellular processes. Edge-to-edge separation distance between $GABA_{B2}$ and SSTR4 membrane-associated gold particle pairs were measured and the distribution of the separation distance between immunogold labeled $GABA_{B2}$ and SSTR4 pairs was determined[69,70]. In astrocytic processes, pairs of immunogold labeled $GABA_{B2}$ and SSTR4 with an edge-to edge distance within 50 nm, were also localized with respect to the closest AZ margin of symmetric synapses. Lateral position of a pair was defined as the distance along the plasma membrane from the AZ edge to the middle point between the two particles, and measured using ImageJ. For experiments in KO mice and relative controls, microscopical fields containing spines, axon terminals and astrocytic processes with at least one gold particle for $GABA_{B2}$ analysis, proximal and distal dendrites, axon terminals, and astrocytic processes for SSTR4 analysis were randomly selected. For both pre- and post-embedding studies, all material from WT and KO mice was processed in parallel. Acquisition of ultramicroscopical fields and density analysis of WT and KO mice were performed in a blind manner.

Immohistochemistry and cell counting. For the evaluation of the number of GCaMP6f-expressing astrocytes and neurons we prepared 100 µm thick brain slices from young and adult animals injected with AAV-ChR2 and AAV2/5.GfaABC.cyto.GCaMP6. Slices were fixed in cold 4% PFA for 2 h, washed with PBS and processed for double immunofluorescence staining. First, we incubated floating sections for 1 h in the Blocking Serum (BS: 1% BSA, 2% goat serum and 1% horse serum in PBS) and 0.2% TritonX-100. We then performed a second incubation with primary antibodies mixed and diluted in BS and 0,02% TritonX-100 (16 h at 4 °C). Primary antibodies used were: anti-NeuN antibody (RRID:AB_2298772, 1:400 mouse, Millipore MAB377) plus anti-GFP (RRID:AB_221477, 1:200 rabbit, Invitrogen Thermo-Scientific, A21311), and anti-glial fibrillary acidic protein (GFAP, RRID:AB_10013382, 1:300 rabbit, Dako, Denmark, Z0334) plus anti-GFP (RRID: AB_221568, 1:200 mouse, Invitrogen Thermo-Scientific, A11120). The anti-GFP antibodies were used to enhance the GCaMP6f fluorescence. After washing with PBS, slices were incubated for 2 h at room temperature with secondary antibodies conjugated with Alexa Fluor-488 (for staining GFP) and with Alexa Fluor-633 (for staining NeuN or GFAP; Invitrogen Thermo-Scientific, 1:500). Slices were then washed and mounted on glass coverslips. Negative controls were performed in the absence of the primary antibodies. For the evaluation of the number of PV- and SST-interneurons expressing ChR2, PV-cre/tdTomato and SST-cre/tdTomato double-transgenic mice were injected at P0 with AAV1.EF1a.DIO.hChR2(H134R)-eYFP.WPRE.hGH (see above for details). Four weeks after virus injection, mice were anesthetized with urethane (2 g/kg) and perfused transcardially with 0.9% saline solution, followed by 4% PFA in 0.1 M PB, pH 7.4. Brains were post-fixed for 6 h, cryoprotected in a 30% sucrose solution in 0.1 M PB pH 7.4 and frozen. Free-floating coronal serial sections (40 µm) from injected PV-cre/tdTomato and SST-cre/tdTomato mice were collected and stained against parvalbumin or somatostatin, respectively. The following primary antibodies were used: anti-parvalbumin (RRID: AB_477329, 1:1000 mouse, Sigma P3088) and anti-somatostatin (RRID: AB_2255365, 1:200 rat, Millipore MAB 354). Secondary antibodies consisted of: goat anti-mouse 647 (RRID: AB_141725, 1:800, Molecular Probes A21236) and goat anti-rat 647 (RRID:AB_141778, 1:800, Molecular Probes A21247). Sections were mounted on SuperFrost slides (Molecular Probes), air dried, and coverslipped in polyvinyl alcohol with diazabicyclo-octane (DABCO). Confocal image *z*-stacks were captured through the thickness of the slice at 1 µm steps and used for double-labeled cell count using an open source ImageJ plugin.

Data analysis. Detection of astrocyte ROI containing Ca^{2+} elevations was performed with ImageJ in a semi-automated manner using the GECIquant plugin[20]. The software was used to identify ROIs corresponding first to the soma (>30 µm^2; confirmed by visual inspection), then to the proximal processes (>20 µm^2 and not corresponding to the soma) and finally to the microdomains (between 1 and 20 µm^2 corresponding to neither the soma nor the proximal processes). All pixels within each ROI were averaged to give a single time course F(t). Analysis of Ca^{2+} signals was performed with ImageJ (NIH) and a custom software developed in MATLAB 7.6.0 R2008 A (Mathworks, Natick, MA, USA). To compare relative changes in fluorescence between different cells, we expressed the Ca^{2+} signal for each ROI as $dF/F_0 = (F(t) - F_0)/(F_0)$. We then defined as *baseline trace* for each ROI the points of the Ca^{2+} trace with absolute values smaller than twice the standard deviation of the overall signal. Significant Ca^{2+} events were then selected with a supervised algorithm as follows. Firstly, a new standard deviation was calculated on the *baseline trace*, and all local maxima with absolute values exceeding twice this new standard deviation were identified. Secondly, of these events, we considered significant only those associated with local calcium dynamics with amplitude larger than threefold the new standard deviation. The amplitude of each Ca^{2+} event was measured from the 20th percentile of the fluorescent trace interposed between its maximum and the previous significant one (see Supplementary Fig. 17). Essentially, this procedure combines a threshold measured from the global baseline with a stricter threshold computed from a local baseline. We adopted this method to reduce artefacts from the recording noise superimposed on the slow astrocytic dynamics and from slow changes in baseline due to physiological or imaging drifts. All the Ca^{2+} traces were visually inspected to exclude the ROIs dominated by noise. For all experiments, we calculated the number of active ROIs and for each ROI corresponding to the soma, proximal processes and microdomains the frequency, and the amplitude of the Ca^{2+} signal. All the Ca^{2+} peaks were aligned to their onset to compute the average Ca^{2+} peak (Supplementary Fig. 17). The onset of each Ca^{2+} event was defined as the last time point when its fluorescence trace was below one standard deviation of the baseline. Finally, the time onset of all detected Ca^{2+} events was reported in raster plots and peristimuls time histograms (PSTH). These procedures were applied for the analysis of both in vivo and brain slice data. To provide an estimate of the change in the overall microdomain activity per astrocyte following PV or SST interneuron stimulation, the number of individual microdomains (active ROIs) and the average frequency of Ca^{2+} microdomain events per cell were measured under the different experimental conditions. Then, these values were averaged across all astrocytes to obtain the bar graphs reported in the figures. A response ratio (RR; Fig. 8a) that describes the change in the response of astrocytic processes to successive stimuli was calculated as follows. Firstly, for each astrocyte the response to a given interneuron stimulation was measured by the number of active ROIs, frequency and amplitude of Ca^{2+} peaks at proximal and fine processes. These values were normalized to their corresponding baseline values, pooled and averaged. Secondly, the astrocyte RR was defined as the ratio of the second to the first response to 10 (or 30) pulse activation of PV or SST interneurons.

Mean IPSCs peak amplitudes in Supplementary Fig. 13 were fitted to the double exponential equation $A(t) = A1^*\exp(-x/t1) + A2^*\exp(-x/t2)$, where $A1$ and $A2$ are the amplitude of the fast and the slow decay component and $t1$ and $t2$ are the corresponding decay time constants.

Statistical analysis. Data were tested for normality before statistical analysis. For the number of ROIs and the frequency of astrocytic Ca^{2+} events, we used paired Student's *t*-test (on normal data distribution) or paired sample Wilcoxon signed-rank test (on non-normal data distribution). For the RR, one sample Wilcoxon signed-rank test was used. For cumulative distribution comparisons, we applied the Kolmogorov–Smirnov test. For EM data, normality test and statistical analysis were performed using GraphPrism v.4.0 (GraphPad Software, San Diego, CA, USA). Given the non-normal distribution of data, Mann–Whitney test and Kruskal Wallis with Dunn's multiple comparison test were used. Pairwise statistical comparisons of each value of the astrocyte response to a given stimulation was carried out with respect to basal values. The astrocytes response to the two successive 10 (or 30) pulse stimulation was also similarly evaluated. All results are presented as mean ± SEM. Results were considered statistically significant at $p \leq 0.05$. $^*p \leq 0.05$, $^{**}p \leq 0.01$, $^{***}p \leq 0.001$. The exact *p*-values for each set of data are reported in the Supplementary Table 4.

Data availability. Data presented in this work are available from the corresponding author upon reasonable request.

Received: 18 January 2017 Accepted: 14 December 2017
Published online: 08 January 2018

References

1. Ascoli, G. A. et al. Petilla terminology: nomenclature of features of GABAergic interneurons of the cerebral cortex. *Nat. Rev. Neurosci.* **9**, 557–568 (2008).
2. Markram, H. et al. Interneurons of the neocortical inhibitory system. *Nat. Rev. Neurosci.* **5**, 793–807 (2004).
3. Hu, H., Gan, J. & Jonas, P. Interneurons. Fast-spiking, parvalbumin$^+$ GABAergic interneurons: from cellular design to microcircuit function. *Science* **345**, 1255263 (2014).
4. Urban-Ciecko, J. & Barth, A. L. Somatostatin-expressing neurons in cortical networks. *Nat. Rev. Neurosci.* **17**, 401–409 (2016).
5. Araque, A. et al. Gliotransmitters travel in time and space. *Neuron* **81**, 728–739 (2014).
6. Bazargani, N. & Attwell, D. Astrocyte calcium signaling: the third wave. *Nat. Neurosci.* **19**, 182–189 (2016).
7. Schummers, J., Yu, H. & Sur, M. Tuned responses of astrocytes and their influence on hemodynamic signals in the visual cortex. *Science* **320**, 1638–1643 (2008).
8. Takata, N. et al. Astrocyte calcium signaling transforms cholinergic modulation to cortical plasticity in vivo. *J. Neurosci.* **31**, 18155–18165 (2011).
9. Navarrete, M. et al. Astrocytes mediate in vivo cholinergic-induced synaptic plasticity. *PLoS Biol.* **10**, e1001259 (2012).
10. Paukert, M. et al. Norepinephrine controls astroglial responsiveness to local circuit activity. *Neuron* **82**, 1263–1270 (2014).
11. Haydon, P. G. & Carmignoto, G. Astrocyte control of synaptic transmission and neurovascular coupling. *Physiol. Rev.* **86**, 1009–1031 (2006).
12. Rusakov, D. A. Disentangling calcium-driven astrocyte physiology. *Nat. Rev. Neurosci.* **16**, 226–233 (2015).
13. Haim, L. B. & Rowitch, D. H. Functional diversity of astrocytes in neural circuit regulation. *Nat. Rev. Neurosci.* **18**, 31–41 (2017).
14. Beenhakker, M. P. & Huguenard, J. R. Astrocytes as gatekeepers of $GABA_B$ receptor function. *J. Neurosci.* **30**, 15262–15276 (2010).
15. Shigetomi, E., Tong, X., Kwan, K. Y., Corey, D. P. & Khakh, B. S. TRPA1 channels regulate astrocyte resting calcium and inhibitory synapse efficacy through GAT-3. *Nat. Neurosci.* **15**, 70–80 (2012).
16. Christian, C. A. & Huguenard, J. R. Astrocytes potentiate GABAergic transmission in the thalamic reticular nucleus via endozepine signaling. *Proc. Natl Acad. Sci. USA* **110**, 20278–20283 (2013).
17. Zhang, F. et al. Optogenetic interrogation of neural circuits: technology for probing mammalian brain structures. *Nat. Protoc.* **5**, 439–456 (2010).
18. Chen, T. W. et al. Ultrasensitive fluorescent proteins for imaging neuronal activity. *Nature* **499**, 295–300 (2013).
19. Shigetomi, E. et al. Imaging calcium microdomains within entire astrocyte territories and endfeet with GCaMPs expressed using adeno-associated viruses. *J. Gen. Physiol.* **141**, 633–647 (2013).
20. Srinivasan, R. et al. Ca^{2+} signaling in astrocytes from *Ip3r2*$^{-/-}$ mice in brain slices and during startle responses in vivo. *Nat. Neurosci.* **18**, 708–717 (2015).
21. Grosche, J. et al. Microdomains for neuron–glia interaction: parallel fiber signaling to Bergmann glial cells. *Nat. Neurosci.* **2**, 139–143 (1999).
22. Kanemaru, K. et al. In vivo visualization of subtle, transient, and local activity of astrocytes using an ultrasensitive Ca^{2+} indicator. *Cell Rep.* **8**, 311–318 (2014).
23. Gentet, L. J. et al. Unique functional properties of somatostatin-expressing GABAergic neurons in mouse barrel cortex. *Nat. Neurosci.* **15**, 607–612 (2012).
24. Polack, P. O., Friedman, J. & Golshani, P. Cellular mechanisms of brain state-dependent gain modulation in visual cortex. *Nat. Neurosci.* **16**, 1331–1339 (2013).
25. Nimmerjahn, A., Kirchhoff, F., Kerr, J. N. & Helmchen, F. Sulforhodamine 101 as a specific marker of astroglia in the neocortex in vivo. *Nat. Methods* **1**, 31–37 (2004).
26. Shigetomi, E., Jackson-Weaver, O., Huckstepp, R. T., O'Dell, T. J. & Khakh, B. S. TRPA1 channels are regulators of astrocyte basal calcium levels and long-term potentiation via constitutive D-serine release. *J. Neurosci.* **33**, 10143–10153 (2013).
27. Kuga, N., Sasaki, T., Takahara, Y., Matsuki, N. & Ikegaya, Y. Large-scale calcium waves traveling through astrocytic networks in vivo. *J. Neurosci.* **31**, 2607–2614 (2011).
28. Xu, H., Jeong, H. Y., Tremblay, R. & Rudy, B. Neocortical somatostatin-expressing GABAergic interneurons disinhibit the thalamorecipient layer 4. *Neuron* **77**, 155–167 (2013).
29. Pfeffer, C. K., Xue, M., He, M., Huang, Z. J. & Scanziani, M. Inhibition of inhibition in visual cortex: the logic of connections between molecularly distinct interneurons. *Nat. Neurosci.* **16**, 1068–1076 (2013).
30. Overstreet, L. S., Jones, M. V. & Westbrook, G. L. Slow desensitization regulates the availability of synaptic GABA(A) receptors. *J. Neurosci.* **20**, 7914–7921 (2000).
31. van den Pol, A. N. Neuropeptide transmission in brain circuits. *Neuron* **76**, 98–115 (2012).
32. Masmoudi, O. et al. Somatostatin down-regulates the expression and release of endozepines from cultured rat astrocytes via distinct receptor subtypes. *J. Neurochem.* **94**, 561–571 (2005).
33. Somvanshi, R. K. & Kumar, U. D-opioid receptor and somatostatin receptor-4 heterodimerization: possible implications in modulation of pain associated signaling. *PLoS ONE* **9**, e85193 (2014).
34. Gassmann, M. et al. Redistribution of $GABA_{B(1)}$ protein and atypical $GABA_B$ responses in $GABA_{B(2)}$-deficient mice. *J. Neurosci.* **24**, 6086–6097 (2004).
35. Helyes, Z. et al. Impaired defense mechanism against inflammation, hyperalgesia, and airway hyperreactivity in somatostatin 4 receptor gene-deleted mice. *Proc. Natl Acad. Sci. USA* **106**, 13088–13093 (2009).
36. Pasti, L., Pozzan, T. & Carmignoto, G. Long-lasting changes of calcium oscillations in astrocytes. A new form of glutamate-mediated plasticity. *J. Biol. Chem.* **270**, 15203–15210 (1995).
37. Pasti, L., Volterra, A., Pozzan, T. & Carmignoto, G. Intracellular calcium oscillations in astrocytes: a highly plastic, bidirectional form of communication between neurons and astrocytes in situ. *J. Neurosci.* **17**, 7817–7830 (1997).
38. Perea, G. & Araque, A. Properties of synaptically evoked astrocyte calcium signal reveal synaptic information processing by astrocytes. *J. Neurosci.* **25**, 2192–2203 (2005).
39. Sibille, J., Zapata, J., Teillon, J. & Rouach, N. Astroglial calcium signaling displays short-term plasticity and adjusts synaptic efficacy. *Front. Cell Neurosci.* **9**, 189 (2015).
40. Schipke, C. G., Haas, B. & Kettenmann, H. Astrocytes discriminate and selectively respond to the activity of a subpopulation of neurons within the barrel cortex. *Cereb. Cortex* **18**, 2450–2459 (2008).
41. Urban-Ciecko, J., Fanselow, E. E. & Barth, A. L. Neocortical somatostatin neurons reversibly silence excitatory transmission via GABAb receptors. *Curr. Biol.* **25**, 722–731 (2015).
42. Makino, H. & Komiyama, T. Learning enhances the relative impact of top-down processing in the visual cortex. *Nat. Neurosci.* **18**, 1116–1122 (2015).
43. Stefanelli, T., Bertollini, C., Luscher, C., Muller, D. & Mendez, P. Hippocampal somatostatin interneurons control the size of neuronal memory ensembles. *Neuron* **89**, 1074–1085 (2016).
44. Mariotti, L., Losi, G., Sessolo, M., Marcon, I. & Carmignoto, G. The inhibitory neurotransmitter GABA evokes long-lasting Ca^{2+} oscillations in cortical astrocytes. *Glia* **64**, 363–373 (2016).
45. Perea, G. et al. Activity-dependent switch of GABAergic inhibition into glutamatergic excitation in astrocyte-neuron networks. *Elife* **5**, e20362 (2016).
46. Kang, J., Jiang, L., Goldman, S. A. & Nedergaard, M. Astrocyte-mediated potentiation of inhibitory synaptic transmission. *Nat. Neurosci.* **1**, 683–692 (1998).
47. Serrano, A., Haddjeri, N., Lacaille, J. C. & Robitaille, R. GABAergic network activation of glial cells underlies hippocampal heterosynaptic depression. *J. Neurosci.* **26**, 5370–5382 (2006).
48. Navarrete, M. & Araque, A. Endocannabinoids mediate neuron-astrocyte communication. *Neuron* **57**, 883–893 (2008).
49. Gould, T. et al. $GABA_B$ receptor-mediated activation of astrocytes by gamma-hydroxybutyric acid. *Philos. Trans. R. Soc. Lond. B Biol. Sci.* **369**, 20130607 (2014).

50. Nimmerjahn, A., Mukamel, E. A. & Schnitzer, M. J. Motor behavior activates Bergmann glial networks. *Neuron* **62**, 400–412 (2009).
51. Thrane, A. S. et al. General anesthesia selectively disrupts astrocyte calcium signaling in the awake mouse cortex. *Proc. Natl Acad. Sci. USA* **109**, 18974–18979 (2012).
52. Katona, L. et al. Sleep and movement differentiates actions of two types of somatostatin-expressing GABAergic interneuron in rat hippocampus. *Neuron* **82**, 872–886 (2014).
53. Baraban, S. C. & Tallent, M. K. Interneuron diversity series: Interneuronal neuropeptides–endogenous regulators of neuronal excitability. *Trends Neurosci.* **27**, 135–142 (2004).
54. Turecek, R. et al. Auxiliary $GABA_B$ receptor subunits uncouple G protein betagamma subunits from effector channels to induce desensitization. *Neuron* **82**, 1032–1044 (2014).
55. Marin, P. et al. Somatostatin potentiates the a1-adrenergic activation of phospholipase C in striatal astrocytes through a mechanism involving arachidonic acid and glutamate. *Proc. Natl Acad. Sci. USA* **88**, 9016–9020 (1991).
56. Fatatis, A., Holtzclaw, L. A., Avidor, R., Brenneman, D. E. & Russell, J. T. Vasoactive intestinal peptide increases intracellular calcium in astroglia: synergism with alpha-adrenergic receptors. *Proc. Natl Acad. Sci. USA* **91**, 2036–2040 (1994).
57. Rocheville, M. et al. Receptors for dopamine and somatostatin: formation of hetero-oligomers with enhanced functional activity. *Science* **288**, 154–157 (2000).
58. Pfeiffer, M. et al. Heterodimerization of somatostatin and opioid receptors cross-modulates phosphorylation, internalization, and desensitization. *J. Biol. Chem.* **277**, 19762–19772 (2002).
59. Muller, W., Heinemann, U. & Berlin, K. Cholecystokinin activates CCKB-receptor-mediated Ca-signaling in hippocampal astrocytes. *J. Neurophysiol.* **78**, 1997–2001 (1997).
60. Dugue, G. P., Dumoulin, A., Triller, A. & Dieudonne, S. Target-dependent use of co-released inhibitory transmitters at central synapses. *J. Neurosci.* **25**, 6490–6498 (2005).
61. Zucca, S. et al. An inhibitory gate for state transition in cortex. *Elife* **6**, e26177 (2017).
62. Melone, M., Ciappelloni, S. & Conti, F. A quantitative analysis of cellular and synaptic localization of GAT-1 and GAT-3 in rat neocortex. *Brain Struct. Funct.* **220**, 885–897 (2013).
63. Xu, X., Roby, K. D. & Callaway, E. M. Immunochemical characterization of inhibitory mouse cortical neurons: three chemically distinct classes of inhibitory cells. *J. Comp. Neur.* **518**, 389–404 (2010).
64. Peters, A., Palay, S. L. & Webster, H. D. F. in *The Fine Structure of the Central Nervous System: Neurons and Their Supportive Cells* (ed. Press, O. U.) 276–295 (Oxford University Press, New York, 1991).
65. Phend, K. D., Rustioni, A. & Weinberg, R. J. An osmium-free method of epon embedment that preserves both ultrastructure and antigenicity for post-embedding immunocytochemistry. *J. Histochem. Cytochem.* **43**, 283–292 (1995).
66. Phend, K. D., Weinberg, R. J. & Rustioni, A. Techniques to optimize post-embedding single and double staining for amino acid neurotransmitters. *J. Histochem. Cytochem.* **40**, 1011–1020 (1992).
67. Tyler, W. J. & Pozzo-Miller, L. D. BDNF enhances quantal neurotransmitter release and increases the number of docked vesicles at the active zones of hippocampal excitatory synapses. *J. Neurosci.* **21**, 4249–4258 (2001).
68. Racz, B. & Weinberg, R. J. The subcellular organization of cortactin in hippocampus. *J. Neurosci.* **24**, 10310–10317 (2004).
69. Storey, S. M. et al. Loss of intracellular lipid binding proteins differentially impacts saturated fatty acid uptake and nuclear targeting in mouse hepatocytes. *Am. J. Physiol. Gastrointest. Liver Physiol.* **303**, G837–G850 (2012).
70. Amiry-Moghaddam, M. & Ottersen, O. P. Immunogold cytochemistry in neuroscience. *Nat. Neurosci.* **16**, 798–804 (2013).

Acknowledgements

We are grateful to T. Pozzan, S. Vicini, and P. Magalhaes for their valuable comments on the manuscript and discussions. We also thank B.S. Khakh and R. Srinivasan for help in the use of the GECIquant software. The work was supported by Telethon Italy Grant GGP12265, Cariparo Foundation, National Research Council Aging Project, Fondo per gli Investimenti della Ricerca di Base Grant RBAP11×42L, PRIN 2015-W2N883_001 and Marie Skłodowska-Curie ITN, EU-GliaPhD to G.C., Istituto Italiano di Tecnologia, European Research Council (ERC, NEURO-PATTERNS), FP7-Health (DESIRE), and MIUR FIRB (RBAP11×42L) to T.F. and PRIN (2010JFYFY2), INRCA intramural funds, UNIVPM, and Fondazione di Medicina Molecolare to F.C.

Author contributions

L.M. performed in vivo Ca^{2+} imaging experiments with the collaboration of M.G.-G. and A.C., developed the software for Ca^{2+} data analysis and analyzed data. G.L. and L.M. performed the Ca^{2+} imaging experiments in brain slices and analyzed astrocytic Ca^{2+} signals with the collaboration of M.Z. and A.L.. G.L., L.M., M.S., and I.M. performed the patch-clamp recording experiments in brain slices. M.S., I.M., A.L., S.B., and L.M.R. performed AAV injections and control experiments in brain slices. C.V. provided the SSR4 KO mice and B.B. the $GABA_{B2}$ KO mice. F.C. and T.F. contributed to the design of EM and electrophysiological experiments in vivo that were performed by M.M., with the contribution of A.P. and A.F., respectively. A.C. and S.B. performed control experiments on ChR2 and GCaMP6f expression. G.C. designed the study and wrote the manuscript with inputs from all the authors.

Additional information

Supplementary Information accompanies this paper at https://doi.org/10.1038/s41467-017-02642-6.

Competing interests: The authors declare no competing financial interests.

Reprints and permission information is available online at http://npg.nature.com/reprintsandpermissions/

Publisher's note: Springer Nature remains neutral with regard to jurisdictional claims in published maps and institutional affiliations.

Neuroscience Letters xxx (xxxx) xxx–xxx

Contents lists available at ScienceDirect

Neuroscience Letters

journal homepage: www.elsevier.com/locate/neulet

Dynamic interactions between GABAergic and astrocytic networks

Annamaria Lia[a,b], Micaela Zonta[a,b,*], Linda Maria Requie[a,b], Giorgio Carmignoto[a,b]

[a] University of Padua, Department of Biomedical Sciences, Padua, Italy
[b] CNR, Neuroscience Institute, Padua, Italy

ARTICLE INFO

Keywords:
Astrocytes
Interneurons
GABA
Calcium signaling
Synaptic transmission

ABSTRACT

Brain network activity derives from the concerted action of different cell populations. Together with interneurons, astrocytes play fundamental roles in shaping the inhibition in brain circuitries and modulating neuronal transmission. In this review, we summarize past and recent findings that reveal in neural networks the importance of the interaction between GABAergic signaling and astrocytes and discuss its physiological and pathological relevance.

1. Introduction

The dynamic communication among different types of neurons in the brain is finely tuned to achieve a fast and accurate computation of incoming sensory signals, which ultimately governs cognitive and motor functions. Over the last two decades, a growing body of evidence revealed that astrocytes, a functionally heterogeneous class of glial cells in the brain [1], are not merely passive supporters of brain function, but they rather actively participate in information processing. The study of neuron-astrocyte interactions has brought to the concept of the tripartite synapse in which astrocytic processes, which enwrap the pre- and post-synaptic neuronal elements, contribute to synaptic transmission modulation. Astrocytes possess a wide variety of plasma membrane receptors and respond to neurotransmitters with intracellular [Ca^{2+}] elevations. The consequent release of gliotransmitters, such as glutamate, D-serine and ATP establishes a bidirectional communication with neurons, which contributes to different forms of short- and long-term plasticity of synaptic transmission [2]. The release of these molecules from activated astrocytes can involve different pathways and mechanisms, some of which depend on intracellular calcium increases and vesicular release, others - unrelated to calcium signal - on plasma membrane transporters or channels [3].

While numerous *in situ* and *in vivo* studies explored the role of the astrocytes in glutamatergic, cholinergic and noradrenergic signaling pathways [4–6], the involvement of astrocytes in GABAergic pathways has been poorly investigated. GABAergic inhibitory signals are generated by a very heterogeneous class of interneurons in terms of firing properties, molecular markers, somatic, dendritic and axonal morphology and represent a fundamental operation in brain neural networks [7–10]. Most importantly, the signaling diversity of the different types of GABAergic interneurons to post-synaptic neurons is crucial to generate the functional heterogeneity of brain circuits [11]. Two key interneuron types are the Somatostatin-expressing (SST) and the Parvalbumin-expressing (PV) interneurons. The former target the tuft dendrites of principal cells providing an efficient control of dendritic signal integration, the latter target different sub-compartments of principal cells: the PV basket cells target the soma and the proximal dendrites, while the PV chandelier cells target the axon initial segment. PV interneurons are, therefore, in a privileged position to control the timing of the action potential firing. Interneurons subtypes are also interconnected, with SST interneurons being inhibited by vasoactive intestinal peptide (VIP) interneurons and, in turn, inhibiting PV interneurons [12]. During development, SST interneurons also exert an important role in the synaptic maturation of PV interneurons [13]. Recent *in vivo* studies highlighted some distinct features of SST and PV interneurons. In the hippocampus SST interneurons regulate the size of neuronal memory ensembles, therefore determining the size of cellular engram [14]. In the neocortex, the transition to active wakefulness modulates the activity of SST interneurons in a layer-specific way, essentially depending on the degree of VIP interneuron or cholinergic innervation, with consequences on dendritic inhibition of different principal cells [15]. In the medial entorhinal cortex, a key component for neuronal representation of the space in mammalian brain, PV and SST interneurons interact with distinct, spatially modulated subpopulations of cells. Interestingly, PV interneurons are needed to specifically tune the activity of grid and speed cells, while SST interneurons are recruited to maintain the spatial specificity in cells [16].

Understanding how interneurons - and possibly different interneuron subtypes - interact with astrocytes, and whether these glial cells integrate GABAergic communication is fundamental to widen our

* Corresponding author at: Department of Biomedical Sciences, via Ugo Bassi 58/b, 35131 Padova, Italy.
E-mail address: micaela.zonta@cnr.it (M. Zonta).

https://doi.org/10.1016/j.neulet.2018.06.026
Received 20 February 2018; Received in revised form 12 June 2018; Accepted 13 June 2018

comprehension of brain circuit function. In this review, we will discuss the following raising issues: i) the astrocytic response to GABAergic signals; ii) the relevance of GABA-activated astrocytes (GAAs) in distinct brain circuits; iii) the astrocytic ability to influence GABAergic transmission; iv) the physiological and pathological relevance of interneuron-astrocyte interplay.

2. Activation of astrocytes by GABA

The expression in astrocytes of ionotropic and metabotropic GABA (γ-Aminobutyric acid) receptors (Rs) as well as of GABA transporters (GATs) indicate that astrocytes have the potential to sense GABAergic signals. Direct evidence that astrocytes can respond to GABA was obtained in electrophysiological studies firstly in acutely isolated astrocytes [17,18] and later in hippocampal, retinal and cerebellar slices [19–21], where astrocytes were shown to possess functional $GABA_AR$s similar to those observed in neurons. However, while the activation of $GABA_A$Rs leads to hyperpolarization in mature neurons, it drives a depolarizing current in astrocytes. This different effect is dependent on the high expression in astrocytes of the $Na^+/K^+/Cl^-$ cotransporter (NKCC1) that maintains in these cells a larger intracellular concentration of Cl^- ions with respect to neurons, thus inverting the transmembrane gradient. This event contributes to regulate extracellular $[Cl^-]$ levels [22], thereby buffering extracellular chloride and ultimately allowing to maintain an efficient GABAergic signaling. The possible physiological consequence of Cl^--mediated astrocytic depolarization is still a matter of debate. Unlike neurons, astrocytes are electrically non-excitable cells and exhibit a form of excitability that relies on intracellular Ca^{2+} elevations. The first clue of this Ca^{2+}-based form of excitability in astrocytes was obtained in the early 1990 s, when the application of Ca^{2+} imaging techniques to cultured astrocytes revealed that these cells respond to neurotransmitters with intracellular Ca^{2+} elevations [23,24]. This property of astrocytes was confirmed in different brain regions where astrocytes respond with Ca^{2+} elevations to the synaptic release of different neurotransmitters [33,34,35,25–27]. The neurotransmitter GABA makes no exception to this rule, evoking astrocytic Ca^{2+} events that were mediated by the activation of ionotropic $GABA_A$ and/or metabotropic $GABA_B$Rs [28] (Fig.1A–B). Calcium elevations mediated by $GABA_A$Rs activation are dependent on Ca^{2+} influx from extracellular space through voltage-sensitive Ca^{2+} channels (VOCCs), activated upon membrane depolarization. In contrast, the mechanism of $GABA_B$R-mediated Ca^{2+} events has been shown to involve G proteins and Ca^{2+} release from internal stores [29,30]. Indeed, the specific $GABA_B$R agonist baclofen (BAC) fails to induce astrocytic Ca^{2+} elevations in mice lacking the IP_3R type 2 ($IP3R2^{-/-}$), which in the brain is mainly, if not exclusively, expressed in astrocytes [31,32]. Additionally, astrocytic Ca^{2+} signaling upon GABA activation depends also on $G_{i/o}$ protein activation, as it occurs in neurons [30]. Several studies demonstrated that GABA activation of astrocytes can be also mediated by GATs. Olfactory bulb astrocytes enwrapping GABAergic synapses were shown to respond to synaptically released GABA with intracellular Ca^{2+} events that were fully prevented by GAT blockers [33]. In a more recent study, Boddum and co-workers similarly found that activation of GAT3 induces astrocytic Ca^{2+} increases in the hippocampus [34]. The general mechanism that drives intracellular Ca^{2+} increases in astrocytes upon GAT activation depends on the co-transport of GABA and Na^+. The increase in intracellular Na^+ concentration that follows GAT activity leads to the inverse operation of the Na^+/Ca^{2+} exchanger (NCX) with a consequent increase in cytosolic $[Ca^{2+}]$ [33] (Fig.1C).

2.1. Astrocytes activated by different GABAergic interneurons

A topic of interest concerning GABA-activated astrocytes is to characterize the dynamics and properties of Ca^{2+} signals evoked by GABA. Taking advantage of the genetically encoded Ca^{2+} indicator GCaMP3, it has been demonstrated that GABA evokes at the soma and the processes of neocortical astrocytes oscillatory and long-lasting Ca^{2+} responses both *in situ* and *in vivo* [30] (Fig. 2A–C). Noteworthy, these responses were shown to possess a form of plasticity, which depends on the subtype of GABAergic interneurons recruiting astrocytes [35]. A selective optogenetic light pulse activation of ChR2-expressing PV or SST interneurons, in both slice and *in vivo* preparations of the mouse somatosensory cortex (SSCx), was indeed observed to evoke weak and robust $GABA_B$R-mediated Ca^{2+} elevations, respectively. Furthermore, astrocytic Ca^{2+} elevations were depressed after repetitive stimulation of PV interneurons, but they were potentiated after repetitive stimulation of SST interneurons. The potentiated Ca^{2+} response was shown to crucially depend on the neuropeptide SST, co-released with GABA by SST interneurons, suggesting that different interneurons may avail of the concurrent release of GABA and neuropeptides to differentially recruit astrocytes to their specific circuits. Overall, this study unveils the existence in the brain of specific interneuron type-astrocyte networks in which astrocytes not only discriminate the GABAergic signaling from different interneuron subtypes, but also retain memory of the previous history of activity in the surrounding interneuron network. These properties of astrocytes are akin to those of memory cells and define a new context that could help to direct future studies on learning and memory mechanisms in brain circuits, specifically with respect to the role played in these phenomena by the neuropeptide Somatostatin and the SST interneurons [14,36–39].

3. Can GABA-activated astrocytes modulate neuronal activity?

The effect of GABA-activated astrocytes (GAAs) on neuronal activity has been mainly explored in the hippocampus, with the first pioneering study published in 1998. In this paper, Kang and collaborators provided evidence that GABA can trigger in hippocampal astrocytes a Ca^{2+} dependent release of glutamate which increases the probability of GABA release onto pyramidal neurons (PyrNs) [40]. This enhancement of inhibitory transmission was strictly dependent on the astrocyte Ca^{2+} response to GABA, since it was abolished when Ca^{2+} elevations were

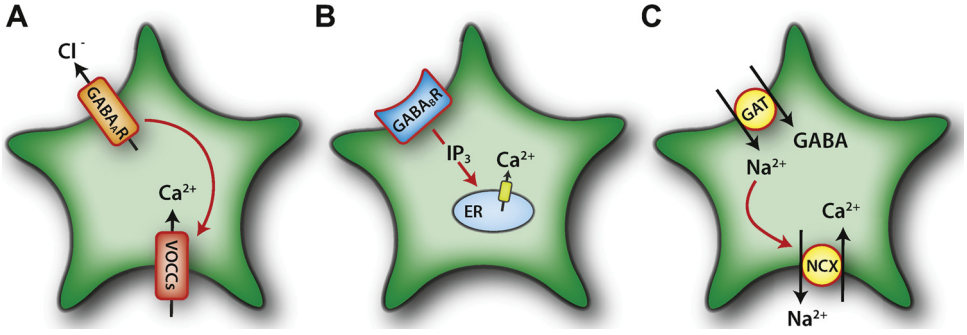

Fig. 1. (A–C) Intracellular pathways leading to Ca^{2+} increase in GABA-activated astrocytes.

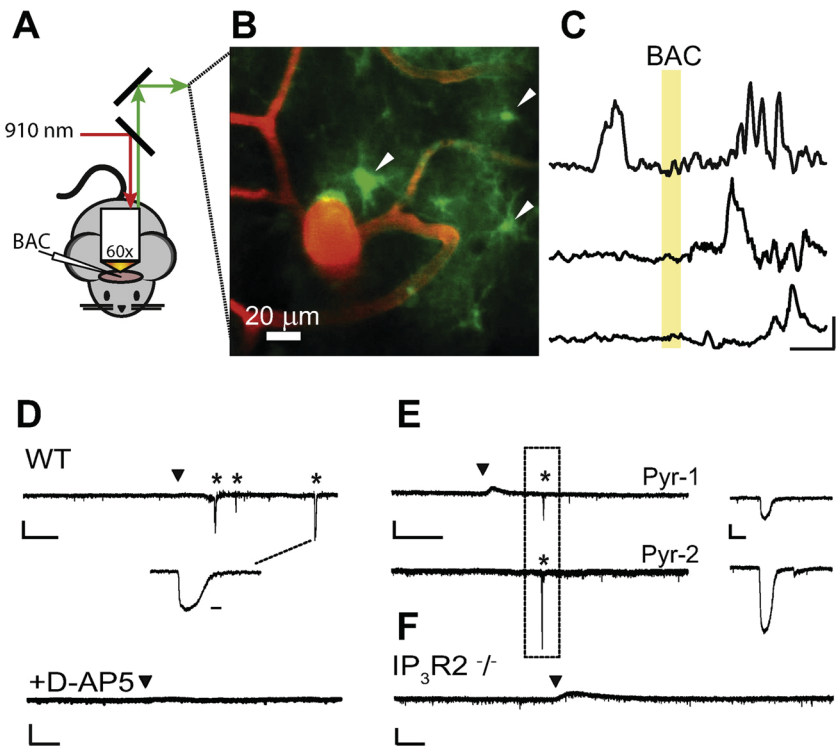

Fig. 2. $GABA_B$ receptor activation induces long-lasting Ca^{2+} oscillations in astrocytes and slow inward currents in pyramidal neurons. (A-C) Experiments in anaesthetized mice. (**A**) Schematic representation of the two-photon *in vivo* set up. The excitation wavelength 910 nm excites both Dextran-TRITC and GCaMP3. (**B**) Maximal projection of blood vessels filled with Dextran-TRITC and astrocytes expressing GCaMP3 in layer I/II of SSCx (right). White arrowheads indicate three representative astrocytes soma. (**C**) Ca^{2+} traces before and after a BAC application. Yellow area marks the local BAC application (scale bars: 20% DF/F_0, 50 s). **(D–F) GABA-activated astrocytes evoke SICs in pyramidal neurons.** Representative whole cell currents from single pyramidal neurons (**D**) or a pair (**E**) of adjacent pyramidal neurons (90 mm apart; Pyr-1 and -2) showing the occurrence of SICs (asterisks) after a BAC local application (black arrowheads) to layer V SSCx in a WT mouse and the absence of SICs upon a similar BAC application in presence of D-AP5 (D, bottom trace) and in $IP3R2^{-/-}$ mice (**F**). (Scale bars: For single recordings: 1 min, 100 pA; enlarged SIC: 500 ms; for paired recording and D-AP5: 20 s, 100 pA and 2 s for the enlarged SIC) *From Mariotti et al., 2015* [30] (For interpretation of the references to colour in this figure legend, the reader is referred to the web version of this article).

blocked by $GABA_BR$ antagonists or by the insertion of the Ca^{2+} chelator BAPTA into the astrocytic *syncytium*. Less than a decade later, it was reported that in the same CA1 region of hippocampus, glutamate released from GAAs can also act on presynaptic group II/III metabotropic glutamate receptors (mGluRs) and cause a transient reduction in glutamate release probability at glutamatergic axon terminals, a phenomenon known as transient heterosynaptic depression (tHD) [41]. Beside glutamate, other gliotransmitters released by GAAs can modulate synaptic strength. The group of Robitaille reported that astrocytes are directly involved in another form of heterosynaptic depression (HD) in hippocampal circuits, which depends on astrocytic release of ATP, its conversion to adenosine and activation of presynaptic $A1R_S$, finally decreasing glutamate release probability [42]. More relevant for the role of GAAs, it was reported that both astrocytic Ca^{2+} responses and HD were dependent on $GABA_BR$ activation. The astrocytic influence on HD can also involve the specific astrocytic GABA transporter GAT-3. In hippocampal astrocytes, GAT-3 activation leads to a Ca^{2+}- dependent release of ATP/adenosine, that acting on presynaptic A1Rs causes a diffused inhibition of neuronal glutamate release, contributing to the homeostatic control of network activity [34]. So far, we presented how GAAs can contribute to "diffusion" of inhibition in hippocampal networks. Unexpectedly, astrocytes have also the potential to decode interneuron activity and convert inhibitory into excitatory signals, as unveiled in Perea [43]. Minimal Schaffer collateral stimulation was paired with applications of depolarizing pulses to an individual hippocampal interneuron, while assessing the response of a synaptically connected pyramidal neuron. Depending on the strength of interneuron activation, resulting in single APs or AP bursts, this experimental protocol resulted in inhibition or potentiation of CA3-CA1 synapses, respectively. While inhibition was dependent on presynaptic $GABA_AR$s, burst-induced potentiation relied on $GABA_BR$ activation and it was accompanied by Ca^{2+} elevations in astrocytes. Depletion of internal Ca^{2+} stores through thapsigargin perfusion and selective BAPTA loading in the astrocytic *syncytium* both succeeded in abolishing not only Ca^{2+} elevations in astrocytes but also the synaptic potentiation. The same downstream effects were obtained in the presence of $GABA_B$ receptor antagonists and using an astrocyte-specific $GABA_BR1$ knockout mouse. As expected, the deletion of $GABA_BR$s in astrocytes hampered the potentiation upon interneuron bursts, while leaving intact the inhibitory effect of single AP induction, confirming that GAAs are necessary for this potentiation. Again, slight variations in the context and the molecular players, in this case CA3-CA1 synapse and astrocytic glutamate acting on presynaptic mGluRI, determine the final effect of GAAs on the neurotransmission modulation.

The role of GAAs in tuning neuronal activity has been explored also in the cortex in a recent paper by Mariotti [30]. In this study, the authors chose to monitor, as a marker of neuronal activation by astrocytic release of glutamate, slow inward currents (SICs), events of widely accepted astrocytic origin. SICs are indeed preserved when synaptic transmission is inhibited by TTX and TeNT, and can be induced by a variety of protocols all resulting in astrocytic calcium increases, from metabotropic receptor activation to calcium uncaging in individual astrocytes [44]. Single and dual-cell patch clamp recordings were performed from PyrNs in the presence of TTX and low frequency glutamatergic SICs were recorded (Fig. 2D-F). $GABA_BR$ activation with exogenous application of BAC, beside inducing long-lasting Ca^{2+} elevations in astrocytes, increased the frequency and the synchronization of SICs in PyrNs. When the same experiments were repeated in $IP3R2^{-/-}$ mice, BAC effects were abolished. These results clearly indicate that GAAs can modulate neuronal activity also in the cortex, and report another example of astrocytes turning a local transient inhibition in a delayed excitation.

Overall, the above discussed studies highlight the complexity of the astrocyte signaling and reveal that the specificities in the action of astrocytes are determined by the type of synaptic circuit, neurotransmitter system and region involved (Fig. 3A).

4. Astrocytic modulation of GABAergic transmission

After the pioneering study of Kang in 1998 [40], the ability of astrocytes to influence inhibitory transmission has been neglected for a long time. Over the last decade, different studies resumed this aspect and shed light into the potential effect of astrocytes on inhibitory transmission (Fig. 3B). A variety of stimuli was used to induce

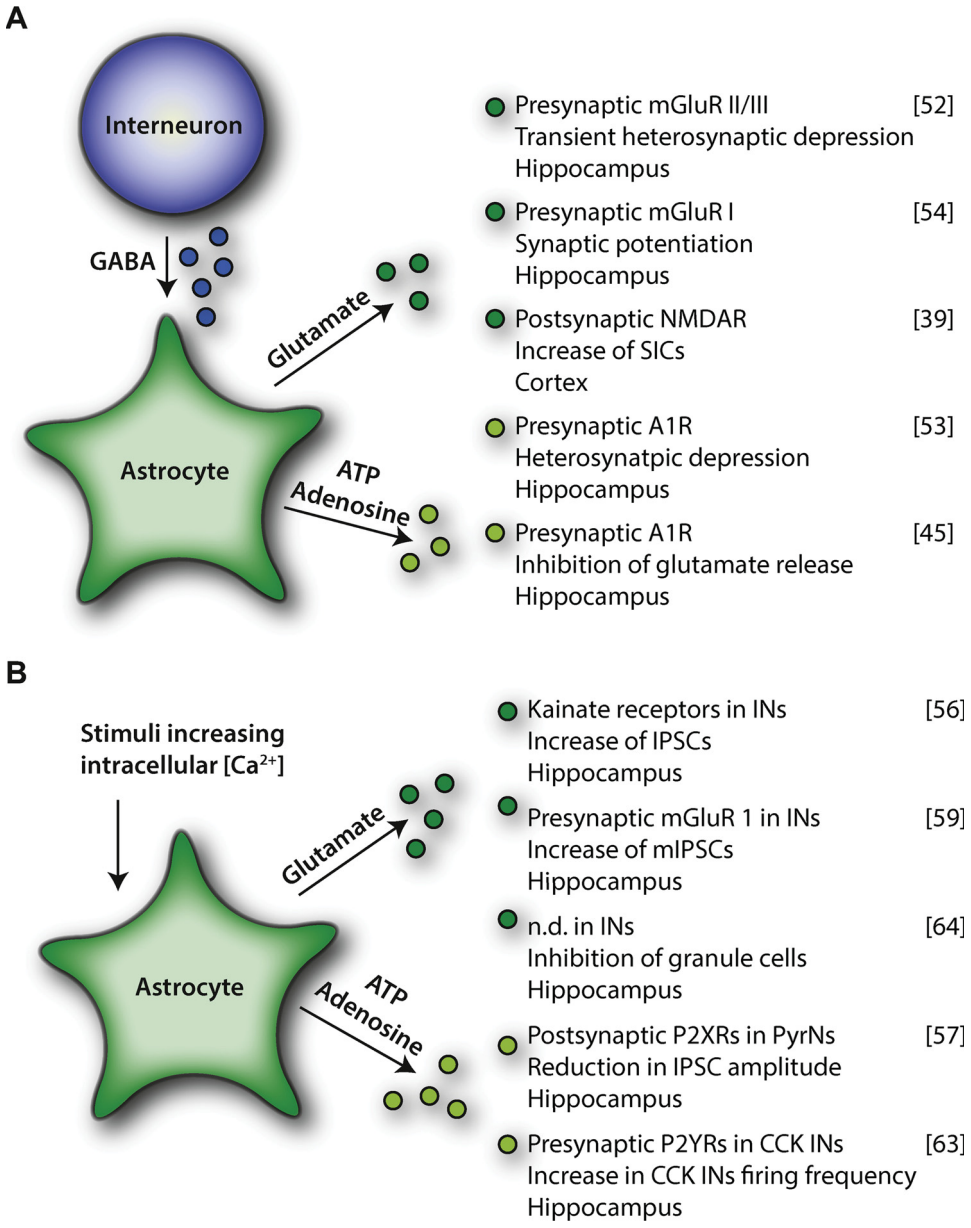

Fig. 3. (A) Modulation of neuronal activity from GABA-activated astrocytes. **(B)** Gliotransmitter-mediated modulation of inhibitory transmission.

gliotransmitter release, from UV light flashes or optogenetic tools, to more physiological stimulation of neuronal afferents to the brain region of interest. It was found that astrocytic Ca^{2+} increases triggered by UV-light pulses induce an increase in the frequency of spontaneous IPSCs (sIPSCs) in hippocampal CA1 interneurons of the stratum radiatum. This effect was dependent on the direct activation of kainate receptors in interneurons following astrocytic glutamate release [45]. In the SSCx, Lalo and colleagues conversely reported an astrocytic modulation of both phasic and tonic inhibition affecting postsynaptic targets rather than GABAergic presynaptic sites [46]. Astrocytes were activated through photolysis of NP-EGTA or application of TFLLR or N-methyl-D-aspartate receptor (NMDAR), which lead to the vesicular release of ATP ultimately acting on neuronal P2XRs. The consequent intracellular Ca^{2+} increase induced a phosphorylation-dependent downregulation of $GABA_A$Rs, and reduced IPSCs amplitude. Accordingly, in a transgenic mouse model with impaired vesicular ATP release, *i.e.* the dnSNARE mice [47], both the IPSCs and the tonic GABA current were significantly larger than in wild- type (WT) mice. These data support the idea that astrocytic ATP release can affect both synaptic and extrasynaptic GABAergic signaling. More recently, the use of optogenetic tools to directly stimulate astrocytes has allowed to further evaluate the potential role of astrocyte activation in the modulation of neuronal network. Light stimulation of ChR2-expressing astrocytes in the visual cortex induced a short-term enhancement of both excitatory and inhibitory synaptic transmission onto PyrNs [48]. This effect depends on astrocytic glutamate acting on presynaptic mGluR1a, as already described in a large variety of brain areas [49–51]. A similar stimulation of ChR2-expressing astrocytes in the hippocampal area CA1 results in differential changes in the activity of neuronal populations, causing a decrease in the firing frequency of hippocampal PyrNs and a firing frequency increase in a selective population of interneurons in this region, *i.e.* cholecystokinin (CCK) interneurons [52]. These effects were mediated by the astrocytic release of ATP. ATP-derived adenosine binds to A1Rs on PyrNs and induces hyperpolarization *via* activation of GIRK channels, while the direct activation of P2YRs in CCK interneurons inhibits the two-pore domain K^+ channels, thus leading to membrane depolarization. This ChR2-mediated activation of astrocytes can mimic the high levels of astrocytic activation occurring in several

pathological conditions, such as stroke and epilepsy. In these brain disorders, ATP released by astrocytes may differentially modulate GABAergic and glutamatergic neurons finally resulting in a global reduction of hippocampal excitatory output. Optogenetic techniques were also applied to indirectly activate hippocampal astrocytes *via* light stimulation of septal cholinergic interneurons, as it is described in Pabst et al. [53]. In this paper, optogenetic activation of cholinergic neurons causes intracellular Ca^{2+} increases in hilar astrocytes through nicotinic receptors. The consequent release of glutamate from astrocytes recruits hilar inhibitory interneurons, thus leading to a slow inhibition of hippocampal granule cells through astrocytic intermediates.

Beside releasing gliotransmitters that directly influence GABAergic transmission at pre- or post-synaptic sites, astrocytes can modulate neuronal excitability by controlling the extracellular GABA concentration *via* GATs. This action of astrocytes is especially relevant when network activity is increased. In a recent paper, Jacob et al. [54] demonstrated that GAT1/3 activity can be negatively influenced by ATP signaling through activation of P2Y1Rs in cortical astrocytes. The intracellular signaling pathway underlying this phenomenon depends on IP3-mediated Ca^{2+} release from the endoplasmic reticulum. The increased intracellular Ca^{2+} concentration raises the activity of NCX eventually leading, as previously described, to the reduction of GAT mediated GABA uptake. Therefore, the effect on GABA transport may be important in the generation of a negative feedback loop that increases the extracellular GABA concentration to brake neuronal firing. Importantly, GATs can even revert their direction and release GABA in the extracellular space under conditions in which network activity may lead to excitotoxic effects, as highlighted in Heja's work [55]. Indeed, during enhanced neuronal network activity the increased excitatory amino acid transporter 2 (EAAT2) activity, leads to GABA release after the reversal of GATs. This causes a final increase of tonic inhibition on nearby CA1 PyrNs, demonstrating a direct conversion of glutamatergic excitation to GABAergic inhibition in the brain.

5. Physiological and pathological relevance of GABA-Astrocytes interplay

In the previous chapters, we explored the direct effect of GABA on astrocytic activity and, more importantly, the influence of GAAs on neuronal activity and synaptic transmission. In this last section, we focus our attention on the physiological and pathological relevance of these interactions. Indeed, it remains largely undefined whether and how distinct GABAergic signaling to astrocytes impacts complex behaviors. Evidence for such a role has been provided in a study investigating in the mouse visual cortex the contribution of GABAergic interneurons in the processing of visual stimuli [48]. In this study, performed in anesthetized mice, optogenetic activation of ChR2-expressing astrocytes modulates the response selectivity of visual cortical neurons. The authors evaluated the visual response to oriented drifting gratings by recording from L2/3 excitatory and different inhibitory neurons. After astrocyte stimulation, PV interneurons displayed an enhancement in the baseline firing rate, a parameter independent of spontaneous activity that measures the overall level of visually driven responses. Such an increase in the baseline predicts a reduction in the Orientation Selectivity Index (OSI). Indeed, after astrocyte photostimulation, PV interneurons showed a robust reduction in OSI. Conversely, the effect of astrocyte activation on excitatory PyrNs and SST interneurons was variable and less clear. Notably, using a specific mGluR1a blocker (AIDA), the authors could demonstrate that the ability of astrocytes to regulate visual tuning properties of PV cortical interneurons is mediated by mGluR1a activation. This work complements previous *in vivo* results showing that the transient blockade of astrocyte glutamate transporters prolongs the orientation-tuning response [4] and that astrocyte-specific deletion of IP3R2-mediated Ca^{2+} responses abolishes adaptation-induced changes in orientation-tuning curves [56]. To our knowledge, this work is the only one that correlates an astrocyte-mediated activation of inhibitory neurons with a physiological response. The reciprocal interactions between GABAergic interneurons and astrocytes in the healthy brain probably represent an important phenomenon in the dynamic control of brain circuit activities. This leads to the question of whether a dysfunction in these interactions is involved in brain disorders characterized by a change in the efficacy of GABAergic transmission and brain circuit hyperexcitability. Under pathological conditions, astrocytes become hypertrophic and reactive [57]. One of the diseases in which the role of reactive astrocytes has been extensively explored is temporal lobe epilepsy (TLE), the most common form of focal epilepsy [58]. In this pathology, network hyperexcitability is accompanied by neuronal loss and reactive astrocytosis both in hippocampus and associated temporal lobe structures. In 2010, Ortinski and colleagues [59] tried to isolate the effect of astrocytosis on network hyperexcitability in hippocampal CA1 region, by assessing the effect on synaptic transmission of virus-induced reactive astrocytosis. They found that an early effect of astrocytosis is a decrease in glutamine synthesis in astrocytes, which is fundamental for the production of both glutamate and GABA. The consequent reduction in the pool of GABA available for synaptic release, in the region of reactive astrocytosis, leads to a selective deficit in inhibitory, but not excitatory, transmission. This defect leads to network hyperexcitability, a common feature of different mouse model of TLE.

Another pathophysiological condition characterized by neuronal hyperexcitability is the spreading depression (SD). This phenomenon can occur in different pathological conditions, such as migraine with aura, stroke and brain injuries [60]. Very recently, a new cellular event that involves both astrocytes and GABA has been described in SD [61]. SD is characterized by propagating waves of neuronal and glia depolarization, followed by a recovery phase. After an initial astrocytic Ca^{2+} wave, SD was shown to promote an oscillatory Ca^{2+} activity in astrocytes during the recovery phase, accompanied by an increase in SICs occurrence in nearby neurons, indicative of an increase in glia to neuron transmission [44]. Experimental results showed that the oscillatory Ca^{2+} activity in astrocytes did not require synaptic transmission, since it persisted in the presence of TTX or AMPA receptor antagonists, and it was independent on purinergic and glutamatergic receptors. Interestingly, during SD an increase in extracellular GABA has been reported [62,63] and, as previously described, long-lasting Ca^{2+} oscillations can be induced in astrocytes by activation of $GABA_BRs$ [30]. Accordingly, by using $GABA_BR$ antagonists the authors succeeded in abolishing both the oscillatory Ca^{2+} activity in astrocytes and the enhancement of SICs in neurons. The mechanisms at the basis of network hyperexcitability reported in these two studies recapitulate two important aspects already discussed in this review. The first is the ability of astrocytes to modulate GABA levels through different mechanisms, in this case by controlling the availability of its precursor glutamine, the second is the role of GAAs and gliotransmission in regulating neuronal network excitability.

The relationship between GABA and astrocytes has been investigated in different papers also in relation with Alzheimer's disease (AD). AD is the most common form of dementia, characterized by frequent association with extracellular deposits of Aβ-plaques and intraneuronal accumulation of neurofibrillary tangles [64]. In 2014, two different laboratories revealed the detrimental role of GABA released from reactive astrocytes in different mouse models of AD. Wu et al. [65] investigated GABA effects in the dentate gyrus (DG), *i.e.* the gateway of cortical input to the hippocampus that is crucially involved in learning and memory, of 5xFAD mice as well as in brain samples from human AD patients [66]. They found an unusual high GABA content in reactive astrocytes of the DG only in the presence of fully developed Aβ-plaques (in 6–8 months old mice and in human brains from AD patients). This was accompanied by an augmented expression of glutamic acid decarboxylase (GAD), *i.e.* the enzyme involved in GABA synthesis, and of the GABA transporter GAT3/4. In order to verify the possibility that GATs mediate GABA release from reactive astrocytes, the authors

focused their attention on tonic inhibition in the DG of 5xFAD mice, where GABA released by reactive astrocytes generates a tonic GABA current mediated by $GABA_AR$ activation on nearby neurons [67]. They found that DG cells from 6 to 8 months old 5xFAD mice showed a larger tonic GABA current with respect to age-matched WT mice, that was abolished by specifically blocking GAT3/4. Noteworthy, inhibitors of GAT3/4 or $GABA_AR$ were also able to rescue behavioral memory deficits in 5xFAD mice. In the same year, Jo and colleagues [68] published a similar study using, beside the 5xFAD mouse model, the APP/PS1 AD model. These authors confirmed the abnormal GABA release in DG and showed that it involves an increased extrusion of Ca^{2+} through the glutamate and GABA-permeable bestrophin-1 channel (Best1), that is highly expressed at the astrocytic microdomains near synapses [69]. The authors previously demonstrated that this mechanism is physiologically present in the cerebellum [70] whereas in hippocampus tonic GABA release in physiological conditions is low [71]. GABA released from astrocytes through Best-1 channel activates both $GABA_AR$ and $GABA_BR$, leading to a presynaptic form of inhibition that hampers neurotransmitter release. The main consequence is an impairment of LTP and cognitive functions, caused by a reduction in spike probability at the perforant-path-to-dentate-granule-cell synapse. Astrocytic GABA release plays therefore, a central role in AD influencing both neuronal activity and cognitive functions.

Despite the evidence of a strict relationship between GABAergic and astrocytic networks in different brain regions, our knowledge of how this interaction is correlated to physiological processes remains unsatisfactory. A long way is ahead to clarify the relevance of these mechanisms in behavioral contexts. Exploring *in vivo* this crucial aspect will open new perspectives in the comprehension of brain physiology and, at the same time, it will help the development of new therapeutic strategies in brain diseases.

Acknowledgments

The original work by the authors was supported by Telethon Italy Grant GGP12265, Cariparo Foundation, National Research Council Aging Project, Fondo per gli Investimenti della Ricerca di Base Grant RBAP11 × 42 L, PRIN 2015-W2N883_001 and Marie Skłodowska-Curie ITN, EU-GliaPhD to G.C.

References

[1] A. Verkhratsky, M. Nedergaard, Physiology of astroglia, Physiol. Rev. 98 (2018) 239–389.
[2] A. Araque, G. Carmignoto, P.G. Haydon, S.H. Oliet, R. Robitaille, A. Volterra, Gliotransmitters travel in time and space, Neuron 81 (2014) 728–739.
[3] V. Parpura, R. Zorec, Gliotransmission: exocytotic release from astrocytes, Brain Res. Rev. 63 (2010) 83–92.
[4] J. Schummers, H. Yu, M. Sur, Tuned responses of astrocytes and their influence on hemodynamic signals in the visual cortex, Science 320 (2008) 1638–1643.
[5] M. Navarrete, G. Perea, D. Fernandez de Sevilla, M. Gomez-Gonzalo, A. Nunez, E.D. Martin, A. Araque, Astrocytes mediate in vivo cholinergic-induced synaptic plasticity, PLoS Biol. 10 (2012) e1001259.
[6] M. Paukert, A. Agarwal, J. Cha, V.A. Doze, J.U. Kang, D.E. Bergles, Norepinephrine controls astroglial responsiveness to local circuit activity, Neuron 82 (2014) 1263–1270.
[7] H. Markram, M. Toledo-Rodriguez, Y. Wang, A. Gupta, G. Silberberg, C. Wu, Interneurons of the neocortical inhibitory system, Nat. Rev. Neurosci. 5 (2004) 793–807.
[8] T. Klausberger, P. Somogyi, Neuronal diversity and temporal dynamics: the unity of hippocampal circuit operations, Science 321 (2008) 53–57.
[9] B. Rudy, G. Fishell, S. Lee, J. Hjerling-Leffler, Three groups of interneurons account for nearly 100% of neocortical GABAergic neurons, Dev. Neurobiol. 71 (2011) 45–61.
[10] A. Kepecs, G. Fishell, Interneuron cell types are fit to function, Nature 505 (2014) 318–326.
[11] P. Somogyi, G. Tamas, R. Lujan, E.H. Buhl, Salient features of synaptic organisation in the cerebral cortex, Brain Res. Brain Res. Rev. 26 (1998) 113–135.
[12] C.K. Pfeffer, M. Xue, M. He, Z.J. Huang, M. Scanziani, Inhibition of inhibition in visual cortex: the logic of connections between molecularly distinct interneurons, Nat. Neurosci. 16 (2013) 1068–1076.
[13] S.N. Tuncdemir, B. Wamsley, F.J. Stam, F. Osakada, M. Goulding, E.M. Callaway, B. Rudy, G. Fishell, Early somatostatin interneuron connectivity mediates the maturation of deep layer cortical circuits, Neuron 89 (2016) 521–535.
[14] T. Stefanelli, C. Bertollini, C. Luscher, D. Muller, P. Mendez, Hippocampal somatostatin interneurons control the size of neuronal memory ensembles, Neuron 89 (2016) 1074–1085.
[15] W. Munoz, R. Tremblay, D. Levenstein, B. Rudy, Layer-specific modulation of neocortical dendritic inhibition during active wakefulness, Science 355 (2017) 954–959.
[16] C. Miao, Q. Cao, M.B. Moser, E.I. Moser, Parvalbumin and somatostatin interneurons control different space-coding networks in the medial entorhinal cortex, Cell 171 (2017) 507–521 e517.
[17] H. Kettenmann, K.H. Backus, M. Schachner, Aspartate, glutamate and gamma-aminobutyric acid depolarize cultured astrocytes, Neurosci. Lett. 52 (1984) 25–29.
[18] D.D. Fraser, S. Duffy, K.J. Angelides, J.L. Perez-Velazquez, H. Kettenmann, B.A. MacVicar, $GABA_A$/benzodiazepine receptors in acutely isolated hippocampal astrocytes, J. Neurosci. 15 (1995) 2720–2732.
[19] B.A. MacVicar, F.W. Tse, S.A. Crichton, H. Kettenmann, GABA-activated Cl^- channels in astrocytes of hippocampal slices, J. Neurosci. 9 (1989) 3577–3583.
[20] B. Clark, P. Mobbs, Transmitter-operated channels in rabbit retinal astrocytes studied in situ by whole-cell patch clamping, J. Neurosci. 12 (1992) 664–673.
[21] T. Muller, J.M. Fritschy, J. Grosche, G.D. Pratt, H. Mohler, H. Kettenmann, Developmental regulation of voltage-gated K^+ channel and $GABA_A$ receptor expression in Bergmann glial cells, J. Neurosci. 14 (1994) 2503–2514.
[22] K. Egawa, J. Yamada, T. Furukawa, Y. Yanagawa, A. Fukuda, Cl^- Homeodynamics in gap-junction-coupled astrocytic networks on activation of GABAergic synapses, J. Physiol. 591 (2013) 3901–3917.
[23] A.H. Cornell-Bell, S.M. Finkbeiner, M.S. Cooper, S.J. Smith, Glutamate induces calcium waves in cultured astrocytes: long-range glial signaling, Science 247 (1990) 470–473.
[24] A.C. Charles, J.E. Merrill, E.R. Dirksen, M.J. Sanderson, Intercellular signaling in glial cells: calcium waves and oscillations in response to mechanical stimulation and glutamate, Neuron 6 (1991) 983–992.
[25] A. Araque, E.D. Martin, G. Perea, J.I. Arellano, W. Buno, Synaptically released acetylcholine evokes Ca2+ elevations in astrocytes in hippocampal slices, J. Neurosci. 22 (2002) 2443–2450.
[26] F. Ding, J. O'Donnell, A.S. Thrane, D. Zeppenfeld, H. Kang, L. Xie, F. Wang, M. Nedergaard, Alpha1-adrenergic receptors mediate coordinated Ca2+ + signaling of cortical astrocytes in awake, behaving mice, Cell. Calcium 54 (2013) 387–394.
[27] L. Pasti, A. Volterra, T. Pozzan, G. Carmignoto, Intracellular calcium oscillations in astrocytes: a highly plastic, bidirectional form of communication between neurons and astrocytes in situ, J. Neurosci. 17 (1997) 7817–7830.
[28] M. Nilsson, P.S. Eriksson, L. Ronnback, E. Hansson, GABA induces Ca^{2+} transients in astrocytes, Neuroscience 54 (1993) 605–614.
[29] S.D. Meier, K.W. Kafitz, C.R. Rose, Developmental profile and mechanisms of GABA-induced calcium signaling in hippocampal astrocytes, Glia 56 (2008) 1127–1137.
[30] L. Mariotti, G. Losi, M. Sessolo, I. Marcon, G. Carmignoto, The inhibitory neurotransmitter GABA evokes long-lasting Ca^{2+} oscillations in cortical astrocytes, Glia (2015).
[31] D.N. Hertle, M.F. Yeckel, Distribution of inositol-1,4,5-trisphosphate receptor isotypes and ryanodine receptor isotypes during maturation of the rat hippocampus, Neuroscience 150 (2007) 625–638.
[32] A.H. Sharp, F.C. Nucifora Jr, O. Blondel, C.A. Sheppard, C. Zhang, S.H. Snyder, J.T. Russell, D.K. Ryugo, C.A. Ross, Differential cellular expression of isoforms of inositol 1,4,5-triphosphate receptors in neurons and glia in brain, J. Comp. Neur. 406 (1999) 207–220.
[33] M. Doengi, D. Hirnet, P. Coulon, H.C. Pape, J.W. Deitmer, C. Lohr, GABA uptake-dependent Ca^{2+} signaling in developing olfactory bulb astrocytes, Proc. Natl. Acad. Sci. U. S. A. 106 (2009) 17570–17575.
[34] K. Boddum, T.P. Jensen, V. Magloire, U. Kristiansen, D.A. Rusakov, I. Pavlov, M.C. Walker, Astrocytic GABA transporter activity modulates excitatory neurotransmission, Nat. Commun. 7 (2016) 13572.
[35] L. Mariotti, G. Losi, A. Lia, M. Melone, A. Chiavegato, M. Gomez-Gonzalo, M. Sessolo, S. Bovetti, A. Forli, M. Zonta, L.M. Requie, I. Marcon, A. Pugliese, C. Viollet, B. Bettler, T. Fellin, F. Conti, G. Carmignoto, Interneuron-specific signaling evokes distinctive somatostatin-mediated responses in adult cortical astrocytes, Nat. Commun. 9 (2018) 82.
[36] L.J. Gentet, Y. Kremer, H. Taniguchi, Z.J. Huang, J.F. Staiger, C.C. Petersen, Unique functional properties of somatostatin-expressing GABAergic neurons in mouse barrel cortex, Nat. Neurosci. 15 (2012) 607–612.
[37] J. Urban-Ciecko, E.E. Fanselow, A.L. Barth, Neocortical somatostatin neurons reversibly silence excitatory transmission via GABAb receptors, Curr. Biol. 25 (2015) 722–731.
[38] J. Urban-Ciecko, A.L. Barth, Somatostatin-expressing neurons in cortical networks, Nat. Rev. Neurosci. 17 (2016) 401–409.
[39] H. Makino, T. Komiyama, Learning enhances the relative impact of top-down processing in the visual cortex, Nat. Neurosci. 18 (2015) 1116–1122.
[40] J. Kang, L. Jiang, S.A. Goldman, M. Nedergaard, Astrocyte-mediated potentiation of inhibitory synaptic transmission, Nat. Neurosci. 1 (1998) 683–692.
[41] M. Andersson, F. Blomstrand, E. Hanse, Astrocytes play a critical role in transient heterosynaptic depression in the rat hippocampal CA1 region, J. Physiol. 585 (2007) 843–852.
[42] A. Serrano, N. Haddjeri, J.C. Lacaille, R. Robitaille, GABAergic network activation of glial cells underlies hippocampal heterosynaptic depression, J. Neurosci. 26 (2006) 5370–5382.
[43] G. Perea, R. Gomez, S. Mederos, A. Covelo, J.J. Ballesteros, L. Schlosser,

A. Hernandez-Vivanco, M. Martin-Fernandez, R. Quintana, A. Rayan, A. Diez, M. Fuenzalida, A. Agarwal, D.E. Bergles, B. Bettler, D. Manahan-Vaughan, E.D. Martin, F. Kirchhoff, A. Araque, Activity-dependent switch of GABAergic inhibition into glutamatergic excitation in astrocyte-neuron networks, Elife 5 (2016).

[44] T. Fellin, O. Pascual, S. Gobbo, T. Pozzan, P.G. Haydon, G. Carmignoto, Neuronal synchrony mediated by astrocytic glutamate through activation of extrasynaptic NMDA receptors, Neuron 43 (2004) 729–743.

[45] Q.S. Liu, Q. Xu, G. Arcuino, J. Kang, M. Nedergaard, Astrocyte-mediated activation of neuronal kainate receptors, Proc. Natl. Acad. Sci. U. S. A. 101 (2004) 3172–3177.

[46] U. Lalo, O. Palygin, S. Rasooli-Nejad, J. Andrew, P.G. Haydon, Y. Pankratov, Exocytosis of ATP from astrocytes modulates phasic and tonic inhibition in the neocortex, PLoS Biol. 12 (2014) e1001747.

[47] O. Pascual, K.B. Casper, C. Kubera, J. Zhang, R. Revilla-Sanchez, J.Y. Sul, H. Takano, S.J. Moss, K. McCarthy, P.G. Haydon, Astrocytic purinergic signaling coordinates synaptic networks, Science 310 (2005) 113–116.

[48] G. Perea, A. Yang, E.S. Boyden, M. Sur, Optogenetic astrocyte activation modulates response selectivity of visual cortex neurons in vivo, Nat. Commun. 5 (2014) 3262.

[49] M.L. Sun, Y.Q. Yu, Role of astrocytes in sensory processing in central nervous system, Zhejiang Da Xue Xue Bao Yi Xue Ban 40 (2011) 673–679.

[50] M. Navarrete, A. Araque, Endocannabinoids potentiate synaptic transmission through stimulation of astrocytes, Neuron 68 (2010) 113–126.

[51] M. Gomez-Gonzalo, M. Navarrete, G. Perea, A. Covelo, M. Martin-Fernandez, R. Shigemoto, R. Lujan, A. Araque, Endocannabinoids induce lateral long-term potentiation of transmitter release by stimulation of gliotransmission, Cereb. Cortex 25 (2015) 3699–3712.

[52] Z. Tan, Y. Liu, W. Xi, H.F. Lou, L. Zhu, Z. Guo, L. Mei, S. Duan, Glia-derived ATP inversely regulates excitability of pyramidal and CCK-positive neurons, Nat. Commun. 8 (2017) 13772.

[53] M. Pabst, O. Braganza, H. Dannenberg, W. Hu, L. Pothmann, J. Rosen, I. Mody, K. van Loo, K. Deisseroth, A.J. Becker, S. Schoch, H. Beck, Astrocyte intermediaries of septal cholinergic modulation in the hippocampus, Neuron 90 (2016) 853–865.

[54] P.F. Jacob, S.H. Vaz, J.A. Ribeiro, A.M. Sebastiao, $P2Y_1$ receptor inhibits GABA transport through a calcium signalling-dependent mechanism in rat cortical astrocytes, Glia 62 (2014) 1211–1226.

[55] L. Heja, G. Nyitrai, O. Kekesi, A. Dobolyi, P. Szabo, R. Fiath, I. Ulbert, B. Pal-Szenthe, M. Palkovits, J. Kardos, Astrocytes convert network excitation to tonic inhibition of neurons, BMC Biol. 10 (2012) 26.

[56] N. Chen, H. Sugihara, J. Sharma, G. Perea, J. Petravicz, C. Le, M. Sur, Nucleus basalis-enabled stimulus-specific plasticity in the visual cortex is mediated by astrocytes, Proc. Natl. Acad. Sci. U. S. A. 109 (2012) E2832–2841.

[57] L.M. Osborn, W. Kamphuis, W.J. Wadman, E.M. Hol, Astrogliosis: an integral player in the pathogenesis of Alzheimer's disease, Prog. Neurobiol. 144 (2016) 121–141.

[58] J. Wetherington, G. Serrano, R. Dingledine, Astrocytes in the epileptic brain, Neuron 58 (2008) 168–178.

[59] P.I. Ortinski, J. Dong, A. Mungenast, C. Yue, H. Takano, D.J. Watson, P.G. Haydon, D.A. Coulter, Selective induction of astrocytic gliosis generates deficits in neuronal inhibition, Nat. Neurosci. 13 (2010) 584–591.

[60] M. Lauritzen, J.P. Dreier, M. Fabricius, J.A. Hartings, R. Graf, A.J. Strong, Clinical relevance of cortical spreading depression in neurological disorders: migraine, malignant stroke, subarachnoid and intracranial hemorrhage, and traumatic brain injury, J. Cereb. Blood Flow. Metab. 31 (2011) 17–35.

[61] D.C. Wu, R.Y. Chen, T.C. Cheng, Y.C. Chiang, M.L. Shen, L.L. Hsu, N. Zhou, Spreading depression promotes astrocytic calcium oscillations and enhances gliotransmission to hippocampal neurons, Cereb. Cortex (2017) 1–13.

[62] R.M. Clark, G.G. Collins, The release of endogenous amino acids from the rat visual cortex, J. Physiol. 262 (1976) 383–400.

[63] M. Fabricius, M. Lauritzen, Transient hyperemia succeeds oligemia in the wake of cortical spreading depression, Brain Res. 602 (1993) 350–353.

[64] D.J. Selkoe, Alzheimer's disease: genes, proteins, and therapy, Physiol. Rev. 81 (2001) 741–766.

[65] Z. Wu, Z. Guo, M. Gearing, G. Chen, Tonic inhibition in dentate gyrus impairs long-term potentiation and memory in an Alzheimer's [corrected] disease model, Nat. Commun. 5 (2014) 4159.

[66] R.P. Kesner, A behavioral analysis of dentate gyrus function, Prog. Brain Res. 163 (2007) 567–576.

[67] S.G. Brickley, I. Mody, Extrasynaptic $GABA_A$ receptors: their function in the CNS and implications for disease, Neuron 73 (2012) 23–34.

[68] S. Jo, O. Yarishkin, Y.J. Hwang, Y.E. Chun, M. Park, D.H. Woo, J.Y. Bae, T. Kim, J. Lee, H. Chun, H.J. Park, D.Y. Lee, J. Hong, H.Y. Kim, S.J. Oh, S.J. Park, H. Lee, B.E. Yoon, Y. Kim, Y. Jeong, I. Shim, Y.C. Bae, J. Cho, N.W. Kowall, H. Ryu, E. Hwang, D. Kim, C.J. Lee, GABA from reactive astrocytes impairs memory in mouse models of Alzheimer's disease, Nat. Med. 20 (2014) 886–896.

[69] D.H. Woo, K.S. Han, J.W. Shim, B.E. Yoon, E. Kim, J.Y. Bae, S.J. Oh, E.M. Hwang, A.D. Marmorstein, Y.C. Bae, J.Y. Park, C.J. Lee, TREK-1 and Best1 channels mediate fast and slow glutamate release in astrocytes upon GPCR activation, Cell 151 (2012) 25–40.

[70] S. Lee, B.E. Yoon, K. Berglund, S.J. Oh, H. Park, H.S. Shin, G.J. Augustine, C.J. Lee, Channel-mediated tonic GABA release from glia, Science 330 (2010) 790–796.

[71] B.E. Yoon, S. Jo, J. Woo, J.H. Lee, T. Kim, D. Kim, C.J. Lee, The amount of astrocytic GABA positively correlates with the degree of tonic inhibition in hippocampal CA1 and cerebellum, Mol. Brain 4 (2011) 42.

Ringraziamenti

"Qual è la mia missione? La molla scatenante di un viaggio che cambia la vita è tutta in questa domanda. Fino a un certo punto rispondere non serve: quando devi formarti, prepararti, quando professionalmente non sei ancora nessuno e hai tutto da imparare, ti basta sentire il vento della giusta direzione e seguirlo, la missione è semplicemente un'intuizione, il contenuto della passione che brucia le tue energie migliori."

Da **Invisibile agli occhi** - ***W. Fasser & M. Orlandi***

Raccogliere tutti i grazie più o meno seri che nascono spontanei dopo tre anni di dottorato in poche righe è difficile, soprattutto per chi, come me, tende ad essere abbastanza prolissa (come Giorgio potrebbe confermare). Ma è doveroso almeno provarci. Ho deciso di iniziare questi ringraziamenti con una frase che, secondo me, nasconde diverse tappe fondamentali di ogni PhD student.

Il primo anno *"non sei ancora nessuno e hai tutto da imparare'*, il secondo anno vive di intuizioni miste a una passione che cresce, il terzo anno, ahimè, *"brucia le tue energie migliori*" (soprattutto se per qualche strana e sfortunata coincidenza astrale la tesi ti tocca scriverla d'estate, a Marina di Padova).

É il momento di partire in questo viaggio sul treno dei ricordi e dei perché… Da questo treno vedo quella che in tanti, parlando del nostro laboratorio, hanno descritto come un'isola felice. Certo ci sono i problemi, le incomprensioni, le piccole beghe quotidiane ma di fondo… insieme stiamo bene. Quindi… Grazie.

Grazie a Cristina, per il supporto continuo e sempre puntuale in questi tre anni. Grazie soprattutto per un'umanità che non è così comune e per le domande giuste che mi ha fatto prima del progress del primo anno, mi hanno fatto capire cosa non sapevo e quanto ancora potevo crescere e… faremo gli esperimenti con gli inibitori del CCE!

Grazie a Giorgio, per l'entusiasmo che riesce a trasmettere e per i suoi continui voli pindarici. Grazie per il continuo stressarci sull'avvicinarci il più possibile alla perfezione e alzare la famosa asticella. Grazie per tutte le sue correzioni, anche se pensa che io non lo ascolti quasi mai. Grazie

perché, anche se spesso chiude la porta in faccia al nostro casino, in fondo, a volte, ne fa parte anche lui.

Grazie a Lindaccia, per tutte le (dis)avventure che abbiamo passato insieme…per il panino con la mortadella alle 8.30 del mattino a Bologna, per Edimburgo (polka, polka, polka), per le due settimane a Parigi senza bagno in camera ma con tanti pains au chocolat per colazione… per gli infiniti "aspetta che controllo se ho chiuso la bombola" … insomma grazie e… sempre allegri bisogna stare! (Sa l'ha vist cus'è?)

Grazie a M&M's, per gli amici Michele Sex e Michele Jr., perché sono state (ahimè tocca usare il passato) due presenze fondamentali, nella loro assoluta diversità! Grazie a Michele Sex per essere stato il mio primo mentore. Per avermi insegnato, a suon di affabili insulti e tanta pazienza, cosa vuol dire provare senza sosta finché non ne esce fuori qualcosa di buono (simbolo la pipetta di uno dei miei primi, e ultimi, patch incollata sul muro dell'SP5!) e per avermi lasciato in eredità la sua fantastica scrivania. Grazie a Michele Jr, perché il mio primo anno oltre ad aver condiviso una scrivania, un pc, una sedia e uno sgabello abbiamo affrontato insieme tutti i disagi degli inizi… il buio del periodo PCR del venerdì sera alle 19, pulizia gabbie e stanza 9… fino a dar vita, insieme alla Lindaccia, all'efferata banda del buco.

Grazie ad Angela, perché è una compagna di banco piena di risorse e di allegria. Grazie perché ha la lacrima facile tanto quanto me, perché riesce a fare i versi di tutti gli animali, perché le piace conoscere e condividere canzoni, video, testi e chi più ne ha più ne metta. Perchè ha sempre ragione… anche se la mano da pallavolista… quella no, non va bene!

Grazie a Marta, per la sua infinita passione per questo lavoro e per il suo senso critico, per la sua incredibile tenacia e per la sua estrema correttezza. Grazie per la sacher con la marmellata al mandarino, per gli sfoghi a inizio giornata e per i consigli cinematografici!

Grazie a Gabri, per aver pensato insieme a Cristina ad iniziare un progetto sull'Alzheimer. Grazie per i preziosi consigli (… anche quelli sulle Canarie) e grazie per l'esperienza del suo matrimonio libero e multicolore.

Grazie a Letizia, purtroppo in lab abbiamo condiviso poco tempo insieme però è bastato per trovarci bene, per avere qualche buona dritta e il prezioso consiglio… se credi in un esperimento fallo.

Grazie a Qui, Quo e Qua (alias Vanessa, Mislav e Rosi) che hanno abbassato l'età media del lab (già molto bassa!!!) e nonostante abbiano creato un po' di agitazione, propria di ogni nuovo arrivo, sono diventati in breve parte integrante del gruppo. Grazie a Rosi per il *severa ma giusta* (che mi ricorda tanto quello che penso di Michele Sex) e per la nota minions che ha preso piede in lab… e a Vanessa e Mislav per i loro vivaci e divertenti battibecchi!

Grazie al trio Autifony, per i lab-meeting a sfondo abbuffata e non solo. Grazie anche a tutti quelli che hanno soggiornato per un breve periodo nel nostro Lab, perché anche se per poco abbiamo condiviso sushi, risate, esperimenti, inizi, Gerry… pezzi di vita.

Grazie a chi popola i corridoi del Vallisneri, per gli infiniti "ciao" che si dicono durante una giornata di lavoro. Grazie alla chat del disagio, simbolo di rapporti che sono andati al di là del condividere uno stesso laboratorio e che hanno trovato i binari giusti per ritrovarsi. Un grazie speciale a Rosa, per essere stata la prima ad aver creduto in me.

Grazie a tutto il laboratorio Pozzan e alla Prof.ssa Pizzo che hanno pazientemente accettato la musica, il karaoke e soprattutto il casino proveniente dalla stanza due fotoni.

Grazie a Paulo, per i giochi di logica e i krumiri.

Grazie a tutti i colleghi incontrati nelle varie scuole…perché andare ai congressi diventa sempre un ritrovare amici lontani. Grazie anche a tutte le persone con cui ho avuto il piacere di collaborare e che mi hanno dato modo di crescere e responsabilizzarmi.

Dulcis in fundo… Grazie a Miky. Potrei scrivere tranquillamente altre tre pagine per dare il giusto peso alle millemila esperienze insieme. Grazie alle, in questo caso fortunate, coincidenze astrali fatte di codici MATLAB che ti hanno permesso di capire (con un delay di quasi un anno) che ero un effettivo membro del laboratorio e che insieme lavoriamo bene. Grazie perché il nostro è sempre stato un lavorare l'una accanto all'altra. Grazie per avermi insegnato a giocare con gli elementi ottici (ora scrivo anche power meter correttamente!) e ad aprire la mente per trovare sistemi fai-da-te e sistemare le cose. Grazie perché è stato un onere insistere ma un onore poi vederti davvero

riprendere a fare esperimento e per aver creduto insieme a me nella whisker stimulation. Grazie perché il tuo essere giustificatrice sociale compensa la mia poca diplomazia, e viceversa. Grazie per le nottate di esperimento (indimenticabili le passeggiate nel carrello della spesa e le 6 del mattino con i Purkinje neurons) concluse spesso con una sana partita a Machiavelli. Grazie perché questo progetto insieme è più divertente. Grazie per tutto quello che abbiamo condiviso anche fuori dal lab e per essere ormai un punto di riferimento, ma questo lo sapevi già!

Bene… mi apro alla chiusura di questo viaggio sul treno dei ricordi e dei perché. Ho deciso di limitarmi a ripercorrere questi tre anni senza uscire fuori dai "*confini della scienza*". Gli altri grazie arriveranno in modi e tempi diversi.

Chiudo con una frase presa sempre da **Invisibile agli occhi**:

"La mia dignità di uomo non emerge solo quando dimostro di saper fare da me,
ma anche quando accetto di non saper fare a meno degli altri."

La bellezza della scienza in fondo è anche questa.

All is **Groovy**